

**DEPOSITION OF METAL ISLANDS,
METAL CLUSTERS AND METAL
CONTAINING SINGLE MOLECULES
ON SELF-ASSEMBLED MONOLAYERS**

Deposition of Metal Islands, Metal Clusters and Metal Containing Single Molecules
on Self-Assembled Monolayers.

Emiel Speets

Thesis University of Twente, Enschede, The Netherlands

ISBN 90-365-2169-6

This work has been financially supported by the Nanolink program of the MESA⁺
Institute for Nanotechnology, University of Twente.

Publisher:

Print Partners Ipskamp, Postbus 33, 7500 AH Enschede, The Netherlands

<http://www.ppi.nl>

© Emiel Adrianus Speets, Enschede, 2005

Cover design: Emiel Speets

Cover Illustration: Saguaro cacti in the Sonoran Desert near the Saguaro National
Park in southern Arizona, USA.

No part of this work may be reproduced by print, photocopy or any other means
without the permission in writing from the publisher.

DEPOSITION OF METAL ISLANDS, METAL CLUSTERS AND METAL CONTAINING SINGLE MOLECULES ON SELF-ASSEMBLED MONOLAYERS

PROEFSCHRIFT

ter verkrijging van
de graad van doctor aan de Universiteit Twente,
op gezag van de rector magnificus,
prof.dr.W.H.M. Zijm,
volgens besluit van het College van Promoties
in het openbaar te verdedigen
op vrijdag 1 april 2005 om 16.45 uur

door

Emiel Adrianus Speets

geboren op 27 september 1976
te Midwoud

Dit proefschrift is goedgekeurd door:

Promotor: Prof. Dr. Ir. D. N. Reinhoudt

Assistent-promotor: Dr. B. J. Ravoo

*“Come gather 'round people
Wherever you roam
And admit that the waters
Around you have grown
And accept it that soon
You'll be drenched to the bone.
If your time to you
Is worth savin'
Then you better start swimmin'
Or you'll sink like a stone
For the times they are a-changin'.”*

Bob Dylan.

Contents

Chapter 1	Introduction	1
1.1	References	4
Chapter 2	Self-Assembled Monolayers in Electronic Devices	5
2.1	Introduction	6
2.2	SAMFETs and other electronic devices	9
2.3	Electronic measurements of SAMs	15
2.3.1	Permanent devices relying on top electrode evaporation	15
2.3.2	Non-permanent devices	19
2.3.3	Scanning probe techniques	23
2.4	Single molecule electronic measurements	29
2.4.1	Conductivity measurements of single molecules using STM	29
2.4.2	Conductivity measurements of single molecules using conducting probe AFM	30
2.4.3	Conductivity measurements using other nanoscale molecular junctions	32
2.5	Conclusion and outlook	36
2.6	References	37
Chapter 3	Self-Assembled Monolayers of Difunctional and of Conducting Molecules	43
3.1	Introduction	44
3.2	Preparation of self-assembled monolayers	45

3.2.1	SAMs of alkyldithiols on gold	45
3.2.2	SAMs of biphenyldithiol on gold	49
3.2.3	SAMs of thio-acetate protected thiols on gold	51
3.3	Insertion of <i>para</i> -1,4-di(phenylethynyl-4'-thioacetyl)benzene (1) in decanethiol SAMs	54
3.4	Conclusions	56
3.5	Experimental procedures	57
3.6	References	59

Chapter 4 Fabrication of Arrays of Gold Islands on Self-Assembled Monolayers using Pulsed Laser Deposition through Nanosieves 63

4.1	Introduction	64
4.2	Pulsed laser deposition	66
4.2.1	Target ablation	68
4.2.2	Nanosieves as shadow masks	69
4.3	Deposition of gold islands on SAMs	72
4.3.1	Insulation of the gold islands from the gold substrate by the SAM	73
4.3.2	Electrochemical investigation of the insulation of the gold islands	75
4.4	Conclusions	78
4.5	Experimental procedures	78
4.6	References	80

Chapter 5	Pulsed Laser Deposition of Noble Metal Clusters on SAMs	83
5.1	Introduction	84
5.2	Preparation of nanometer size metal clusters	85
5.3	Deposition of metal clusters on SAMs	90
5.4	Conclusions	94
5.5	Experimental procedures	94
5.6	References	96
Chapter 6	Scope of Pulsed Laser Deposition of Metals on Self-Assembled Monolayers	97
6.1	Introduction	98
6.2	Variations of substrate, SAM and deposited metal in PLD on SAMs	99
6.2.1	Deposition of various metals	99
6.2.1.1	Pattern replication in shadow mask deposition	99
6.2.1.2	Morphology of deposited metal islands on SAMs	101
6.2.2	Deposition on various substrates	104
6.2.3	Other sieves	106
6.3	Pattern enhancement of pulsed laser deposited metal patterns using electroless deposition	107
6.3.1	PLD and ELD on SAMs on SiO ₂	108
6.3.2	PLD and ELD on SAMs on Au	109
6.4	Conclusions	111
6.5	Experimental procedures	112
6.6	References	113

Chapter 7	Surface-Confined Single Molecules: Assembly and Disassembly of Nanosize Coordination Cages on Gold (111)	115
7.1	Introduction	116
7.2	Large cavitands and cages	117
7.3	Surface assembly	118
7.4	Conclusions	124
7.5	Experimental procedures	125
7.6	References	126
	Summary	129
	Samenvatting	133
	Dankwoord	137
	Curriculum Vitae	141

Chapter 1

Introduction

Nanotechnology is in a sense the logic follow-up of microtechnology but it is on the other hand a totally new branch of science. Where microtechnology was mainly ruled by the chip industry for the preparation of micron size components and photolithography was the main tool, nanotechnology is much broader.

Nanotechnology is a combination of different fields in natural sciences, the goal of which is the manipulation, integration and use of objects with sizes ranging from submicron to sub-nanometer (single atoms). Biomolecules,¹ self-assembled supramolecular systems,² photolithography,³ nanofabrication,⁴ materials science⁵ and electronics⁶ all are part of this expanding and popular field. Nanotechnology should provide answers and solutions in the fields of, among others, medicine, environmental science and electronics. Although commercial prospects are solid, large scale commercialization might take another ten years.⁷

Molecular electronics⁸ is one of the most interesting new fields that has emerged from nanotechnology. Molecular electronics is concerned with the use of molecules or molecular assemblies as functional parts of electronic devices, ranging from dye-sensitized solar cells to transistors. Molecular electronics for use in computer chips has become appealing for two reasons. Firstly, the fabrication of smaller devices on chips using conventional lithographic techniques becomes increasingly difficult and costly,⁹ and secondly semiconductors, insulators and metals behave differently on the nanometer scale, giving fundamental problems for working

devices.¹⁰ The use of molecules as insulators and rectifiers might solve these limitations.¹¹

A big advantage of using molecules in electronic devices is that synthetic chemistry can afford a virtually endless number of different molecules, tailor-made for specific electronic functions. The ultimate goal of molecular electronics is the integration of organic molecules, biomolecules, carbon nanotubes¹² and nanoclusters in working nanocomputers.¹³ Examples of molecular electronics are intramolecular charge transfer for light harvesting,¹⁴ conduction, switching and the use of self-assembled monolayers (SAMs) of functional molecules.

SAMs are one-molecule thick layers of organic molecules on surfaces that have been applied in many fields in science and in nanotechnology since they were first reported.^{15,16} Their use as functional part in electronic devices has very recently received major attention.¹⁷ SAMs have suitable dimensions to be integrated in nanoscale electrical circuits. Depending on the molecules, they can perform several functions, which are presently performed by semiconductors or metals in conventional chips, like conduction, switching, rectification and insulation. Moreover, the use of SAMs might even have advantages over conventional materials and techniques when it comes to making smaller Integrated Circuits (IC's).

With the development of scanning probe tools such as scanning tunneling microscopy (STM)¹⁸ and atomic force microscopy (AFM)¹⁹ systematic investigation of molecular electronics became feasible. Still, newer and better microscopes are the key to innovative nanotechnology research.²⁰ Self-assembled monolayers can be analyzed for their electronic properties from the single molecule scale²¹ up to square millimeter areas.²²

The research that is described in this thesis focuses on the use of self-assembled monolayers (SAMs) in molecular electronics and single molecule chemistry. SAMs are used as a platform for functionalization by deposition of metal or insertion of single molecules.

In Chapter 2 an overview will be given of the use of SAMs in electronic devices and the measurement of the electrical properties of single molecules. The focus will be on the importance of the contact between molecules and electrodes, device fabrication and analysis using various single-molecule probing techniques.

In Chapter 3 the preparation of SAMs with thiol headgroups from dithiols and dithioacetates will be described. 1,4-Di(phenylethynyl-4'-thioacetyl)benzene is inserted in pre-existing decanethiol SAMs. X-ray photoelectron spectroscopy (XPS), STM, contact angle goniometry and electrochemistry were used to analyze these SAMs.

Chapter 4 describes the fabrication of Au-SAM-Au sandwich structures using Pulsed laser deposition (PLD) through a nanosieve. This mild technique to deposit metals on SAMs is explained and the arrays of islands of deposited Au are analyzed using AFM. Using electrochemical reduction of Cu from a CuSO₄ solution a distinction can be made between islands that are electrically insulated by the SAM and non-insulated islands.

In Chapter 5 the deposition of small metal clusters using PLD is described. Transmission Electron Microscopy was used to investigate the Au, Pd and Pt clusters, which had nm sizes. Metal clusters were deposited on SAMs, and STM and conducting probe AFM were used to prove that the clusters were positioned on top of the SAMs.

In Chapter 6 the scope of PLD on SAMs is investigated. Various metals are deposited on various SAMs on Au and SiO₂. Sieves with different patterns are used to deposit small amounts of metal on SAM, which are then used as a catalyst for electroless deposition. Solid Cu structures could be fabricated using a minimal gas phase metal deposition followed by chemical growth of Cu.

Finally, Chapter 7 deals with the single molecule insertion and detection of nanosize coordination cages and cavitands on gold using AFM. Cages with a large internal volume, formed by the self-assembly of two large thioether functionalized cavitand molecules, could be attached to a gold surface by insertion from solution in a preformed SAM and could subsequently be disassembled and reassembled.

1.1 References

¹ N. Ramachandran, E. Hainsworth, B. Bhullar, S. Eisenstein, B. Rosen, A. Y. Lau, J. C. Walter, L. Labaer, *Science* **2004**, 305, 86-90.

² D. N. Reinhoudt, M. Crego-Calama, *Science* **2002**, 295, 2403-2407.

³ G. M. Wallraff, W. D. Hinsberg, *Chem. Rev.* **1999**, 99, 1801-1822.

⁴ S. R. Quake, A. Scherer, *Science* **2000**, 290, 1536-1540.

- ⁵ (a) R. K. Soong, G. D. Bachand, H. P. Neves, A. G. Olkhovets, H. G. Craighead, C. D. Montemagno, *Science* **2000**, 290, 1555-1558; (b) T. L. Morkved, P. Wiltzius, H. M. Jaeger, D. G. Grier, T. A. Witten, *Appl. Phys. Lett.* **1994**, 64, 422-424.
- ⁶ (a) Y. Cui, C. M. Lieber, *Science* **2001**, 291, 851-853; (b) D. I. Gittins, D. Bethell, D. J. Schiffrin, R. J. Nichols, *Nature* **2000**, 408, 67-69.
- ⁷ R. Paull, J. Wolfe, P. Hébert, M. Sinkula, *Nature Biotech.* **2003**, 21, 1144-1147.
- ⁸ D. H. Cobden, *Nature* **2001**, 409, 32-33.
- ⁹ T. Ito, S. Okazaki, *Nature* **2000**, 406, 1027-1031.
- ¹⁰ J. M. Tour, *Acc. Chem. Res.* **2000**, 33, 791-804.
- ¹¹ J. M. Tour, *Molecular Electronics*, World Scientific, Singapore, 2003, ISBN981-238-341-7.
- ¹² S. J. Tans, A. R. M. Verschueren, C. Dekker, *Nature* **1998**, 393, 49-52.
- ¹³ G. Y. Tseng, J. C. Ellenbogen, *Science* **2001**, 294, 1293-1294.
- ¹⁴ B. O'Regan, M. Grätzel, *Nature* **1991**, 353, 737-740.
- ¹⁵ R. G. Nuzzo, D. L. Allara, *J. Am. Chem. Soc.* **1983**, 105, 4481-4483.
- ¹⁶ J. Sagiv, *J. Am. Chem. Soc.* **1980**, 102, 92-98.
- ¹⁷ M. A. Reed, J. Chen, A. M. Rawlett, D. W. Price, J. M. Tour, *Appl. Phys. Lett.* **2001**, 78, 3735-3737.
- ¹⁸ G. Binnig, H. Rohrer, C. Gerber, E. Weibel, *Phys. Rev. Lett.* **1982**, 49, 57-61.
- ¹⁹ G. Binnig, C. F. Quate, C. Gerber, *Phys. Rev. Lett.* **1986**, 56, 930-933.
- ²⁰ S. Bunk, *Nature* **2001**, 410, 127-129.
- ²¹ G. K. Ramachandran, J. K. Tomfohr, J. Li, O. F. Sankey, X. Zarate, A. Primak, Y. Terazono, T. A. Moore, A. L. Moore, D. Gust, L. A. Nagahara, S. M. Lindsay, *J. Phys. Chem. B* **2003**, 107, 6162-6169.
- ²² R. Haag, M. A. Rampi, R. E. Holmlin, G. M. Whitesides, *J. Am. Chem. Soc.* **1999**, 121, 7895-7906.

Chapter 2

Self-Assembled Monolayers in Electronic Devices

The use of self-assembled monolayers (SAMs) and single molecules in micro- and nanoscale electronic devices is reviewed. Functioning nanoscale electronic devices in which a SAM is incorporated are described, as well as devices for macroscale electronic analysis of SAMs. The problems and challenges encountered when making such devices like top electrode deposition, short circuits and contacting molecules and electrodes are discussed. The second part of the review deals with single molecule electronics. The different experimental methods and setups used for measuring single molecule electronic properties are described, together with the factors that are important for electrical measurements, such as junction size, junction stability and temperature variation.

2.1 Introduction

Self-assembled monolayers (SAMs) are an excellent tool for surface modification.¹ During the last decades a large number of articles addressing the fundamental properties of SAMs have been published, indicating the importance of these systems and giving a good insight into the structure and properties of a wide variety of SAMs.^{2,3} Many groups work on the application of SAMs in sensing,⁴ surface protection (etch resist),^{5,6,7} protein binding,⁸ lubrication,⁹ surface wettability,¹⁰ surface patterning,¹¹ or lift-off layers.¹²

SAMs can be prepared using a variety of surfaces and organic molecules.² The most common SAMs are sulfur containing molecules (thiols, thioethers, disulfides) on noble metal surfaces^{13,14,15} and siloxanes on SiO_2 ¹⁶ or other substrates.¹⁷ SAMs of carboxylic acids on metal oxides,¹⁸ alkenes on silicon^{19,20} and thiols on GaAs²¹ have also been prepared. In molecular electronics, SAMs of thiols on gold are the combination of choice, because of the electrical conductivity of the gold substrate.

All SAMs contain the same four elements: a substrate, a functional group, (which forms the bond between surface and molecule) a spacer (which can be just an alkyl chain, for good packing of the SAM) and finally the outer surface functionality. In molecular electronics studies the spacer is often a conjugated, electron conducting system. The outer surface functionality can be a substituent that controls only the surface potential (like methyl or perfluoromethyl), but it can also be a chemically reactive group that can bind to other compounds. A schematic drawing is shown in Figure 2.1.

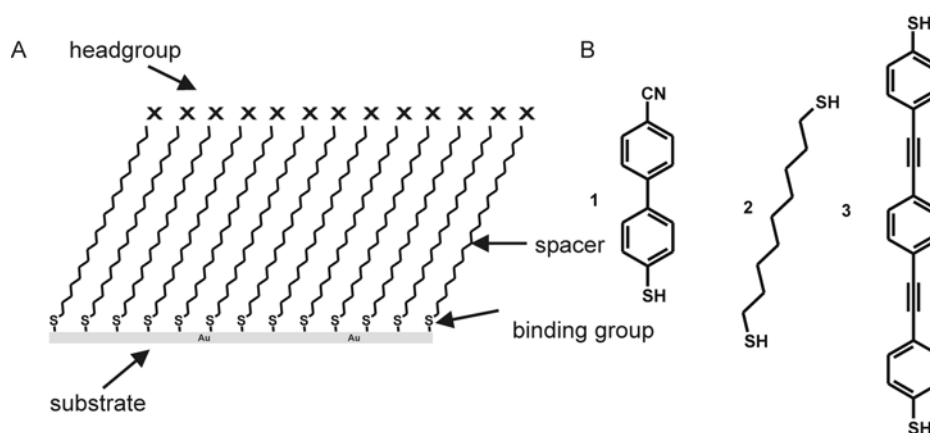


Figure 2.1 (A) Schematic drawing of a self-assembled monolayer of thiolates on gold. (B) Typical molecules used in molecular electronics.

SAMs are easy to prepare without the need for cleanroom conditions. SAMs can be highly ordered and often offer an excellent method to modify a surface with only a small amount of material. In this chapter mainly SAMs on gold are discussed. Gold surfaces can be easily prepared, do not oxidize under normal conditions and are conductive. SAMs are prepared by simply immersing the gold substrate in a solution of the sulfur-containing molecule. A SAM is formed within several hours.

Molecular electronics is based on the use of molecules in electronic circuits in order to perform functions that are known of semiconductors or metals. The well-known Moore's law²² which predicts a doubling of the number of transistors on a chip every 18 months will not be valid forever, as the small dimensions of silicon-based devices will ultimately give rise to fundamental physical problems. Three atom thick oxide layers are not electrically insulating anymore, leading to charge leakage, and silicon loses its (semiconducting) band structure at nanoscale dimensions.²³ Because of the increasing demand for faster computers and higher storage capacities per square inch, electrical devices that incorporate a single or only a few molecules have become of great interest.

The use of single molecules as rectifiers in electronic devices was first proposed in 1974 by Aviram and Ratner.²⁴ They proposed a molecule that would have roughly the properties of a solid-state p-n junction. They described molecules containing an electron-donor and an electron-acceptor part bridged by a spacer group. With the invention of the scanning tunneling microscope (STM) by Binnig and Rohrer²⁵ the field of molecular electronics started to gain momentum. STM provided a tool which could visualize conducting surfaces with atomic resolution and even single atoms could be moved around on a surface and afterwards visualized using the same probe.²⁶ From STM images the crystalline 2-dimensional structure of the sulfur atoms of the thiols could be derived.^{27,28,29,30} The field of molecular electronics has expanded rapidly, ranging from molecular wires,²³ charge transfer processes,³¹ electron transfer at molecule/metal electrode interfaces^{32,33,34} to unimolecular electrical rectifiers.³⁵ Recently, Creery published a review on molecular electronic junctions describing several measurement methods.³⁶ James and Tour published a review on electrical measurements in molecular electronics focusing on the molecular properties.³⁷

Metal-molecule-metal junctions consisting of single molecules or assemblies of molecules (like SAMs) all show generalized electrostatic potential behavior. Figure 2.2 stresses the importance of contact between the molecule and the electrodes. Different molecule/electrode pairs will give different contact resistances (R_1 , R_2). The electronic properties of molecules (R_{mol}) can only be compared for measurements with the same electrodes.

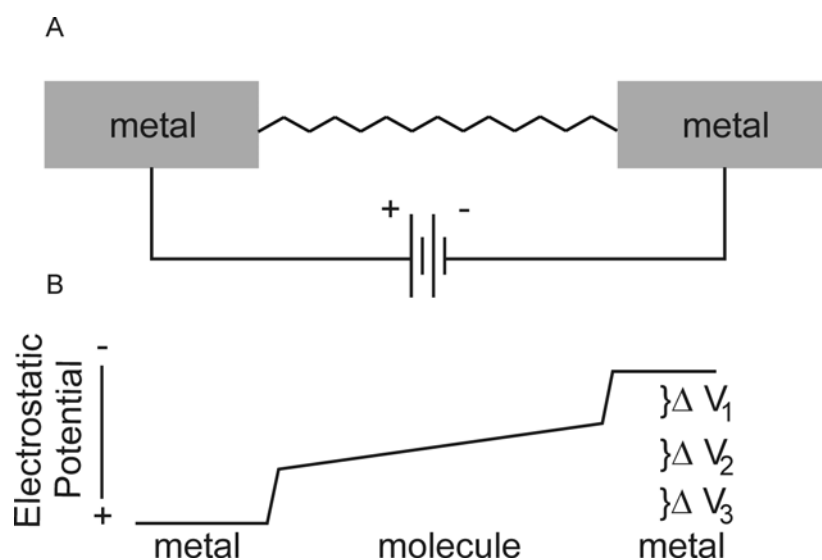


Figure 2.2 (A) Metal-molecule-metal junction. The molecular part can be a single molecule or a SAM. (B) Electrostatic potential corresponding to (A), ΔV_1 and ΔV_3 are the voltage drops caused by the contact between molecule and metal, ΔV_2 is the voltage drop caused by the molecule or SAM (from Wold and Frisbie³⁸).

This Chapter describes three main aspects of molecular electronics. The first aspect is the use of entire SAMs in devices. The SAM is used as functional layer between two electrodes and performs functions such as rectification, switching and charge storage.

The second aspect is the electronic measurement through SAMs. For this, measurement devices are constructed for analysis purposes only. The devices are used to measure properties like resistance and conductivity of the SAM and eventual asymmetric bias response. Crucial elements in the research on devices like these are the deposition of the top electrode on the SAM, the investigation whether the SAM is still intact, and whether there are no short circuits between the two electrodes.

The third aspect is the investigation of electronic properties of single molecules. Molecules are probed for non-symmetrical behavior and resistance to see

whether they might be used in transistors or capacitors respectively. The main advantage of these experiments is that an exact number of molecules, from one to several, are probed and that for this reason the junction structure is well defined. The challenge here is the formation of metal-molecule-metal junctions. AFM and STM can be used for this purpose but other elegant methods have been developed as well.

The focus in this Chapter will be on the design of measurement devices and methods, and the comparison of results obtained from different devices. The measurement of contact resistance, rectifying behavior and conductivity of junctions will also be described. The field of electronic measurements through SAMs is relatively new, and no standard measurement tools and methods have been established. For this reason extensive comparison of values obtained in literature for the resistance of molecules is avoided.

2.2 SAMFETs and other electronic devices

SAMs might be excellent components for the fabrication of nanoscale electronic devices on chips. Because of their thickness, which is in the order of several nanometers, and their tunable electrical properties, they might be used in nanometer scale field effect transistors (FETs) and logic gates. The development of SAM-devices has already led to some interesting results, despite the fact that the electronic properties of SAMs are not yet fully understood. For the application in electronic devices molecules should perform functions like rectification,³⁹ charge storage, switching or capacitance. In this section a few of the most well known devices published in recent literature are described.

Figure 2.3 shows a schematic picture of a self-assembled monolayer field-effect transistor (SAMFET) made by Dekker *et al.*⁴⁰ inspired by a design first proposed by Schön *et al.*⁴¹ The SAM of 4-4'-biphenyldithiolate acts as the semiconductor for electrons moving from the source to the drain if a potential is applied to an aluminum gate, insulated from the gold electrodes by a thin aluminum oxide layer. The SAM functions in such a way that when no bias is applied to the gate electrode, no current is flowing from source to drain.

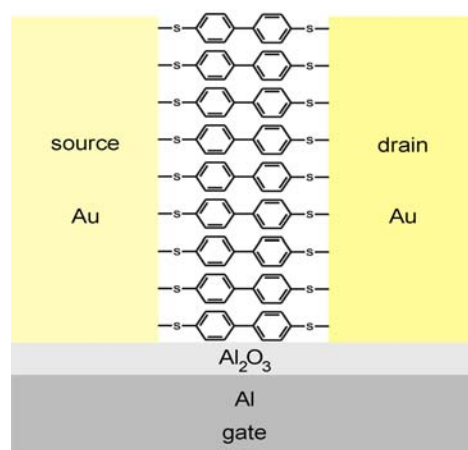


Figure 2.3 Schematic drawing of the functional part of a SAMFET, used by Dekker *et al.*⁴⁰

As with all electronic SAM devices, the second electrode must be contacted to the top part of the SAM (on gold) without the creation of short circuits. Another crucial factor for a working SAMFET is that the molecules used should work as a part of the transistor, in other words they must show rectifying behavior. Dekker *et al.* used five different dithiols and dicyanides and only a small percentage of the devices was not electrically shorted. A few devices using 1,3-benzenedithiol exhibited a weak gate effect. These results were in sharp contrast with the previously reported devices made by Schön *et al.*,⁴¹ which turned out to be fraudulent.⁴² Kagan *et al.* concluded that because of carrier tunneling and device electrostatics the minimum length of molecules used in such a SAMFET should be $> 2.5 - 3$ nm.⁴³ In other words, devices like the SAMFET by Schön *et al.* will never work even if no electrical shorts are present. They concluded that these kinds of SAMFETs would only work with SAMs of longer molecules.

A molecular switch that can open and close an electrical circuit when a bias is applied is another example of the use of molecules for electronic functions. Rotaxanes are mechanically linked ring-shaped molecules around a dumbbell-shaped molecule capable of switching by movement of the ring along the dumbbell.⁴⁴ Stoddart and Heath *et al.* reported a Langmuir-Blodgett (LB) layer of a rotaxane as switching component in a logic gate made from an array of configurable switches⁴⁵ (Figure 2.4). The rotaxane layer was deposited on an aluminum oxide substrate after which a Ti/Al electrode was evaporated on top of the rotaxane layer. The macrocycle should switch position if a bias is applied.

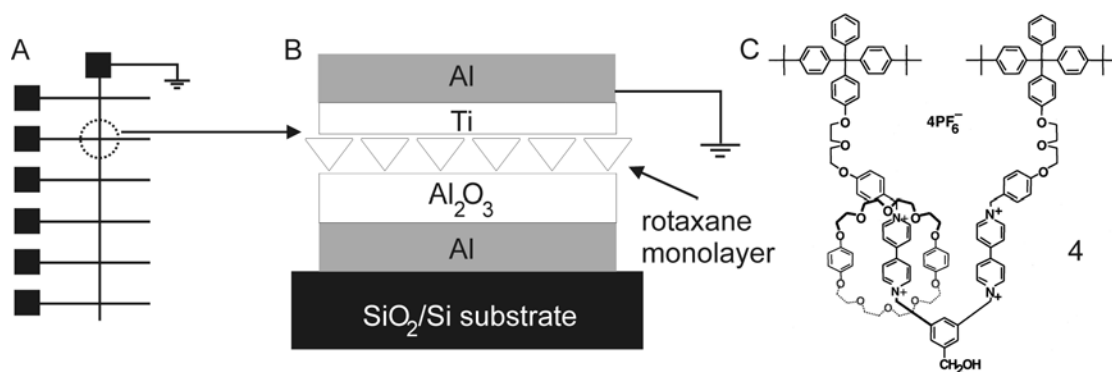


Figure 2.4 Logic gate device using a rotaxane LB layer as constructed by Stoddart and Heath *et al.*⁴⁵ (A) Schematic picture of the cross-wire construction (B) Schematic cross section of a junction (C) Rotaxane (**4**) used in the logic gate.

This system (Figure 2.4 A) provides six different measurement possibilities. The junctions can be electrically probed *via* the larger pads connected by wires that have diameters of several microns. The switchable rotaxane layer is in the middle of the junction and consists of several million molecules per junction. Later work of Stoddart *et al.*⁴⁶ using a comparable device (with platinum as bottom electrode) showed however that the observed reversible-switching behavior ascribed to the rotaxane molecules also occurred when eicosanoic acid molecules were used. The electrical switching and resistance tuning was a function of the molecules, the electrodes and their interfacial interactions, they concluded. Partial reconstruction of the titanium electrode surfaces by electromigration-induced filaments might be the reason for the resistance tuning. The use of the highly reactive titanium as electrode material,⁴⁷ to prevent further diffusion of Al or Au electrode material through the monolayers, makes it difficult to understand what the metal-molecule interface really is like.⁴⁶ Comparable electronic devices have also been made using a [2]catenane switch (consisting of two interconnected ring-shaped molecules). These devices were stable over months and hundreds of switching cycles.⁴⁸

Furthermore SAMs have been used to store electronic charges, which could be read out as well. Reed and Tour *et al.* reported a molecular random access memory (RAM) cell.⁴⁹ A set of conjugated thiols (Figure 2.5) between two gold electrodes (30-50 nm in diameter) was put into a high and a low conductive state (σ) by applying short voltage pulses. The system could be written, by applying a positive voltage pulse, read, and also erased, by applying a negative voltage pulse. Figure 2.6 shows

how this molecular RAM cell works. Only the molecules that contained a nitro group (**5** and **6**) showed this switchable behavior, whereas the molecule with only an amine (**7**) and without substituents could not store a charge. *Via* a two-step reduction the molecule (**5** or **6**) can be reduced to the dianion; current only flows through the SAM after the first reduction step. The mechanism of the current flow is under discussion. Ghosh *et al.* concluded (from modeling energy diagrams) that charge transfer occurred due to oxidation of the chemically bound part of the molecule, and did not involve the nitro group.⁵⁰

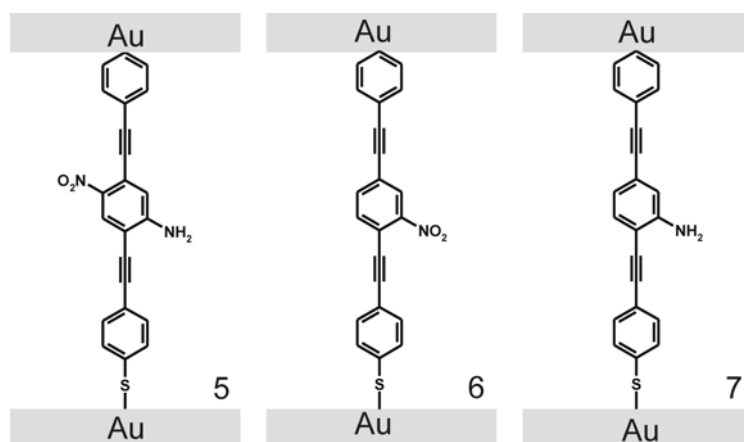


Figure 2.5 Molecules for a random access memory cell.⁴⁹

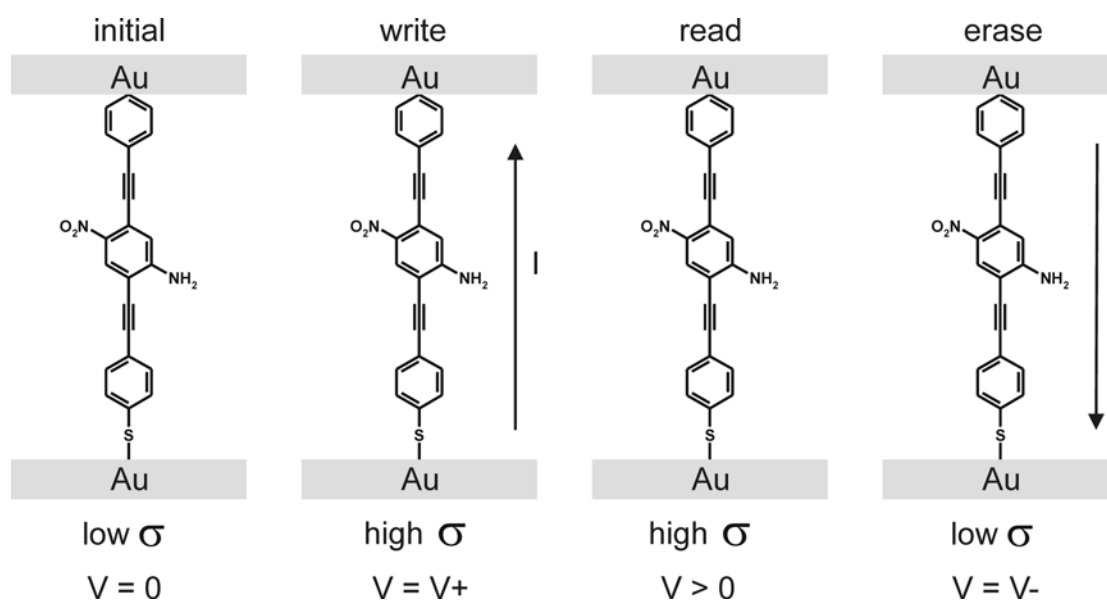


Figure 2.6 Schematic representation showing how the molecular RAM cell works. The arrows indicate the direction in which the current flows.

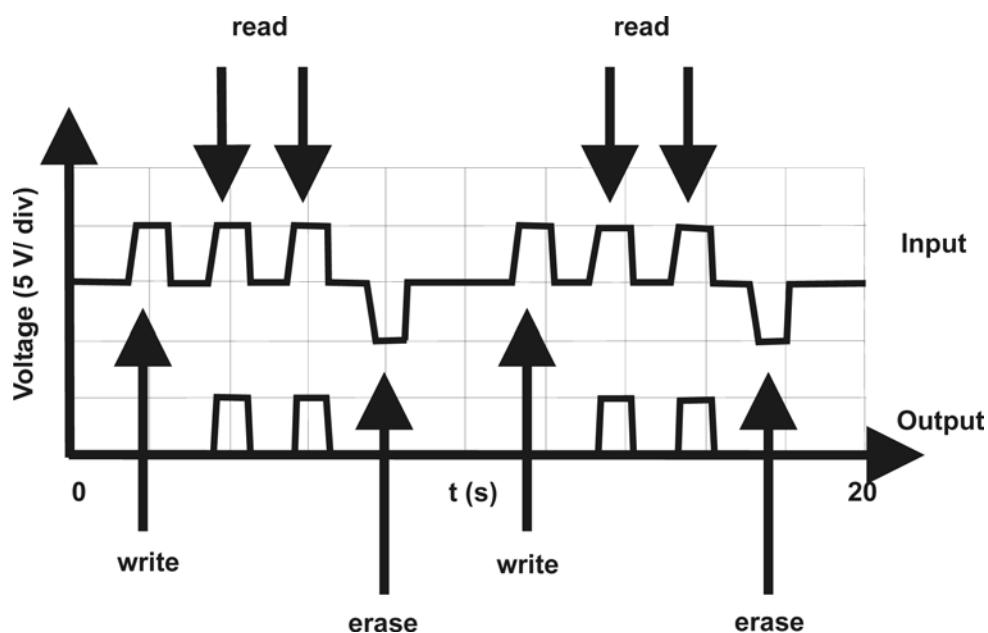


Figure 2.7 Response of the molecular RAM cell to applied voltage pulses (from ref. 49).

In Figure 2.7 the input and output signals of the molecular RAM cell are shown. The device used for the switching experiments was a nanopore, which will be discussed later in this Chapter (2.3.1). The switching is reversible and no device degradation was observed. Molecule **(6)** (Figure 2.5) showed a memory effect. However, in this case the storage was in a low conductive state opposite to that of molecule **(5)**.

Conductive molecules can also be used in electronic circuits as nanoscale switchable electric wires. Tour *et al.* reported the NanoCell (Figure 2.8), which is a disordered array of nanowires and islands, interlinked with molecules, between input/output leads.⁵¹ Two sets of electrodes were deposited on a silicon wafer. The electrodes make contact with an evaporated, discontinuous gold film. This film does not conduct electricity from one electrode to the other. Gold nanowires (diameter 30 nm, length 300-2000 nm) were added to a solution of 1-(phenylethynyl-4'-thioacetyl)-2-nitro-4-(phenylethynyl-4''-thiol)-benzene **(8)** (Figure 2.8 B). The thiols adsorb to the nanowires, leaving the thioacetate groups exposed. Subsequently, the thioacetate groups were deprotected and a NanoCell was immersed in the solution, allowing the nanowires connected by the molecules to be assembled between the electrodes.

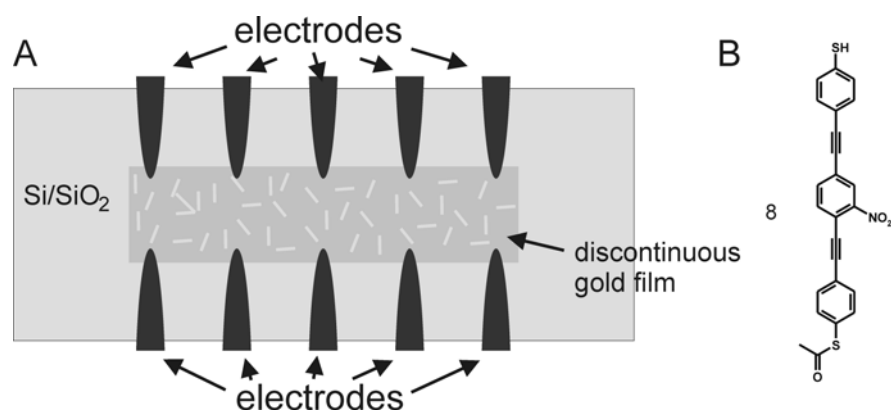


Figure 2.8 (A) NanoCell made by Tour et al. The ten gold electrodes have widths of around $3 \mu\text{m}$ and are spaced $5 \mu\text{m}$ apart. (B) 1-(Phenylethynyl-4'-thioacetyl)-2-nitro-4-(phenylethynyl-4''-thiol)-benzene (**8**).

Between a pair of electrodes, paths consisting of evaporated gold, gold nanowires and conjugated molecules were formed. As in the molecular RAM, this system could be switched when a voltage pulse was applied. The switching was reproducible, although electromigration and nanofilamentary metal formation might also be a mode for current transport. The main advantage of the NanoCell is that it does not require nanolithographic techniques to create junctions. A disadvantage is however that it is never completely clear what causes the measured signals, because the paths through which the current flows have a random length and consist of different materials (molecules, nanowires and evaporated gold).⁵¹ This system gives a perfect example of how an electronic device using functional molecules can be fabricated by 'randomly' self-assembled building blocks. Electronic testing of all pathways between the outer electrodes, using a probe station, gives information about the properties of every possible path between two electrodes.

All these examples show that SAMs can be used to perform functions that until now were performed by semiconductors and metals. Taken together with the possibility to fabricate devices with very small junction dimensions, SAM devices are promising for future use. Understanding the processes that occur during switching, rectification or conductance is of utmost importance for the fabrication of commercial SAM devices.

2.3 Electronic measurements of SAMs

For most applications the electronic properties of a group of molecules (in a SAM) is more important than the properties of one single molecule. The electronic properties in a SAM cannot be derived directly from single molecule properties because for larger electrodes irregularities such as pinholes, surface roughness and influences of the surrounding matrix, like lateral electronic coupling, play a role. Because deposition of a second electrode on the SAM is often difficult⁵² alternative device architectures were designed to measure electronic properties of SAMs. Several of these methods use systems that are not stable and can only be used for measurement purposes, like crosswire junctions or mercury drop electrodes. Other methods use a setup, made using conventional lithography, which in principle can be used as working device as well, containing a SAM assembled on an electrode after which another electrode is evaporated on top of this SAM.

2.3.1 Permanent devices relying on top electrode evaporation

The nanopore (Figure 2.9) developed by Reed *et al.* is an example of a permanent device.⁵³ Via conventional lithography techniques a small pore was created in a silicon nitride membrane. A Au electrode was evaporated on the backside of the device after which a SAM was formed on the exposed gold area, which may be as small as 20 nm in diameter (*ca.* 300 nm²). The second Au electrode was evaporated on the SAM at 77 K at a rate of less than 1 Å s⁻¹ to avoid damage to the SAM. Around 80 % of the devices constructed in this way functioned, and displayed no short circuits.

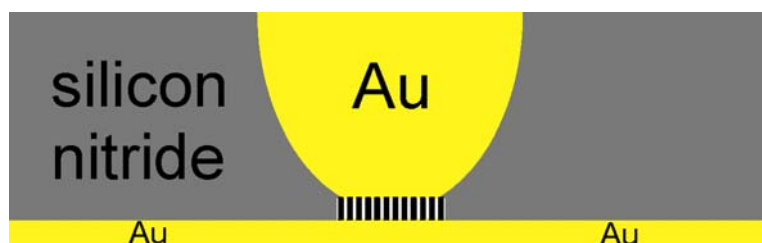


Figure 2.9 Nanopore device as used by Reed *et al.*⁵³ The top electrode is evaporated on the SAM in the pore. Both electrodes are contacted with microprobes.

With this device electron conductivity through alkanethiol SAMs was observed to be temperature-independent (300 K to 80 K), indicating that tunneling is the dominant mechanism.⁵⁴ The direct tunneling current in low bias regimes can be described with equation 1.

$$J \propto \frac{1}{d} \exp(-\beta_0 d) \quad (1)$$

In equation 1 d is the barrier width (thickness of SAM) and β_0 is a bias independent decay coefficient given by equation 2.

$$\beta_0 = \frac{2(2m)^{1/2}}{\hbar} \alpha (\Phi_B)^{1/2} \quad (2)$$

In equation 2 m is the electron mass, Φ_B the barrier height and α a unitless adjustable parameter used when calculating tunneling through molecules.⁵⁵ This through bond tunneling makes inelastic electron spectroscopy possible, which can be used to identify chemical bonds in molecules.⁵⁶

The tunneling current depends exponentially on the thickness of the alkanethiol SAM, with a decay coefficient β .⁵⁷ For the C₈SH, C₁₂SH and C₁₆SH alkanethiols a barrier height Φ_B of 1.39 ± 0.01 eV was determined from the bias dependence of β , as well as a zero-field decay coefficient β_0 of 0.79 ± 0.01 Å⁻¹. Petta *et al.* used a similar setup to measure octanedithiol (HSC₈SH) and hexanedithiol (HSC₆SH) junctions.⁵⁸ Resistances per HSC₈SH molecule are between 30 MΩ and 6 GΩ, HSC₆SH has a resistance of between 11 MΩ and 2 GΩ.

For facile electronic measurements of SAMs a junction with a small surface area should be constructed, of which the top and bottom electrode can be contacted using a macroscale device. The contact points should be outside the junction area because contacting with a macroscale probe would directly damage the SAM. Austin and Chou reported a monolayer diode fabricated using nano-imprint lithography (NIL) for conductivity measurements of SAMs.⁵⁹ They created diodes of 1600 nm². A schematic drawing of their device is shown in Figure 2.10. The advantage of this

method is that by using NIL, standard etching techniques and by simply turning the device 90 degrees for the second deposition very small electrodes can be made, which can probe areas of only a few thousand molecules. However the yield of working devices when using an octadecanethiol ($C_{18}SH$) SAM was only 5 %. The other 95 % of the devices had short circuits between the two electrodes. When using octanethiol (C_8SH) SAMs, which are thinner and less well-packed, no resistance originating from the SAM could be measured. A chip with 40 samples with junction sizes of 200×200 nm down to 40×40 nm was investigated using a semiconductor analyzer. From I/V curves (Figure 2.11) Austin and Chou calculated a resistance per $C_{18}SH$ molecule of 1800 ± 400 M Ω .

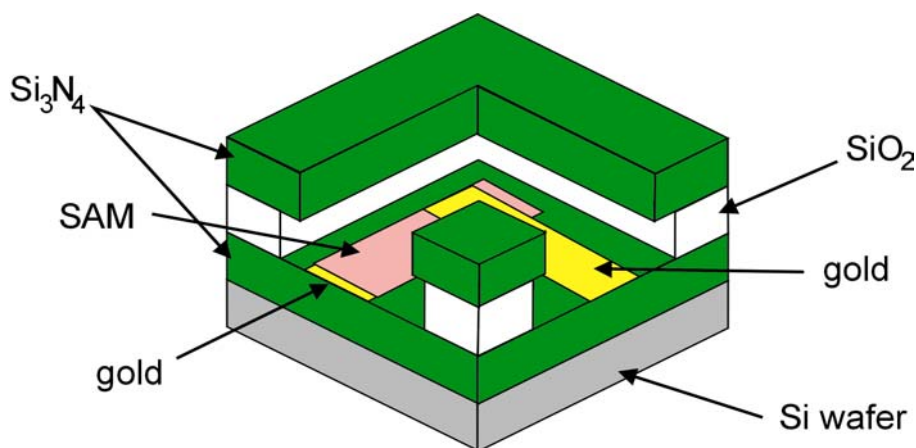


Figure 2.10 Schematic representation of the device used for measuring I/V curves of SAMs by Austin and Chou.⁵⁹

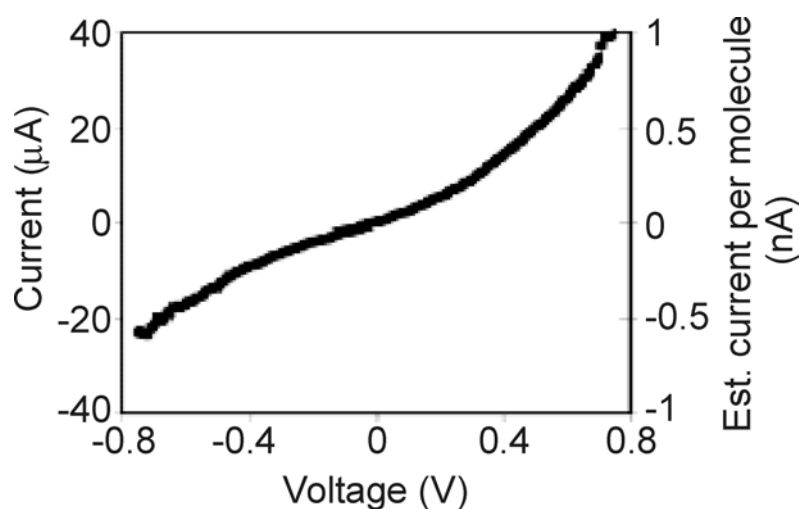


Figure 2.11 Typical I/V characteristic of a $C_{18}SH$ SAM measured in the device shown in Figure 2.10.⁵⁹

Samples usually shorted after 30 to 50 cycles or when more than 1 V was applied. The low resistance per molecule compared to previously reported results, together with the instability of the devices requires more detailed investigation in order to confirm if the measured resistance values are correct.^{60,61}

In a comparative study, Reed *et al.*⁶² measured electronic transport through alkanethiol SAMs of different lengths in three different ways *viz.* by Conducting Probe AFM (CP-AFM) (Section 2.3.3), in a monolithic mesa device (Figure 2.12, a junction with micrometer lateral dimensions constructed via optical lithography on a silicon wafer), and in nanopores (Figure 2.9).

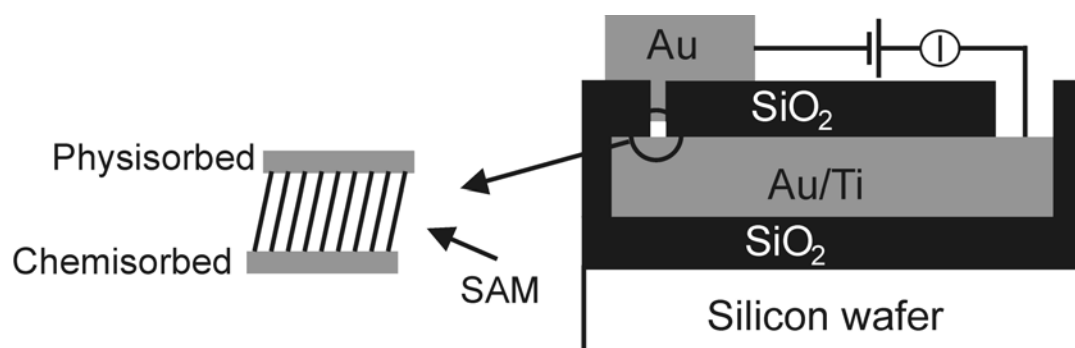


Figure 2.12 Monolithic mesa device used by Reed *et al.* (ref. 62).

Reed *et al.* concluded that CP-AFM was not suitable for electronic transport measurements because of the deformation of the SAM by the tip, especially when different loading forces are used. For this reason it was difficult to conclude whether a correct measurement was performed. Also, the effect of water and other adsorbates is not fully understood. The monolithic mesa (Figure 2.12), with a junction area of $960 \pm 60 \text{ nm}^2$, made it possible to construct many devices on one chip, which were characterized by standard solid state or IC device methods. A large variation of the current density was measured, whereas temperature dependent measurements were however not possible. The yield of working devices without short circuits was only 0.5 %, which is a factor ten lower than that for the nanopores. Probably this has to do with the larger junction size making the statistical chance of pinholes being present in the SAM higher. Reed *et al.* concluded that the nanopore was the only device useful for $I(V,T)$ measurements. The junction diameter of the nanopore (Figure 2.9) was on average only around 50 nm. The nanopore also made temperature dependent measurements possible. These are very important in determining the charge transport

constants and mechanism, because tunneling is temperature independent while ohmic current transport is temperature dependent.

2.3.2 Non-permanent devices

Because top electrode deposition is often a limiting step for device fabrication, alternatives were developed that did not rely on gas phase evaporation of metal on a SAM.

A very elegant way to measure a small area of SAM, circumventing the top electrode deposition step and at the same time allowing simple electronic measurements, is to press two macroscale objects together thus sandwiching a SAM. Kushmerick *et al.*⁶³ measured I/V curves from a so-called cross-wire junction⁶⁴ in which two gold wires of 10 μm diameter, one coated with a SAM, were contacted (Figure 2.13). The wires were brought in contact by deflecting one wire in a magnetic field with the Lorentz force that is generated by a small (< 5 mA) dc current. This method allows the contacting of two electrodes without damaging or deforming the SAM.

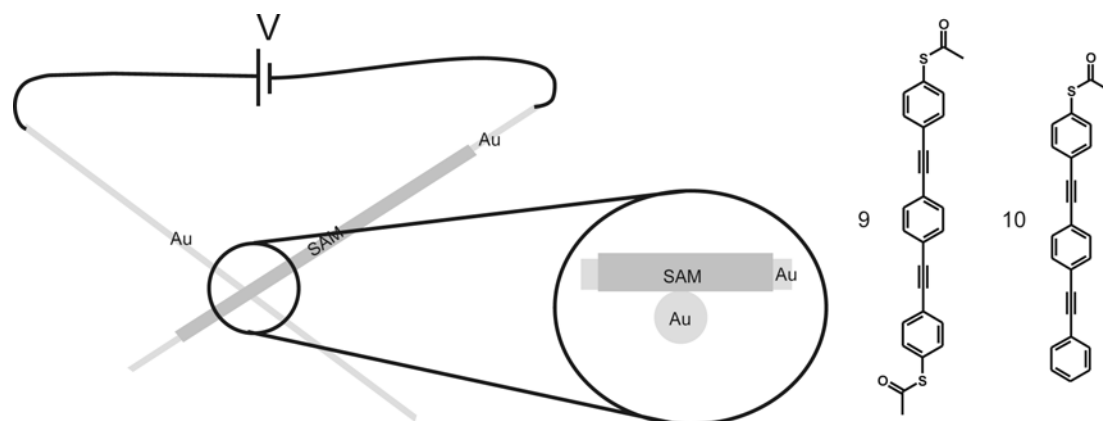


Figure 2.13 Cross-wire junction used by Kushmerick *et al.*⁶³ Two thin wires, one coated with a SAM, were pressed together and the current was measured.

Kushmerick *et al.* compared a symmetrical junction of 1,4-di(phenylethynyl-4'-thioacetyl)benzene (**9**) and an asymmetrical junction of 1-(phenylethynyl-4'-thioacetyl)-4-(phenylethynyl)benzene (**10**). The symmetric molecule acted as a molecular wire whereas the asymmetric junction (in which one wire was only physically connected to a phenyl group) acted as a diode.

From I/V curves through the isonitrile-terminated molecular wire **11** (Figure 2.14 C) in a crosswire junction integer-scaling factors from 1 to 1119 could be determined.⁶⁵ These scaling factors are a measure for the number of molecules through which the current was flowing. Dividing an I/V curve through one of these factors yielded I/V curves corresponding to a single molecule junction (Figure 2.14 B).

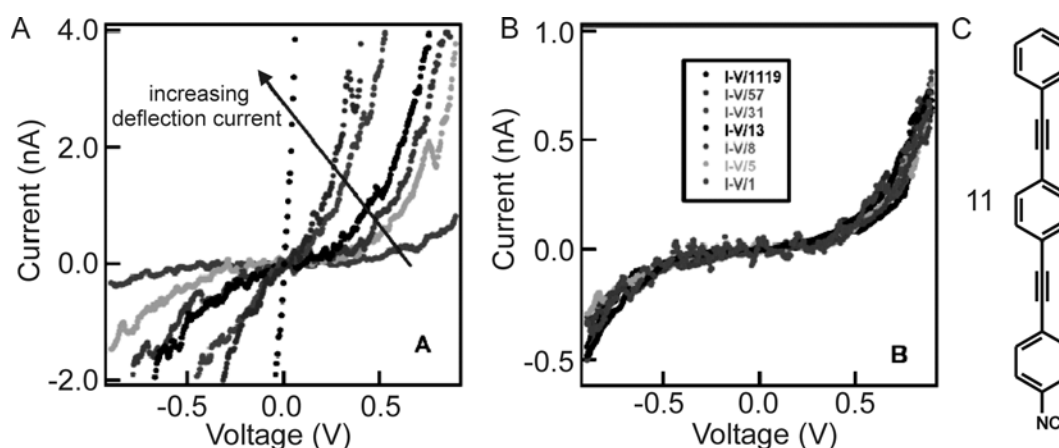


Figure 2.14 (A) I/V curves using a cross-wire junction with isonitrile-oligo(phenylene)-ethynylene molecules. (B) I/V curves divided by integer numbers. (C) 1-(Phenylethynyl-4'-isonitrile)-4-(phenylethynyl)benzene (**11**) (adapted from ref. 65).

Kushmerick *et al.* concluded that there was no lateral electronic coupling along the molecular backbone of the molecules and that they can be seen as individual channels through which electrons can flow (*viz.* in a parallel geometry). The I/V characteristics are weakly asymmetric which is attributed to the fact that on one side the electrode is chemically bound to the gold *via* an isonitrile group while the connection with the other electrode is purely physical *via* the phenyl group. This shows the importance of chemical contact between molecules and electrodes. The cross-wire system was also used to compare the difference in charge transport between a C₁₂ alkanedithiolate, an oligo (phenylene-ethynylene) dithiolate and an oligo (phenylene-vinylene) dithiolate.⁶⁶ Relative values of the junction conductances measured at 0.5 V show that oligo (phenylene-ethynylene) conducts 15 times better than the C₁₂ thiolate. The oligo (phenylene-vinylene) conducts even 46 times better.

Another non-permanent device used for measuring the resistance of molecules uses mercury as the top electrode. Mercury drop junctions for measuring the

electronic properties of SAMs were reported by Whitesides *et al.*⁶⁷, Liu and Yu⁶⁸ and Madja *et al.*⁶⁹ In such a device mercury is coated with a SAM and acts as the top electrode in a metal-SAM-SAM-mercury junction (see Figure 2.15). The top mercury electrode, coated with a SAM does, not diffuse through the other SAM to the SAM-metal interface and makes perfect conformal contact because of its liquid state. When there is no SAM at the mercury electrode, diffusion of the mercury to the bottom electrode takes place.⁷⁰ The bottom electrode consisted of a silver-supported SAM. A difference between these and other devices is that in this system two SAMs are stacked in series between the electrodes.

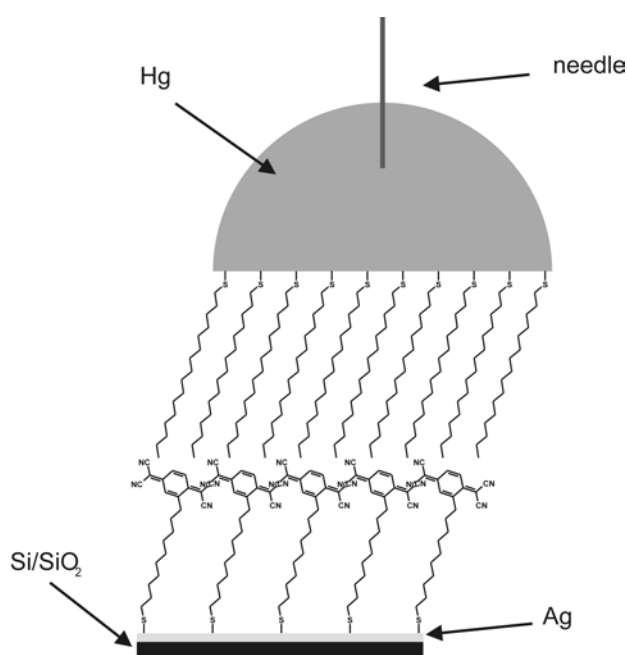


Figure 2.15 Mercury drop junction between a hexadecanethiolate SAM assembled on a mercury drop and a $(TCNQC_{10}S)_2$ SAM assembled on a Ag substrate.

A system in which both electrodes are made from mercury with a junction area of 1.5 mm^2 was used to measure the conductivity of two SAMs in series.⁶⁷ For a junction thickness of 2.9 nm ($C_{10}SH$) to junction thickness 8.9 nm ($C_{33}SH$) the conductivity is $6 \pm 2 \times 10^{-15} \Omega^{-1} \text{ cm}^{-1}$. If electron tunneling would be the charge transport mechanism the resistance would increase exponentially with a factor β for thicker layers. Electron tunneling between the electrodes, as can occur in shorter junction lengths, cannot take place due to the large thickness of these double SAM junctions.⁷¹

Whitesides *et al.* also measured molecular rectification in a mercury drop device using a tetracyanoquinidomethane (TCNQ) terminated dialkyldisulfide (**12**) assembled on a silver electrode.⁷² The mercury drop electrode was coated with a hexadecanethiolate (C₁₆SH) SAM. The ratio of the conductivity in the forward bias to the conductivity in the reverse bias was 9 ± 2 , as calculated from values measured using positive and negative biases at 1 V (Figure 2.16). The current densities for junctions consisting of **12** and alkythiolates of different chain lengths are shown in Figure 2.16.

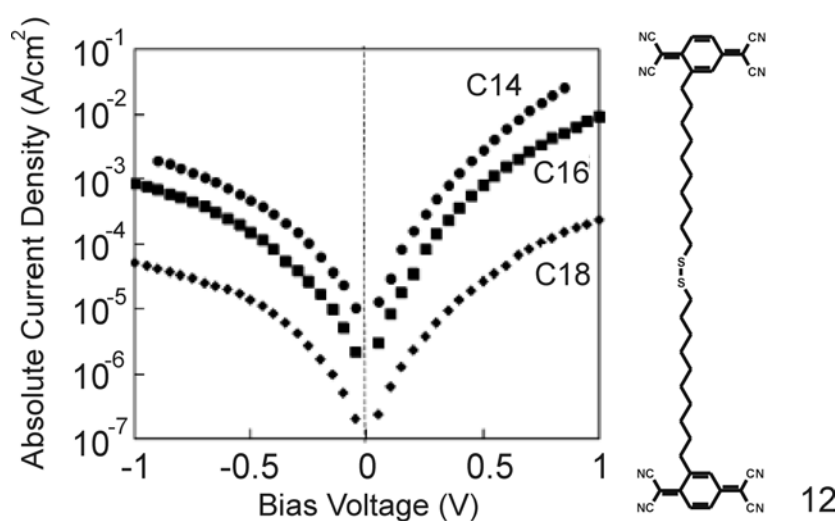


Figure 2.16 Current densities of $J_{Ag-12//Cn-Hg}$ junctions. Negative V values indicate electron flow from the mercury drop to the silver electrode (from ref. 72).

Breakdown voltages (BDVs) of junctions using different solid metal electrodes and alkanethiolate SAMs using the same mercury-drop method were determined.⁷³ The BDVs for C₁₆SH SAMs on Cu, Ag and Hg were twice as high as those for C₁₆SH SAMs on Au. They were dependent on the density (packing and tilt-angle) of the SAM and on the length of the thiols used. Current densities through two SAMs (Hg-SAM-SAM-Ag) were 2×10^{-10} A cm⁻² for C₁₆SH, 1×10^{-6} A cm⁻² for C₈SH, 3×10^{-6} A cm⁻² for oligophenylethiols and 7×10^{-4} A cm⁻² for phenylthiol.⁷⁴

Sek *et al.* used the mercury drop system to measure current through thin mono- and dithiol monolayers.⁷⁵ Their data showed that the conductivity of fully bonded Ag- α,ω -alkanedithiol SAM-Hg junctions is at least 8-95 fold larger than the conductivity of Ag- α,ω -alkanedithiol SAM-Hg junctions only chemically bonded to the Ag electrode and also larger than the conductivity of monothiol SAMs. The

mercury thiolate formation can be prevented if the polarization of the Hg-drop is substantially more negative than the potential of the electrochemical Hg-S formation. The tunneling decay coefficient β is smaller ($0.82 \pm 0.01/\text{CH}_2$) for the fully bound system than for the singly bound dithiol ($1.05 \pm 0.01/\text{CH}_2$) or monothiol ($1.02 \pm 0.06/\text{CH}_2$), indicating a lower energy barrier for long range electron tunneling. These results clearly show the effect of chemical binding between molecule and electrode on the resistance of a junction.

Compared to solid electrodes a mercury drop junction has as advantages that the SAM does not display any grain boundaries, that the contact between electrodes is optimal and that defects in the SAMs as a result of microscopic roughness are minimized. Disadvantages are that temperature-dependent measurements cannot be performed and that single molecule experiments cannot be done because there is a limit for the minimum size of the mercury drop.

2.3.3 Scanning probe techniques

Another kind of non-permanent junction can be made using scanning probe methods. The advantage of using scanning probe techniques, like scanning tunneling microscopy (STM) and conducting probe atomic force microscopy (CP-AFM), is that readily available instruments can be used for the analysis of very small SAM junctions.

As mentioned before in this chapter, CP-AFM^{38,76} is also used for the analysis of thiolate SAMs. The use of CP-AFM in single molecule measurements will be discussed in Chapter 2.4.2. The junction area in CP-AFM measurements on SAMs depends on the shape of the coated tip, but is usually in the range of 20 nm^2 , which means that around 100 molecules (in an alkanethiolate SAM) are analyzed in parallel at the same time. CP-AFM has as advantage over STM that it physically contacts the sample surface during measurement. A bias is applied between conducting tip and substrate, whereas the feedback control uses the force between tip and substrate, as in normal AFM. Because contact between tip and substrate is guaranteed a second measurement can be performed in parallel, *viz.* the electronic analysis. This means that in one analysis both the corresponding height and current images can be obtained. Figure 2.17 shows a schematic picture of a CP-AFM measurement of a SAM.

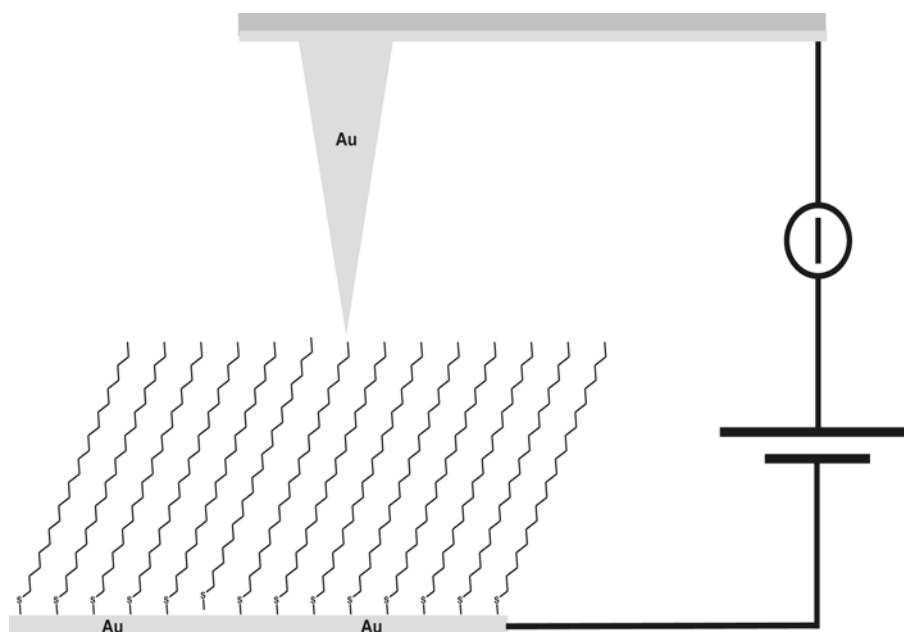


Figure 2.17 CP-AFM setup, scanning a self-assembled monolayer of thiols on gold.

Wold and Frisbie used CP-AFM to investigate the current-voltage behavior of alkanethiolate SAMs of different chain lengths.⁷⁷ The current increases enormously with decreasing chain-length. The logarithm of the resistance correlates linearly with the chain length from C₆ to C₁₀ chains. Densities vary from $2 \times 10^7 \Omega$ for C₆ to $> 10^{10} \Omega$ for a C₁₀ SAM. It was also found that the load applied to the tip influenced the conductance because the tip is pressed into the SAM. These observations can be explained taking into account that tunneling is the main electron transport mechanism.

CP-AFM was also used for a comparison of the electric resistance between monothiol and isonitrile SAMs as a function of chain length.⁷⁸ The logarithm of the resistance of isonitriles on gold vs. the number of methylene groups gave a straight line (Figure 2.18). The contact resistance R_0 , defined as the resistance with 0 methylene groups, was 18500Ω in the case of the thiols and 16700Ω in the case of the isonitriles.

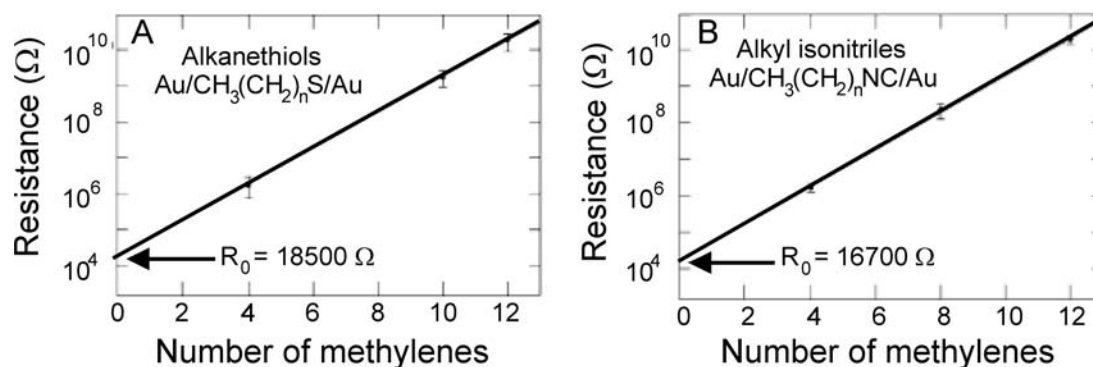
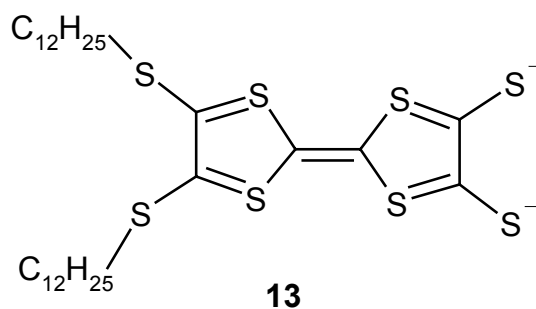


Figure 2.18 Resistance of (A) alkanethiols and (B) alkyl isonitriles with different chain lengths (taken from ref 78).

Frisbie *et al.*⁷⁹ also observed that the contact resistance of Au/molecule/Au junctions was smaller than that of Ag/molecule/Ag junctions. The same experiments were performed using saturated and unsaturated molecular junctions. It was found that the resistance of alkanethiols is higher, especially for longer molecules, compared to oligophenylene SAMs. Frisbie *et al.* also investigated length-dependent transport in molecular junctions of mono- and dithiols on gold, platinum and silver substrates using gold, platinum and silver coated AFM tips.⁸⁰ The contact resistance R_0 decreases with increasing electrode work function and increased applied bias. Chemisorbed contacts (S-metal bonds) have much higher transmission currents than physisorbed contacts (CH₃-metal). However, when dithiols or monothiols were used no difference in the tunneling decay coefficient β was found. Small differences in the Fermi level hardly influenced the tunneling efficiency.⁸⁰

Lindsay and coworkers used CP-AFM to analyze a SAM of 2,3-bis(dodecylthio)-6,7-bis(thiolate)-tetrathiofulvalene (**13**) (Chart 2.19) on Au(111).⁸¹ This molecule has a resistance of 25.7 ± 0.3 GΩ, which makes it a conductor like carotenoids or oligophenylenes. This high conductivity, despite the long alkyl chains, is likely due to the bad packing and tilting of the chains so that only the TTF unit is probed with the tip. For comparison, a 1-octanethiol SAM, which has more or less the same length as the tetrathiafulvalene-unit, has a resistance of $\gg 100$ GΩ.

**Chart 2.19**

The group of Lindsay investigated the electrode-molecule contact by CP-AFM.⁸² They compared I/V curves of monothiol with those of dithiol SAMs. The dithiol SAMs showed three different kinds of I/V curves. The first is observed when the SAM is contacted with the tip for the first time and resembles a monothiol curve, and the current is very sensitive to the contact force. The contact between the SAM and the tip is purely physical. When the tip comes in chemical contact with the thiol terminated SAM, I/V curves that are independent of the load are observed. They show a low current part which has an average current of 4.6 ± 0.7 nA at ± 3 V and a high current part which has an average current of 46 ± 6 nA at ± 3 V. The load independence of the current is a very striking feature of measuring in a chemical contact regime.

Measuring the electronic properties of SAMs by STM has the advantage that the SAM is not physically deformed during the measurement. Because STM relies on tunneling current, which decreases exponentially with distance, STM measures either single or a very small number of molecules. A general feature of STM is the unknown distance between the tip and the surface. It is possible to position the tip in such a way that it barely touches the monolayer surface. When an STM tip is brought closer to a surface, a kink point is observed in the current vs. distance plot (Figure 2.20). At this point the tip is in contact with the SAM surface while exerting minimal force.²⁹

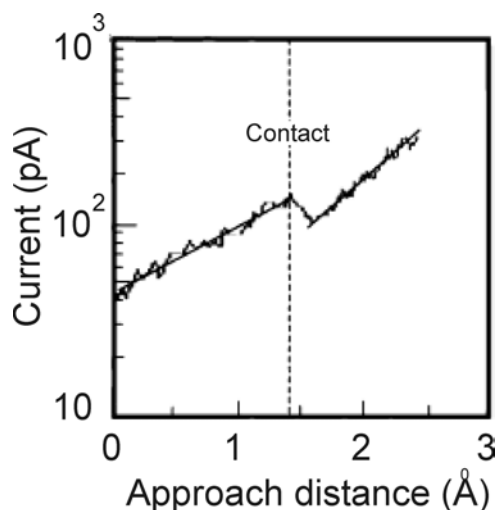


Figure 2.20 I/d curve of a contacting STM tip with a SAM surface (from ref. 29).

Labonté *et al.* performed scanning tunneling spectroscopy (STS) under ultra high vacuum (UHV) conditions.⁸³ They characterized dodecanethiol ($C_{12}SH$), octadecanethiol ($C_{18}SH$) and resorcinarene C_{10} tetrasulfide ($RC_{10}TS$) SAMs on Au(111). One of the most important conclusions of this work was that the tetrasulfide, which has a thickness of 2.0 nm, displayed a higher resistance than $C_{18}SH$. The electrical insulation of $RC_{10}TS$ was comparable to that of a 1.5 nm thick SiO_2 layer on silicon. According to the authors the main reason for this behavior is the mismatch in the orbital overlap of gold and sulfides. This corresponds with XPS data which are almost the same for the bound and the unbound S_{2p} peaks (for thiols and disulfides the shift is 1 eV). Allara and Weiss *et al.* measured for mixed SAMs of C_{10} and C_{12} alkylthiols on gold that the conductivity of the C_{10} thiol was ten times higher than that of the C_{12} thiol.⁸⁴ These measurements were performed using very low currents so that the tip was not in contact with the SAM. The resistance of the system is composed of the tip-SAM gap resistance and the resistance of the SAM.

Dhirani *et al.* measured the rectifying behavior of 1-(phenylethynyl)-4-(phenylethynyl-4'-thiol)benzene (**14**) on Au(111) and Ag(111) using STM.⁸⁵ They found that decanethiol, benzenethiol and the shorter 4-(phenylethynyl)-benzenethiol (**15**) did not show this type of behavior, in other words they did not yield symmetrical I/V curves. Dhirani *et al.* suggested that the rectification of **14** arises from the length of conjugation of the molecular framework and an increase of donor character of the sulfur atom upon adsorption to the metal.

Ashwell *et al.* used STM for the investigation of the rectifying behavior of the donor-acceptor complex $Z\text{-}\beta\text{-[N-(}\omega\text{-acetylthioalkyl-4-quinolinium)]-}\alpha\text{-cyano-4-styryldicyanomethanide (16)}$ (Chart 2.21).⁸⁶ The electrical asymmetry arises from the non-planar donor-(π -bridge)-acceptor moiety. Protonation of **16** disrupts the electron accepting properties of the $\text{C}(\text{CN})_2$ group, resulting in symmetric I/V curves, confirming that the donor-acceptor combination caused the asymmetry. Because the STM tip was not in contact with the molecule contact resistance could not be the reason for the rectification. The use of STM to measure single functional molecules in an inert matrix will be discussed more extensively in Chapter 2.4.1.

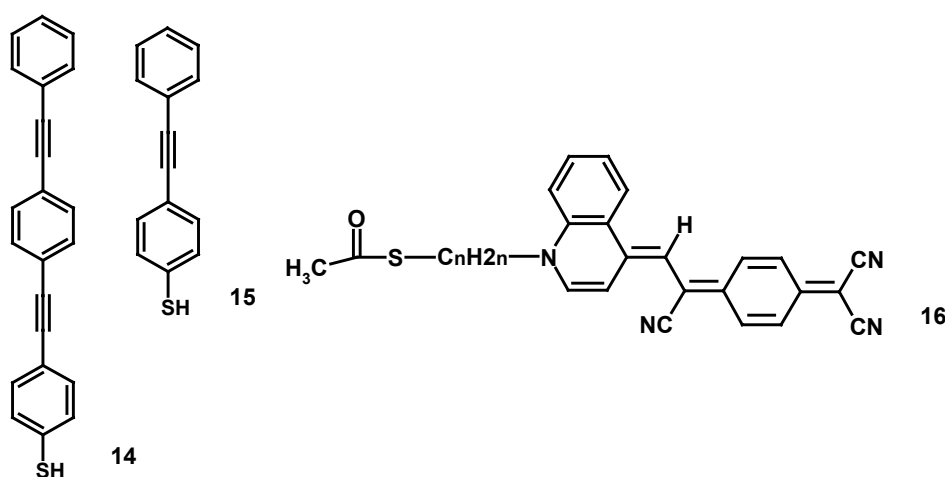


Chart 2.21

Cahen, Lindsay and Frisbie *et al.* published an excellent review in which they compared low-bias room temperature currents through molecules, measured using different techniques.⁸⁷ They addressed the important question whether it is possible to compare results measured using different configurations. They concluded that current/molecule values measured at biases of 0.2 and 0.5 V corresponded reasonably well when measured using CP-AFM, pico-STM, mercury-drop electrodes or nanopores. Measurements with CP-AFM in liquid-cells yielded much lower values, which was ascribed to contact effects. The reason for this extra contact barrier, which might be solvent shells around the probes or reduction of contact areas, should be investigated further.

It has become clear that for electronic measurements of SAMs several factors are very important. First, the contact of the metal electrodes with the organic

molecules. The contact resistance depends very much on the electrode material used. Gold is not the most ideal material for contacting thiol molecules in terms of contact resistance. Compared to for example the silver/molecule junction, the conductivity through a gold/molecule junction is significantly lower. The resistance of a molecule/metal junction is also lower if the molecule is chemically bound to the electrode, instead of just in physical contact. As expected, the size of the junction is very important. Because of irregularities in solid electrode surfaces and grain boundaries in SAMs smaller junction areas yield statistically more working devices. For electronic analysis of SAMs it is furthermore important that temperature-dependent measurements can be done in order to determine whether the electron transport regime is tunneling (which is temperature independent) or through bond (which is temperature dependent).

2.4 Single molecule electronic measurements

Single molecule electronic measurements are of fundamental interest. In this section several methods to electronically probe single molecules are described. One of the most important considerations is that the contact between the molecules and the probe is crucial. This means that there should not only be physical/chemical contact between molecule and electrode, but there should also be an efficient orbital overlap to minimize contact resistance (see Figure 2.2). Different techniques often yield different results, probably caused by the differences in contacting the molecules. Although the sulfur-gold bond is a good tool for wiring molecules for electrical measurements the overlap between the lowest unoccupied molecular orbital (LUMO) of the molecule and the Fermi level of the metal still displays a rather large orbital mismatch.²³ The search for the “best” molecule metal contact is therefore still ongoing.

2.4.1 Conductivity measurements of single molecules using STM

Because of its relative ease of use and its availability STM is one of the most important tools in nanotechnology and in electronic measurements of single molecules. Because an STM tip is not in physical contact with the sample and relies on tunneling current high-resolution images can be obtained.^{88,89} SAMs with chain

lengths up to $\sim C_{12}$ can be imaged. Longer alkanethiolate SAMs have a resistance that is too large to get the STM tip in a tunneling regime, which makes it almost impossible to obtain high-resolution images.

Allara, Tour and Weiss *et al.*⁹⁰ investigated the assembly of highly conjugated oligo-phenyl-ethynylene molecules on gold surfaces. Insertion of the molecules in a non-conductive alkanethiolate matrix led to single assembled, conjugated molecules, whereas co-desorption led to a monolayer with structural disorder. STM could be used to identify single conjugated molecules in a SAM of alkylthiols.

Lately, STM has been used in the analysis of single molecule electronic properties. One method of measuring is the use of gold or silver colloids that are attached to thiol groups sticking out of a mixed SAM.⁹¹ Reactive thiol surfaces that would otherwise stick to the STM tip can be probed in this way and because the measurement is done *via* an attached “electrode” also the contact resistance is taken into account.

An STM-related method to measure single molecule resistance was reported by Xu and Tao.^{92,93} The difference with other STM experiments is that these measurements were performed in solution, and that an Au-coated STM tip was used. The STM tip was repeatedly brought in and out of contact with a gold substrate in a solution of dithiols or 4,4'-bipyridine. Every time the tip comes out of contact with the surface a molecule can assemble between the moving tip and the surface, so that the resistance can be measured. Resistances of the molecules are $10.5 \pm 0.5 \text{ M}\Omega$ for hexanedithiol, $51 \pm 5 \text{ M}\Omega$ for octanedithiol, $630 \pm 50 \text{ M}\Omega$ for decanedithiol and $1.3 \pm 0.1 \text{ M}\Omega$ for 4,4'-bipyridine. The tunneling decay constant for alkanedithiols (β_N) is $1.0 \pm 0.1/\text{CH}_2$.

2.4.2 Conductivity measurements of single molecules using conducting probe AFM

One of the easiest methods to visualize single molecule electronics is to measure the conductivity of a dithiol using a Au-coated conductive AFM-tip. The group of Lindsay used gold colloids, which are attached to thiol groups of the SAM. The colloids are attached from solution, after which the sample is measured. CP-AFM can simultaneously measure a height and a current difference.^{94,95,96} In Figure 2.22 a schematic drawing of a Au-coated AFM-tip that scans a SAM with an inserted

carotene-dithiol molecule (**17**) is shown. The gold colloid is attached via the thiol group that sticks out of the surface of the SAM. The colloid prevents sticking of thiol groups to the probe, ensuring that the AFM-tip remains clean of contaminants. The carotenoid is significantly more conductive than 1,4-di(phenylethynyl-4'-thiol)benzene (**3**), which is often used in molecular electronics.

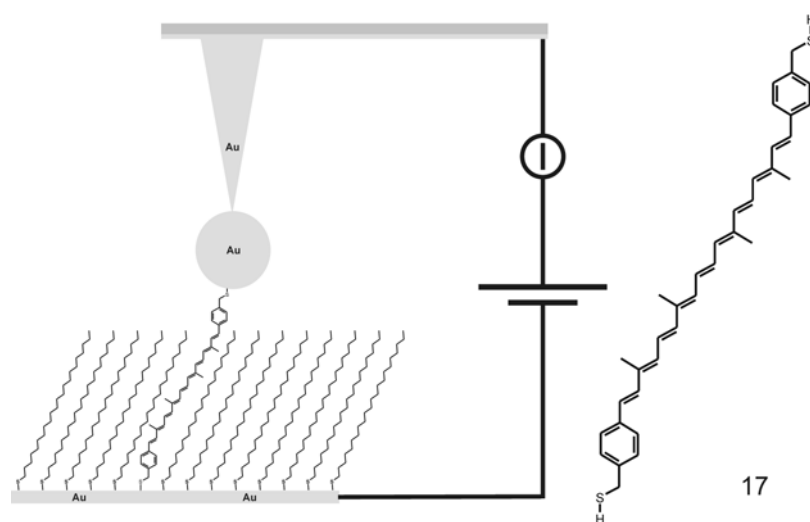


Figure 2.22 Measurement of the electronic properties of a single carotenedithiol molecule as performed by the Lindsay group, using a gold colloid attached to a single molecule (ref. 96).

Colloids attached to dithiols diluted in a monothiol SAM were measured with CP-AFM. The I/V curves were integer multiples of the same curve, i.e. the I/V curve of a single molecule. This made it possible to calculate how many carotenoids were bound to the colloid. The resistance of single inserted octanedithiol molecules in a non-conducting octanethiol SAM was also measured. Figure 2.23 B shows five different I/V curves. If the current values are divided by integer factors (from 1 till 5) all curves overlap (Figure 2.23 C). The octanedithiol molecules (HSC_8SH) have a resistance of $900 \pm 50 \text{ M}\Omega$ in the ohmic region (between -0.1 and $+0.1 \text{ V}$). When this is compared with measurements of alkyl-monothiols (through a non-bonded contact) where the resistances are at least $10^4 \text{ G}\Omega$, this shows the importance of chemical contact in electronic measurements. This experiment also clearly shows that tunneling through non-conducting SAMs occurs through the molecules.

The processes of insertion and colloid attachment could be visualized by STM. The native SAM displayed etch-pits and after insertion, brighter spots corresponding

to the conjugated inserted molecules were visible on defect sites. After the attachment of the colloid also a clear height difference⁹⁷ could be seen.

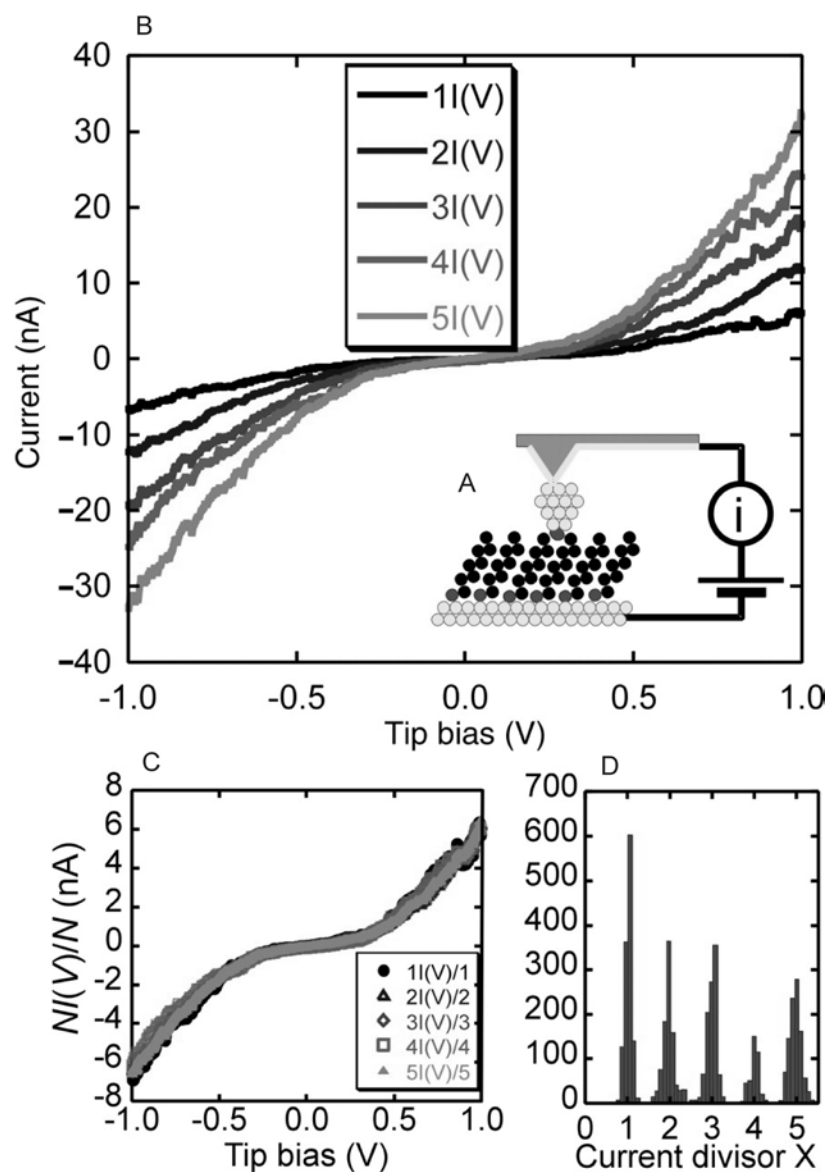


Figure 2.23 (A) Cartoon of the CP-AFM measurement through octanedithiol. (B) I/V curves. (C) I/V curves divided by integer values. (D) Number of molecules bound to one colloid (taken from ref. 95).

2.4.3 Conductivity measurements using other nanoscale molecular junctions

It is conceivable that in probing single molecules with STM or CP-AFM the surrounding SAM matrix interferes with the measurement. It is also not always easy

to determine whether single molecules are measured or instead a small group of molecules. For STM there is always the concern that the tip is not in physical contact with the molecules, whereas for CP-AFM the influence of the applied load, which can compress the sample, plays a role. For this reason other techniques have been developed for single molecule measurements. These techniques rely on the fabrication of a nanoscale junction between two electrodes in which a single di-substituted molecule can be assembled.

Park *et al.*⁹⁸ used a two-electrode system obtained *via* electromigration to make a single atom transistor. The metallic electrodes were made by ramping large voltages over thin gold wires (less than 200 nm in width, 10-15 nm thick) at cryogenic temperatures. During ramping the current was constantly monitored until at a certain point only a tunneling current was recorded which indicates that the wire had broken.⁹⁹ At this point a gap of typically 1-2 nm is formed. When both parts of the metallic wire are coated with a SAM, molecules can bridge this gap. The two parts of the metal wire, which was assembled on a silicon wafer with a 30 nm thick SiO₂ layer, form a drain and a source while the doped silicon wafer can act as the gate (see Figure 2.24). Electronic properties of the molecules can be measured by acquiring I/V curves while the gate voltage is varied. Measurements on [Co(tpy-(CH₂)₅-SH)₂] in the gap at a temperature of less than 100 mK yielded (in 10 % of the cases) I/V curves which show a strongly suppressed current up to a threshold value that depends on the gate voltage V_g, caused by the alkyl chains. After this the current increases in steps. The threshold voltage for conduction could be altered by varying the gate voltage V_g. The steps were present due to the well-defined charge states of the single Co atom in the molecule. The fine structure of the current steps near the voltage thresholds indicates that a single electron transistor has been made. Liang *et al.*¹⁰⁰ reported a single-molecule transistor using the divanadium complex [N,N',N''-trimethyl-1,4,7-triazacyclononane)₂ V₂(CN)₄-(μ-C₄N₄)].

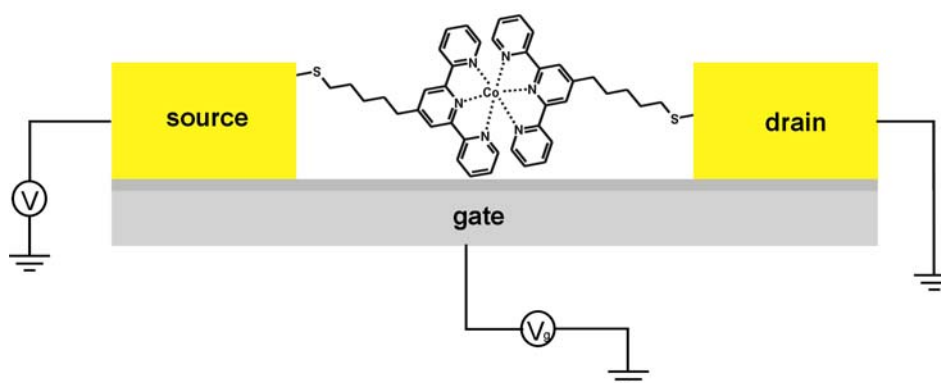


Figure 2.24 Single atom transistor (by Park *et al.*⁹⁸) formed by electromigration of SAM-covered gold wires on a Si/SiO₂ wafer.

Allara *et al.* reported the thermally activated conduction of dithiolates in molecular junctions¹⁰¹ formed *via* this electromigration method of gold wires at 13 K. A single molecule was bound between two nano-electrodes *via* two thiolate-gold bonds. All I/V curves of the asymmetric 1-nitro-2,5-di(phenylethynyl-4'-mercapto)benzene show asymmetric behavior at all temperatures. However, it was difficult to determine whether the junction contained one or more molecules.

Break junctions can also be made by mechanically breaking a thin gold wire instead of using the electromigration technique.¹⁰² The thin gold wire is mechanically broken while the current is measured to monitor the gap formation. Between the two electrodes of the break junction a single molecule can be assembled. In Figure 2.25 a schematic picture of such a break junction is shown. Figure 2.25 A shows the gold wire of the break junction, which in Figure 2.25 B is coated with a SAM (in this case a SAM of p-dithiophenyl). After mechanical breaking the wire was immersed in a solution (Figure 2.25 C), the SAM covers the two opposite electrodes. After the solvent has evaporated, the two electrodes are moved towards each other until a current is measured.

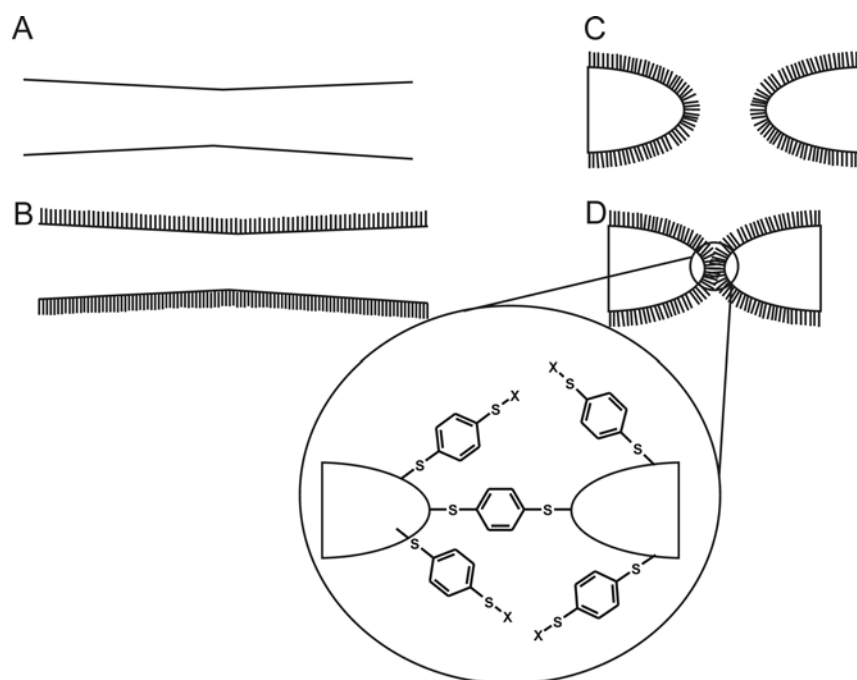


Figure 2.25 Mechanically controlled break junction as published by Reed *et al.*¹⁰² (A) Thin gold wire. (B) Wire coated with a SAM. (C) Coated wire after breaking. (D) Junction formation

Von Löhneysen *et al.* used the mechanically controlled break junction technique to measure a set of three different dithiols (**18-20**) (Figure 2.26).^{103,104,105} The data strongly suggest that they were measuring single molecules. Asymmetric molecules like [1,4-bis((2'-*para*-mercaptophenyl)-ethynyl)-2-acetyl-amino-5-nitrobenzene] (**19**) were compared to symmetric molecules like [9,10-bis((2'-*para*-mercaptophenyl)-ethynyl)-anthracene] (**18**). The *I/V* curves and derived *dI/dU* curves are asymmetrical for **19** and nearly symmetrical for **18**. The third molecule, bis-(triphenylphosphine)-bis-*C*-(4-ethynyl)-phenylthiol-platinum (**20**) contains a Pt atom which dissects the conjugated system. The *I/V* curves of **20** show a larger non-conductive gap.

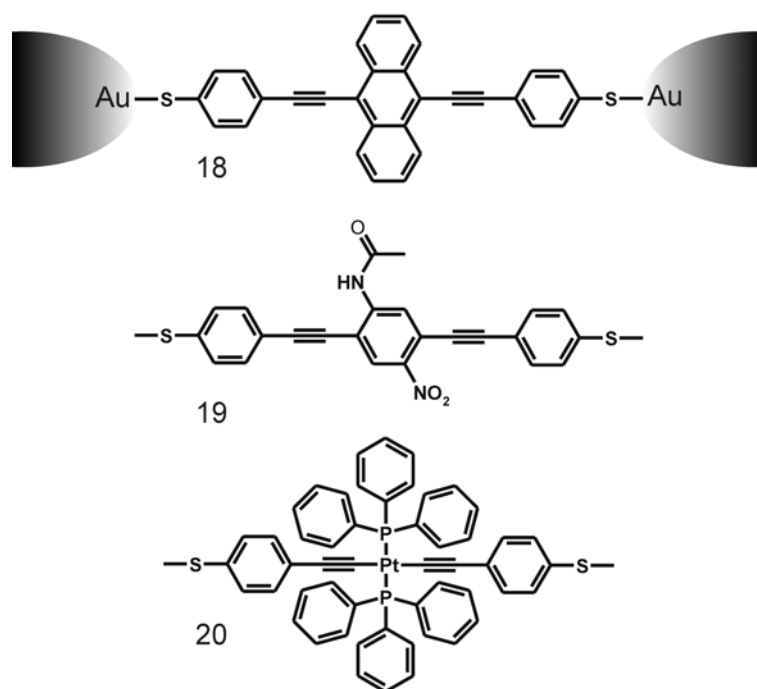


Figure 2.26 Break junction used by von Löhneysen et al. with three different molecules **18**, **19** and **20**.

2.5 Conclusion and outlook

Despite the difficulties in both incorporating molecules in electronic devices and finding the right molecules that function and that are stable enough to last for years molecular electronics will certainly be a very important part of future miniaturized electronics. The enormous number of papers published every year and the large number of researchers working on the subject are proofs of the trust scientists have in these new systems.

Considerable progress has been made in the construction of devices that can measure the electronic properties of SAMs and single molecules. After the molecular electronics hype, which led to numerous papers in high impact journals,¹⁰⁶ scientists are now realizing that much of the conclusions were premature. Several devices do not seem to qualify for molecular electronics¹⁰⁷ because the measured effects were not related to properties of the molecules used but of the device itself.

Now the focus in the field of molecular electronics is aimed at producing consistent results and to relate the properties of the devices to molecular properties. The combination of single molecule analyses and the measurements of SAMs in

devices can be a strong tool to develop the best molecules in the best devices necessary to be applied in the building of small electronic components with large storage capacities.

This thesis deals with surface fabrication and analysis required for making molecular electronic devices. SAMs are investigated for their macroscale electronic properties to test whether they can be used in molecular electronics. A considerable part of this thesis explores the formation of metal-molecule-metal structures and is focused on the fabrication of insulated top-electrodes on SAMs. Pulsed laser deposition is used as a mild technique for the deposition of these top-electrodes. Metal-containing single molecules were investigated to obtain more insight in the positioning, probing and manipulation of single, surface-bound, metal complexes using AFM.

2.6 References

- ¹ A. Ulman, *An Introduction to Ultrathin Organic Films*; Academic Press: Boston USA, **1991**.
- ² A. Ulman, *Chem. Rev.* **1996**, 96, 1533-1554.
- ³ F. Schreiber, *Prog. Surf. Sci.* **2000**, 65, 151-256.
- ⁴ A. Friggeri, F. C. J. M. van Veggel, D. N. Reinhoudt, *Chem. Eur. J.* **1999**, 5, 3595-3602.
- ⁵ A. Kumar, H. A. Biebuyck, N. L. Abbott, G. M. Whitesides, *J. Am. Chem. Soc.* **1992**, 114, 9188-9189.
- ⁶ M. Geissler, H. Schmid, A. Bietsch, B. Michel, E. Delamarche, *Langmuir* **2002**, 18, 2374-2377.
- ⁷ J. C. Love, D. B. Wolfe, M. L. Chabinyc, K. E. Paul, G. M. Whitesides, *J. Am. Chem. Soc.* **2002**, 124, 1576-1577.
- ⁸ M. Lahav, A. Vaskevich, I. Rubinstein, *Langmuir* **2004**, 20, 7365-7367.
- ⁹ M. T. McDermott, J.-B. D. Green, M. D. Porter, *Langmuir* **1997**, 13, 2504-2510.
- ¹⁰ G. B. Sigal, M. Mrksich, G. M. Whitesides, *J. Am. Chem. Soc.* **1998**, 120, 3464-3473.
- ¹¹ Y. Xia, G. M. Whitesides, *Angew. Chem. Int. Ed.* **1998**, 37, 550-575.
- ¹² G. M. Kim, B. J. Kim, E. S. ten Have, F. Segerink, N. F. van Hulst, J. Brugger, *J. Microsc.* **2003**, 209, 267-271.
- ¹³ R. G. Nuzzo, D. L. Allara, *J. Am. Chem. Soc.* **1983**, 105, 4481-4483.

- ¹⁴ A. Kühnle, S. Vollmer, T. R. Linderoth, G. Witte, C. Wöll, F. Besenbacher, *Langmuir* **2002**, 18, 5558-5565.
- ¹⁵ J. C. Love, D. B. Wolfe, R. Haash, M. L. Chabinye, K. E. Paul, G. M. Whitesides, R. G. Nuzzo, *J. Am. Chem. Soc.* **2003**, 125, 2597-2609.
- ¹⁶ J. Sagiv, *J. Am. Chem. Soc.* **1980**, 102, 92-98.
- ¹⁷ B. L. Kropman, D. H. A. Blank, H. Rogalla, *Langmuir* **2000**, 16, 1469-1472.
- ¹⁸ (a) D. L. Allara, R. G. Nuzzo, *Langmuir* **1985**, 1, 45-52; (b) H. Ogawa, T. Chihara, K. Taya, *J. Am. Chem. Soc.* **1985**, 107, 1365-1369.
- ¹⁹ A. B. Sieval, B. van den Hout, H. Zuilhof, E. J. R. Sudhölter, *Langmuir* **2001**, 17, 2172-2181.
- ²⁰ R. L. Cicero, M. R. Linford, C. E. D. Chidsey, *Langmuir* **2000**, 16, 5688-5695.
- ²¹ J. F. Dorsten, J. E. Maslar, P. W. Bohn, *Appl. Phys. Lett.* **1995**, 66, 1755-1757.
- ²² G. E. Moore, *Electronics* **1965**, 38, 114.
- ²³ J. M. Tour, *Acc. Chem. Res.* **2000**, 33, 791-804.
- ²⁴ A. Aviram, M. A. Ratner, *Chem. Phys. Lett.* **1974**, 29, 277.
- ²⁵ G. Binnig, H. Rohrer, C. Gerber, E. Weibel, *Phys. Rev. Lett.* **1982**, 49, 57-61.
- ²⁶ D. M. Eigler, E. K. Schweizer, *Nature* **1990**, 344, 524-526.
- ²⁷ G. E. Poirier, E. D. Pylant, *Science* **1996**, 272, 1145-1148.
- ²⁸ Y. Qian, G. Yang, J. Yu, T. A. Jung, G. Liu, *Langmuir* **2003**, 19, 6056-6065.
- ²⁹ G. Yang, G. Liu, *J. Phys. Chem. B* **2003**, 107, 8746-8759.
- ³⁰ K. Kobayashi, H. Yamada, T. Horiuchi, K. Matsushige, *Appl. Surf. Sci.* **1999**, 144-145, 435-438.
- ³¹ D. M. Adams, L. Brus, C. E. D. Chidsey, S. Creager, C. Creutz, C. R. Kagan, P. V. Kamat, M. Lieberman, S. Lindsay, R. A. Marcus, R. M. Metzger, M. E. Michel-Beyerle, J. R. Miller, M. D. Newton, D. R. Rolison, O. Sankey, K. S. Schanze, J. Yardley, X. Zhu, *J. Phys. Chem. B* **2003**, 107, 6668-6697.
- ³² X.-Y. Zhu, *J. Phys. Chem. B* **2004**, 108, 8778-8793.
- ³³ S. N. Yaliraki, A. E. Roitberg, C. Gonzalez, V. Mujica, M. A. Ratner, *J. Chem. Phys.* **1999**, 111, 6997-7002.
- ³⁴ M. W. Holman, R. Liu, D. M. Adams, *J. Am. Chem. Soc.* **2003**, 125, 12649-12654.
- ³⁵ R. M. Metzger, *Chem. Rev.* **2003**, 103, 3803-3834.
- ³⁶ R. L. Creery, *Chem. Mater.* **2004**, 16, 4477-4496.
- ³⁷ D. K. James, J. M. Tour, *Chem. Mater.* **2004**, 16, 4423-4435.

- ³⁸ D. J. Wold, C. D. Frisbie, *J. Am. Chem. Soc.* **2001**, 123, 5549-5556.
- ³⁹ V. Mujica, M. A. Ratner, A. Nitzan, *Chem. Phys.* **2002**, 281, 147-150.
- ⁴⁰ J.-O. Lee, G. Lientschnig, F. Wiertz, M. Struijk, R. A. J. Janssen, R. Egberink, D. N. Reinhoudt, P. Hadley, C. Dekker, *Nano Lett.* **2003**, 3, 113-117.
- ⁴¹ (a) J. H. Schön, H. Meng, Z. Bao, *Nature* **2001**, 413, 713-716 (retracted);(b) J. H. Schön, H. Meng, Z. Bao, *Science* **2001**, 294, 2138-2140 (retracted);(c) J. H. Schön, Z. Bao, *Appl. Phys. Lett.* **2002**, 80, 847-849 (retracted).
- ⁴² M. R. Beasley (Chair), S. Datta, H. Kogelnik, H. Kroemer, D. Monroe, The “Rreport of the investigation committee on the possibility of scientific misconduct in the work of Hendrik Schön and co-authors” can be found on the internet at the following address http://www.lucnet.com/news_events/pdf/researchreview.pdf.
- ⁴³ C. R. Kagan, A. Afzali, R. Martel, L. M. Gignac, P. M. Solomon, A. G. Schrott, B. Ek, *Nano Lett.* **2003**, 3, 119-124.
- ⁴⁴ (a) J. O. Jeppesen, S. A. Vignon, J. F. Stoddart, *Chem. Eur. J.* **2003**, 9, 4611-4625; (b) C. O. Dietrich-Buchecker, J-P. Sauvage, *Chem. Rev.* **1987**, 87, 795-810.
- ⁴⁵ C. P. Collier, E. W. Wong, M. Belohradsky, F. M. Raymo, J. F. Stoddart, P. J. Kuekes, R. S. Williams, J. R. Heath, *Science* **1999**, 285, 391-393.
- ⁴⁶ D. R. Stewart, D. A. A. Ohlberg, P. A. Beck, Y. Chen, R. Stanley Williams, J. O. Jeppesen, K. A. Nielsen, J. F. Stoddart, *Nano Lett.* **2004**, 4, 133-136.
- ⁴⁷ (a) S. C. Chang, Z. Li, C. N. Lau, B. Larade, R. S. Williams, *Appl. Phys. Lett.* **2003**, 83, 3198-3200; (b) K. Konstadinidis, P. Zhang, R. L. Opila, D. L. Allara, *Surf. Sci.* **1995**, 338, 300-312.
- ⁴⁸ C. P. Collier, G. Mattersteig, E. W. Wong, Y. Luo, K. Beverly, J. Sampaio, F. M. Raymo, J. F. Stoddart, J. R. Heath, *Science* **2000**, 289, 1172-1175.
- ⁴⁹ M. A. Reed, J. Chen, A. M. Rawlett, D. W. Price, J. M. Tour, *Appl. Phys. Lett.* **2001**, 78, 3735-3737.
- ⁵⁰ A. W. Ghosh, F. Zahid, S. Datta, R. R. Birge, *Chem. Phys.* **2002**, 281, 225-230.
- ⁵¹ J. M. Tour, L. Cheng, D. P. Nackashi, Y. Yao, A. K. Flatt, S. K. St. Angelo, T. E. Mallouk, P. D. Franzon, *J. Am. Chem. Soc.* **2003**, 125, 13279-13283.
- ⁵² J. M. Tour, *Molecular electronics*, World Scientific, Singapore 2003 ISBN 981-238-341-7.
- ⁵³ (a) J. Chen, M. A. Reed, A. M. Rawlett, J. M. Tour, *Science* **1999**, 286, 1550-1552; (b) T. Lee, W. Wang, J. F. Klemic, J. J. Zhang, J. Su, M. A. Reed, *J. Phys. Chem. B* **2004**, 108, 8742-8750; (c) W. Wang, T. Lee, I. Kretzschmar, M. A. Reed, *Nano Lett.* **2004**, 4, 643-646; (d) C. Zhou, M. R. Deshpande, M. A. Reed, L. Jones II, J. M. Tour, *Appl. Phys. Lett.* **1997**, 71, 611-613.
- ⁵⁴ W. Wang, T. Lee, M. A. Reed, *Phys. Rev. B* **2003**, 68, 035416.

- ⁵⁵ W. Wang, T. Lee, M. A. Reed, *J. Phys. Chem. B* **2004**, 108, 18398-18407.
- ⁵⁶ A.-S. Hallbäck, N. Oncel, J. Huskens, H. J. W. Zandvliet, B. Poelsema, *Nano Lett.* **2004**, 4, 2393-2395.
- ⁵⁷ S. M. Sze, *Physics of Semiconductor Devices*, 2nd ed. Wiley, New York, 1981.
- ⁵⁸ J. R. Petta, D. G. Salinas, D. C. Ralph, *Appl. Phys. Lett.* **2000**, 77, 4419-4421.
- ⁵⁹ M. D. Austin, S. Y. Chou, *Nano Lett.* **2003**, 3, 1687-1690.
- ⁶⁰ W. Wang, T. Lee, M. A. Reed, *Nano Lett.* **2004**, 4, 533-533.
- ⁶¹ M. D. Austin, S. Y. Chou, *Nano Lett.* **2004**, 4, 535-535.
- ⁶² T. Lee, W. Wang, J. F. Klemic, J. J. Zhang, J. Su, M. A. Reed, *J. Phys. Chem. B* **2004**, 108, 8742-8750.
- ⁶³ J. G. Kushmerick, D. B. Holt, J. C. Yang, J. Naciri, M. H. Moore, R. Shashidhar, *Phys. Rev. Lett.* **2002**, 89, 086802.
- ⁶⁴ S. Gregory, *Phys. Rev. Lett.* **1990**, 64, 689.
- ⁶⁵ J. G. Kushmerick, J. Naciri, J. C. Yang, R. Shashidar, *Nano Lett.* **2003**, 3, 897-900.
- ⁶⁶ J. G. Kushmerick, D. B. Holt, S. K. Pollack, M. A. Ratner, J. C. Yang, T. L. Schull, J. Naciri, M. H. Moore, R. Shashidhar, *J. Am. Chem. Soc.* **2002**, 124, 10654-10655.
- ⁶⁷ M. A. Rampi, O. J. A. Schueller, G. M. Whitesides, *Appl. Phys. Lett.* **1998**, 72, 1781-1783.
- ⁶⁸ Y.-J. Liu, H.-Z. Yu, *ChemPhysChem.* **2002**, 9, 799-802.
- ⁶⁹ K. Slowinski, R. V. Chamberlin, C. J. Miller, M. Majda, *J. Am. Chem. Soc.* **1997**, 119, 11910-11919.
- ⁷⁰ J. Thome, M. Himmelhaus, M. Zharnikov, M. Grünze, *Langmuir* **1998**, 14, 7435-7449.
- ⁷¹ B. Mann, H. Kuhn, *J. Appl. Phys.* **1971**, 42, 4797.
- ⁷² M. L. Chabinye, X. Chen, R. E. Holmlin, H. Jacobs, H. Skulason, C. D. Frisbie, V. Mujica, M. A. Ratner, M. A. Rampi, G. M. Whitesides, *J. Am. Chem. Soc.* **2002**, 124, 11730-11736.
- ⁷³ R. Haag, M. A. Rampi, R. E. Holmlin, G. M. Whitesides, *J. Am. Chem. Soc.* **1999**, 121, 7895-7906.
- ⁷⁴ R. E. Holmlin, R. Haag, M. L. Chabinye, R. F. Ismagilov, A. E. Cohen, A. Terfort, M. A. Rampi, G. M. Whitesides, *J. Am. Chem. Soc.* **2001**, 123, 5075-5085.
- ⁷⁵ S. Sek, R. Bilewicz, K. Slowinski, *Chem. Commun.* **2004**, 404-405.
- ⁷⁶ B. Alpers, S. Cohen, I. Rubinstein, G. Hodes, *Phys. Rev. B* **1995**, 52, 17017-17020.
- ⁷⁷ D. J. Wold, C. D. Frisbie, *J. Am. Chem. Soc.* **2000**, 122, 2970-2971.
- ⁷⁸ J. M. Beebe, V. B. Engelkes, L. L. Miller, C. D. Frisbie, *J. Am. Chem. Soc.* **2002**, 124, 11268-11269.

- ⁷⁹ D. J. Wold, R. Haag, M. A. Rampi, C. D. Frisbie, *J. Phys. Chem. B* **2002**, 106, 2813-2816.
- ⁸⁰ V. B. Engelkes, J. M. Beebe, C. D. Frisbie, *J. Am. Chem. Soc.* **2004**, 126, 14287-14296.
- ⁸¹ E. Gomar-Nadal, G. K. Ramachandran, F. Chen, T. Burgin, C. Rovira, D. B. Amabilino, S. M. Lindsay, *J. Phys. Chem. B* **2004**, 108, 7213-7218.
- ⁸² X. D. Cui, X. Zarate, J. Tomfohr, O. F. Sankey, A. Primak, A. L. Moor, D. Gust, G. Harris, S. M. Lindsay, *Nanotechnol.* **2002**, 13, 5-14.
- ⁸³ A. P. Labonté, S. L. Tripp, R. Reifenger, A. Wei, *J. Phys. Chem. B* **2002**, 106, 8721-8725.
- ⁸⁴ L. A. Bumm, J. J. Arnold, T. D. Dunbar, D. L. Allara, P. S. Weiss, *J. Phys. Chem. B* **1999**, 103, 8122-8127.
- ⁸⁵ A. Dhirani, P.-H. Lin, P. Guyot-Sionnest, R. W. Zehner, L. R. Sita, *J. Chem. Phys.* **1997**, 106, 5249-5253.
- ⁸⁶ G. J. Ashwell, A. Chwialkowska, L. R. H. High, *J. Mater. Chem.* **2004**, 14, 2389-2394.
- ⁸⁷ A. Salomon, D. Cahen, S. Lindsay, J. Tomfohr, V. B. Engelkes, C. D. Frisbie, *Adv. Mater.* **2003**, 15, 1881-1890.
- ⁸⁸ K. Kobayashi, H. Yamada, T. Horiuchi, K. Matsushige, *Appl. Sur. Sci.* **1999**, 144-145, 435-438.
- ⁸⁹ S. Raible, J. Pfeiffer, T. Weiss, W. Clauss, W. Goepel, V. Schurig, D. P. Kern, *Appl. Phys. A* **2000**, 70, 607-611.
- ⁹⁰ M. T. Cygan, T. D. Dunbar, J. J. Arnold, L. A. Bumm, N. F. Shedlock, T. P. Burgin, L. Jones II, D. L. Allara, J. M. Tour, P. S. Weiss, *J. Am. Chem. Soc.* **1998**, 120, 2721-2732.
- ⁹¹ M. Dorogi, J. Gomez, R. Osifchin, R. P. Andres, R. Reifenger, *Phys. Rev. B* **1995**, 52, 9071-9077.
- ⁹² B. Xu, N. J. Tao, *Science* **2003**, 301, 1221-1223.
- ⁹³ M. Mayor, H. B. Weber, *Angew. Chem. Int. Ed.* **2004**, 43, 2882-2884.
- ⁹⁴ A. M. Rawlett, T. J. Hopson, L. A. Nagahara, R. K. Tsui, G. K. Ramachandran, S. M. Lindsay, *Appl. Phys. Lett.* **2002**, 81, 3043-3045.
- ⁹⁵ X. D. Cui, A. Primak, X. Zarate, J. Tomfohr, O. F. Sankey, A. L. Moore, T. A. Moore, D. Gust, G. Harris, S. M. Lindsay, *Science* **2001**, 294, 571-574.
- ⁹⁶ G. K. Ramachandran, J. K. Tomfohr, J. Li, O. F. Sankey, X. Zarate, A. Primak, Y. Terazono, T. A. Moore, A. L. Moore, D. Gust, L. A. Nagahara, S. M. Lindsay, *J. Phys. Chem. B* **2003**, 107, 6162-6169.
- ⁹⁷ STM cannot measure heights correctly, but only measures a current at a certain distance from the sample. The conducting molecules and gold colloids are brighter in a constant current image, because the tip moves away from the surface, and in a constant height image, because of the increase of the current.

- ⁹⁸ J. Park, A. N. Pasupathy, J. I. Goldsmith, C. Chang, Y. Yaish, J. R. Petta, M. Rinkoski, J. P. Sethna, H. D. Abruña, P. L. McEuen, D. C. Ralph, *Nature* **2002**, 417, 722-725.
- ⁹⁹ H. Park, A. K. L. Lim, A. P. Alivisatos, J. Park, P. L. McEuen, *Appl. Phys. Lett.* **1999**, 75, 301-303.
- ¹⁰⁰ W. Liang, M. P. Shores, M. Brokrath, J. R. Long, H. Park, *Nature* **2002**, 417, 725-729.
- ¹⁰¹ Y. Selzer, M. A. Cabassi, T. S. Mayer, D. L. Allara, *J. Am. Chem. Soc.* **2004**, 126, 4052-4053.
- ¹⁰² M. A. Reed, C. Zhou, C. J. Muller, T. P. Burgin, J. M. Tour, *Science* **1997**, 278, 252.
- ¹⁰³ J. Reichert, R. Ochs, D. Beckmann, H. B. Weber, M. Mayor, H. von Löhneysen, *Phys. Rev. Lett.* **2002**, 88, 176804.
- ¹⁰⁴ H. B. Weber, J. Reichert, R. Ochs, D. Beckmann, M. Mayor, H. von Löhneysen, *Physica E* **2003**, 18, 231-232.
- ¹⁰⁵ H. B. Weber, J. Reichert, F. Weigend, R. Ochs, D. Beckmann, M. Mayor, R. Ahlrichs, H. von Löhneysen, *Chem. Phys.* **2002**, 281, 113-125.
- ¹⁰⁶ R. F. Service “Science breakthrough of the year 2001”, *Science* **2001**, 294, 2442-2443.
- ¹⁰⁷ R. F. Service, *Science* **2003**, 302, 556-559.

Chapter 3

Self-Assembled Monolayers of Difunctional and of Conducting Molecules

*The preparation and analysis of self-assembled monolayers of α,ω -bis-functionalized molecules is described. XPS, contact angle goniometry, STM and electrochemistry are used to analyze the order and binding mode of these SAMs. SAMs of 1,9-nonanedithiol SAMs can be prepared in such a way that the order is acceptable and a thiol-terminated surface is obtained. The longer 1,16-hexadecanedithiol does not form ordered SAMs. para-Di(phenylethynyl-4',-thioacetyl)benzene (**1**) was used to make SAMs that are reasonably well ordered. In decanethiol SAMs the in-situ deprotected **1** inserts as clusters of several molecules.*

3.1 Introduction

Alkylthiol, dialkyldisulfide or dialkylsulfide SAMs on noble metal surfaces are the most common SAMs that can be prepared.¹ These SAMs alter the wettability of metal surfaces and protect them, for example against corrosion² or etching.³ The quality of alkylthiol SAMs on gold depends on their length. Short chain alkylthiols like hexanethiol (HT) and octanethiol (OT) form less ordered “liquid-like” SAMs while octadecanethiol (ODT) and eicosanethiol (ET) form more ordered “crystalline like” SAMs.⁴ More interesting and versatile are SAMs of functionalized alkylthiolates. α,ω -Substituted alkanes bind with the sulfur group to the noble metal surface and leave the other functional group exposed. This group can then be used for sensing⁵ or, in patterning, for preferential binding of metal.⁶ In the case of dithiols a reactive surface is obtained that can chemically bind metals. This concept is used in single molecule junctions (Chapter 2) where the difunctionalized molecules assemble between two electrodes. For the preparation of SAMFETs or other devices another advantage of dithiol SAMs over monothiol SAMs is that these reactive surface groups will prevent metal diffusing through the SAM.⁷ Finally, the covalent binding of a molecule to an electrode reduces the contact resistance in the junction. For this reason SAMs made from dithiols are of great interest in molecular electronics (Chapter 2).

The complication of using difunctional molecules like alkyldithiols is that if they are flexible enough they can bind to the surface with both functional groups at the same time. The molecules can lie flat on the surface or form loops, hindering the formation of good quality SAMs.⁸ Disulfide multilayers can be formed as well.⁹ Rigid, conjugated dithiols like biphenyldithiol are more easily oxidized, and for this reason they can oligomerize to form multilayers on a gold surface.^{10,11,12,13} The use of a thioacetate protection group makes storage of these compounds possible. For assembly on a gold surface, the thiol groups can be deprotected *in-situ*.^{11,14} These potential complications are often not discussed in detail in publications. In this chapter several dithiol and dithioacetate SAMs are analyzed using X-ray photoelectron spectroscopy (XPS), Electrochemistry (EC), scanning tunneling microscopy STM and contact angle goniometry.

3.2 Preparation of self-assembled monolayers

3.2.1 SAMs of alkyldithiols on gold

1,9-Nonanedithiol (NDT) SAMs were prepared on evaporated gold substrates. NDT molecules are long and flexible enough to form loops (Figure 3.1). XPS was used to investigate whether sulfur atoms are bound to gold or that they are free, as thiol.¹⁵ Sulfur gives a very weak signal in XPS, so especially when SAMs are used high-sensitivity equipment is necessary. The sulfur signal is split into two peaks corresponding to the $S_{2p\ 3/2}$ and the $S_{2p\ 1/2}$ in the ratio of 2 to 1. The energy difference between both peaks is around 1 eV. The peaks for bound and unbound sulfur partly overlap, with a binding energy for the bound $S_{2p\ 3/2}$ at around 161.8 eV and the peak for the unbound $S_{2p\ 3/2}$ at around 163.1 eV.¹⁶ Even though the sulfur peaks are relatively weak, the difference between the bound and unbound binding energies can be used to determine the conformation.

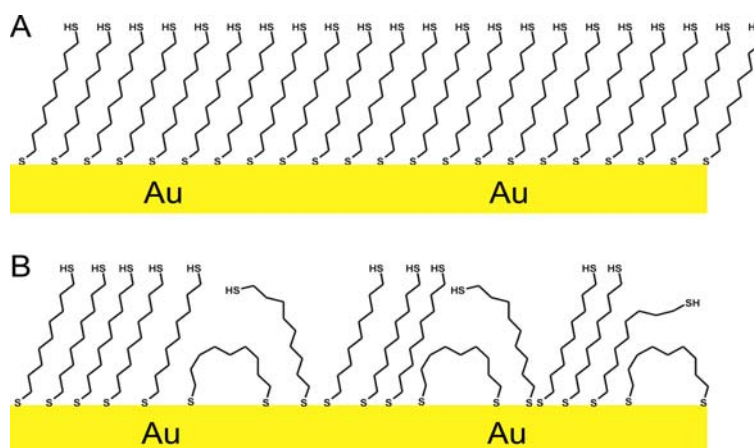


Figure 3.1 Possible structure of a 1,9-nonanedithiol SAM assembled on gold (A) All straight, ordered configuration. (B) Disordered configuration with loops.

Figure 3.2 shows an XPS spectrum of the sulfur S_{2p} region of an NDT SAM made from a ~ 1 mM hexane solution on evaporated gold. The peak was fitted with two double S_{2p} peaks, keeping the full width at half maximum (FWHM) equal (ratio between $S_{2p\ 3/2}$ and $S_{2p\ 1/2}$ is 2:1). The separation of these peaks was 1.21 eV while the separation between the bound and unbound peaks was 1.18 eV.

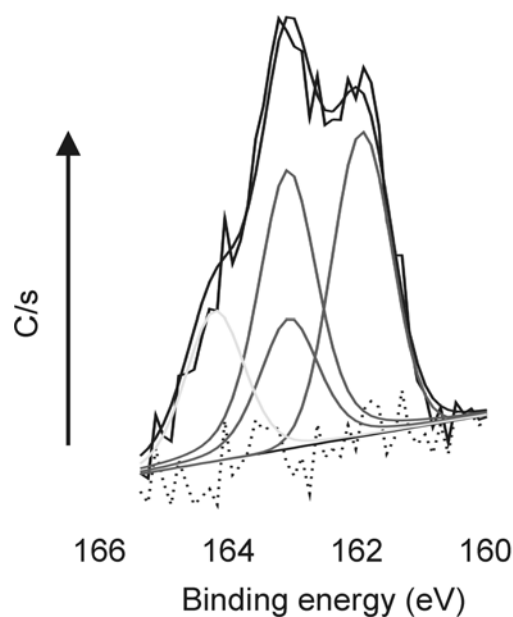


Figure 3.2 S_{2p} region of the XPS spectrum of an NDT SAM made from a 1 mM hexane solution, on 20 nm evaporated gold.

Table 3.1 S_{2p} peak fit data of NDT SAM on gold.^{a,b}

Band	Energy (eV)	FWHM	% Area
$S_{2p\ 3/2}$ bound	162.04	1.13	32.02
$S_{2p\ 1/2}$ bound	163.22	1.13	16.01
$S_{2p\ 3/2}$ unbound	163.25	1.13	34.64
$S_{2p\ 1/2}$ unbound	164.43	1.13	17.32

a $\chi^2 = 1.06$

b pass energy 58.70 eV

Table 3.1 shows that the areas of both $S_{2p\ 3/2}$ peaks are almost equal, indicating an equal number of free sulfur atoms (thiols) and bound sulfur atoms (thiolates). Because of the attenuation of the photoelectrons emitted by atoms that are buried deeper in the SAM, the peak of the bound thiolates is expected to be smaller.¹⁷ Although the error in the fitting of peaks with such low intensities is significant it can be concluded that most of the dithiol molecules are in an upright position on the gold surface with one sulfur (thiolate) bound to the gold and one sulfur (thiol) exposed. Theoretically, partial multilayers could be present together with dithiols connected with both thiols to the surface. Studies in the literature on the multilayer formation process make this seem unlikely.⁹

Contact angles with water for NDT SAMs are $78^\circ \pm 3^\circ$ (advancing) and $47^\circ \pm 6^\circ$ (receding). The significantly lower advancing contact angle compared to alkylthiol SAMs ($> 100^\circ$)¹⁸ is due to the more hydrophilic thiol end group in this SAM. There seems to be no substantial looping of the dithiol molecules. However, the relatively large hysteresis value indicates that the order of this SAM is limited.

Several electrochemical techniques were used to analyze SAMs on conducting surfaces.¹⁹ Using cyclic voltammetry (in a 0.1 M K_2SO_4 solution), performed at different scan speeds (0.1 V s^{-1} , 0.2 V s^{-1} , 0.5 V s^{-1}), a double layer capacitance for the NDT SAM of $\sim 4 \mu\text{F cm}^{-2}$ at -0.2 V was calculated. Resistances measured using electrochemical impedance spectroscopy (EIS)²⁰ (using the redox couple $K_4Fe(CN)_6 / K_3Fe(CN)_6$, both 1 mM) are typically in the order of 800 to 1000 $\Omega \text{ cm}^2$ (Figure 3.3) (a bare good electrode has a charge transfer resistance in the order of 50 $\Omega \text{ cm}^2$). These results all indicate that the SAM is not very well ordered. The reason for the increase in resistance after each scan is not clear. SAMs made from non-purged ethanol often show resistances in the same range as ODT SAMs. This is likely caused by multilayer formation.

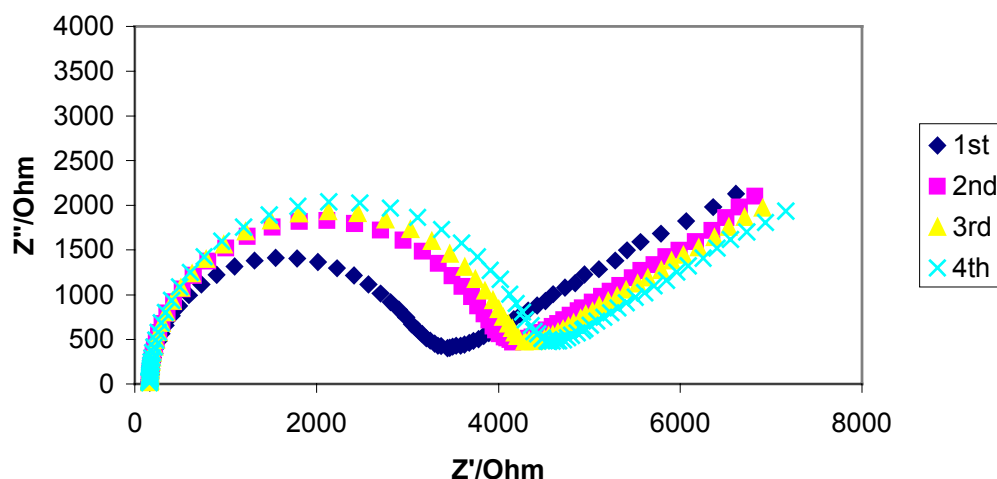


Figure 3.3 Subsequent electrochemical impedance spectra of NDT SAM on gold made with 30 minute intervals.

SAMs on gold were also made with the longer 1,16-hexadecanedithiol (HDDT). The S_{2p} peak in the XPS spectrum of an HDDT SAM is different from that of NDT. Fitting this S_{2p} peak (Figure 3.4) shows that the area of the peaks

corresponding to bound sulfur is $\sim 80\%$. This means that around 20% of the dithiols are bound through one sulfur atom while 80% is bound with both sulfur atoms to the surface. This is in accordance with previously reported results for these SAMs on silver, made from ethanolic solutions.⁸

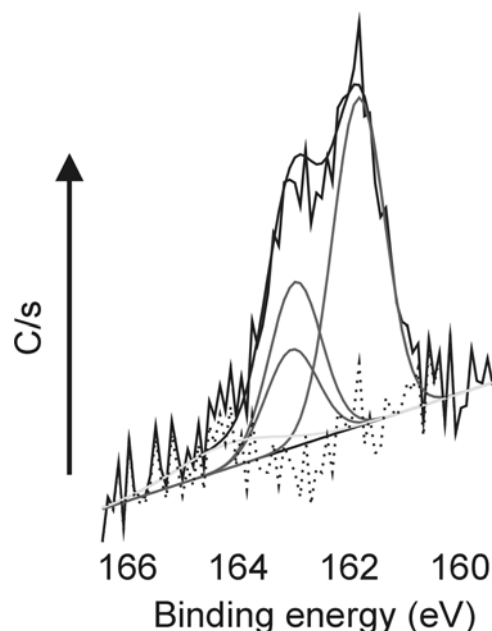


Figure 3.4 S_{2p} region of the XPS spectrum of an HDDT SAM on evaporated gold.

Table 3.2. S_{2p} peak fit data of HDDT SAM on gold.^{a,b}

band	Energy (eV)	FWHM	% area
$S_{2p\ 3/2}$ bound	162.07	1.07	53.11
$S_{2p\ 1/2}$ bound	163.25	1.07	26.55
$S_{2p\ 3/2}$ unbound	163.32	1.07	13.56
$S_{2p\ 1/2}$ unbound	164.50	1.07	6.78

a $\chi^2 = 1.14$

b pass energy 58.70 eV

The XPS spectra show that whereas NDT can be used to make ordered SAMs (with molecules singly bound to the surface), this is not possible for the much longer HDDT. This is most likely due to the length of this molecule, which makes it more flexible so that it can bind with both sulfur atoms to the surface. Contact angles of these SAMs are 116° (advancing) and 60° (receding). These values are much too high for a thiol-terminated surface. The high advancing contact angles probably arise from

exposed, hydrophobic, alkyl chains (possibly caused by oligomerization). The large hysteresis value of 56° suggests that the order of these layers is very poor.

EIS showed that the HDDT SAM formed from a 1 mM solution in chloroform has a charge transfer resistance of around 25 k Ω (Figure 3.5), indicating that the SAM covers the gold electrode and blocks the charge transfer process. However, compared to ODT SAMs (which have approximately the same length), which have resistances of 35 to 150 k Ω cm² ²¹ depending on the quality, the HDDT SAM is a poor resist. The capacitance of this layer was around 8 μ F cm⁻², also indicating a very disordered or thin layer.

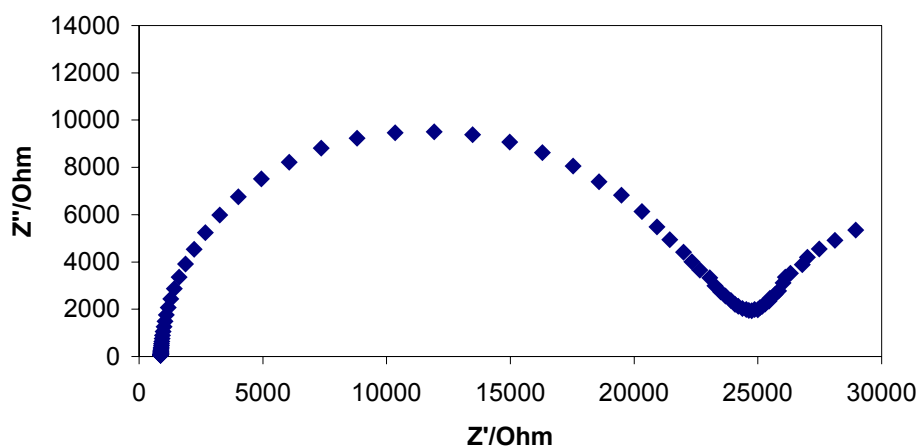


Figure 3.5 Electrochemical impedance spectrum of an HDDT SAM from CHCl₃.

3.2.2 SAMs of biphenyldithiol on gold

Biphenyldithiol (BDT) is a molecule often used for the fabrication of nanoscale electronic devices.²² It can bind metal electrodes on both sides and it is conjugated. XPS analysis (Figure 3.6) showed a much larger free than bound sulfur peak. Apart from the attenuation of the signal of bound sulfur buried in the SAM probably also multilayers of disulfides, formed after oxidation of the thiol groups, are the cause of this observation.^{12,13}

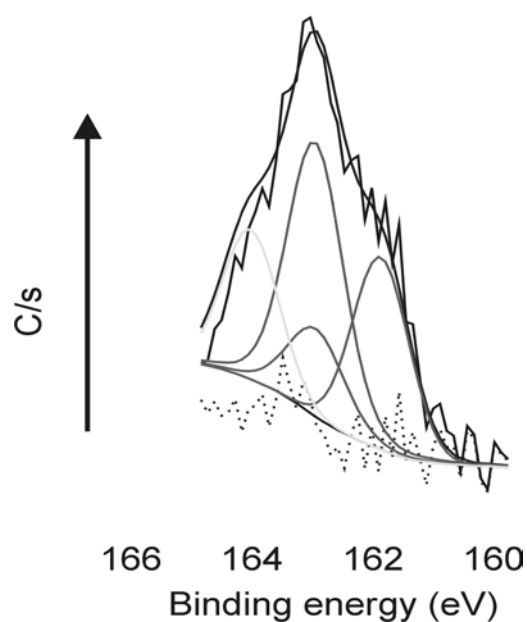


Figure 3.6 S_{2p} region of the XPS spectrum of a BDT SAM on evaporated gold.

Table 3.3 S_{2p} peak fit data of BDT SAM on gold.^{a,b}

band	Energy (eV) ^c	FWHM	% area
$S_{2p\ 3/2}$ bound	162.32	1.21	26.07
$S_{2p\ 1/2}$ bound	163.50	1.21	13.04
$S_{2p\ 3/2}$ unbound	163.52	1.21	40.59
$S_{2p\ 1/2}$ unbound	164.70	1.21	20.30

a $\chi^2 = 1.19$

b pass energy 58.70 eV

c binding energies relative to C_{1s} peak at 284.8 eV. The C_{1s} peak for aromatic carbon is however at a different position than aliphatic carbon

The BDT SAM has an advancing contact angle of 80° and a receding angle of 35° , which is comparable to previously reported results from Bao *et al.*, for a deprotected biphenyl-dithioacetate.²³ The hysteresis value of the contact angles is approximately 45° , which indicates a poor order of BDT SAMs. Electrochemical impedance spectroscopy on BDT SAMs shows (Figure 3.7) that they have very low charge transfer resistance of around $700\ \Omega\ \text{cm}^2$. This can be caused by the molecules lying flat on the substrate rather than standing up in a perpendicular orientation. The very high double layer capacitance calculated from cyclic voltammetry ($\sim 10\ \mu\text{F}\ \text{cm}^{-2}$)

agrees with this. It seems that BDT SAMs are not suitable for the use in electronic devices where a top electrode has to be deposited on the SAM.

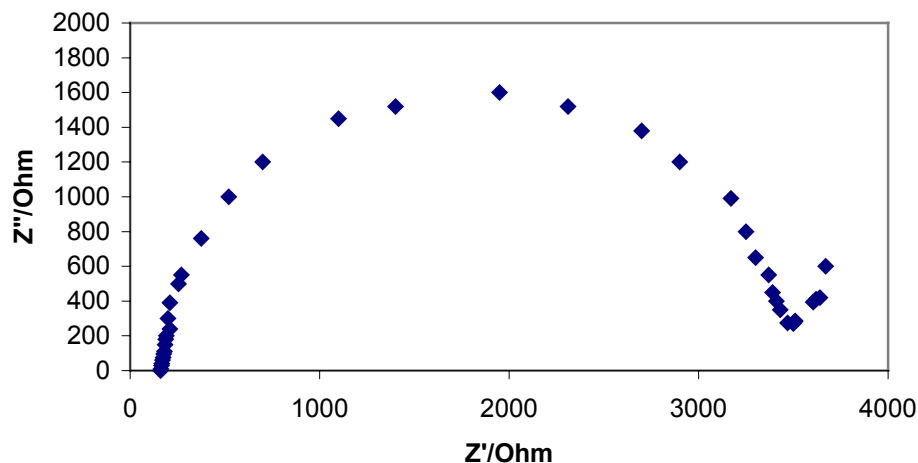


Figure 3.7 Electrochemical impedance spectrum of a BDT SAM from CHCl_3 .

3.2.3 SAMs of thio-acetate protected thiols on gold

Oligo-(phenylene-ethynylene) dithioacetates are a useful class of compounds in molecular electronics because they can bind a noble metal on two sides of the molecule and have a conjugated π -system that can transport electrons.²⁴ Thiols, especially conjugated systems that are prone to oxidation, can be protected as thioacetates. The thioacetate group can be deprotected *in-situ* in solution to yield the corresponding thiolate, which can then bind the gold surface.^{10,14} When deprotecting dithioacetates, reactive thiolate groups are formed which oxidize easily and can then react to form oligomer disulfides. Also auto-deprotection by the gold can occur. In this way SAMs can be made directly from thioacetates.²⁵ When using this method, higher concentrations of thioacetate are necessary to form good SAMs.

SAMs of *para*-di(phenylethynyl-4'-thioacetyl)benzene (**1**) (Figure 3.8) were prepared from chloroform solutions without any further additive to deprotect the thioacetate groups (to prevent oligomerisation) and from THF solutions containing NH_4OH to deprotect the thiol groups.

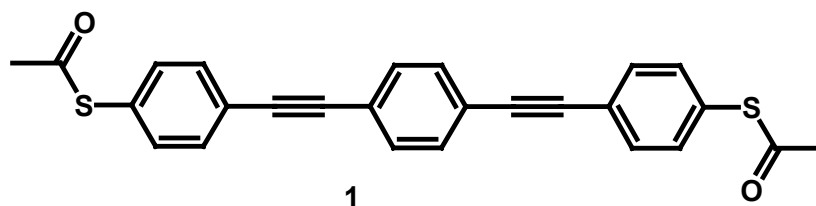


Chart 3.8

A SAM of **1** made from a 0.5 mM solution in CHCl₃ on evaporated gold had an advancing contact angle with water of 72° and a receding contact angle of 54°. The advancing contact angles are slightly lower than of SAMs made from dithiols, which might indicate that the end group is a thioacetate group.

SAMs of **1** were analyzed with cyclic voltammetry (CV), heterogeneous electron transfer (HET) and EIS. CV showed a charging current at -0.2 V of 0.08 μA, which corresponds to a double layer capacitance of 4.52 μF cm⁻². EIS showed (Figure 3.9) charge transfer resistances ranging from 1 to 20 kΩ cm². SAMs made from *in-situ* deprotected dithioacetates have a higher resistance than SAMs made from protected dithioacetates. The quality of these layers made from unprotected **1**, however, was irreproducible.

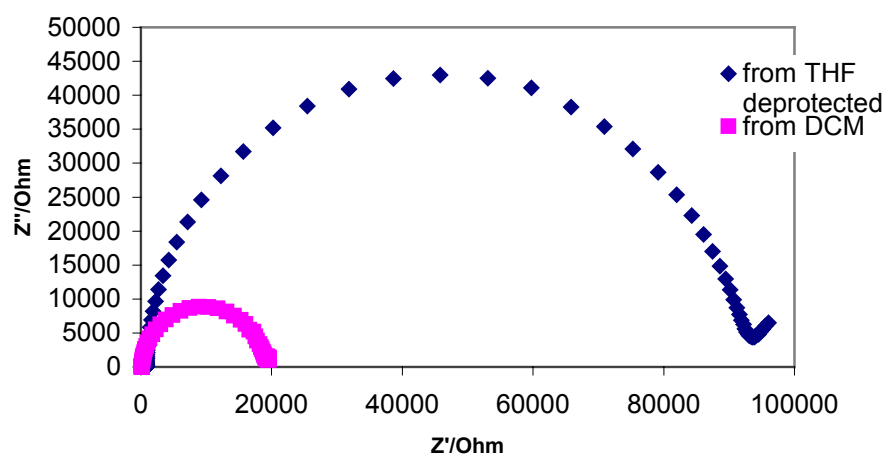


Figure 3.9 Electrochemical impedance spectra of **1** made from dichloromethane and THF (deprotected).

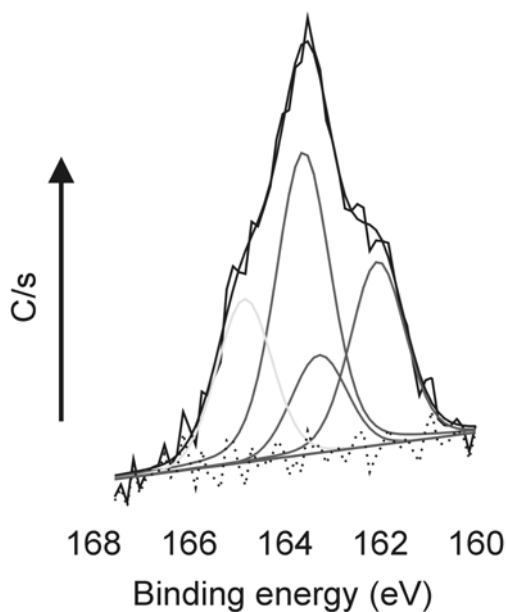


Figure 3.10 S_{2p} region of the XPS spectrum of an **1** SAM prepared from THF (NH_4OH) on evaporated gold.

Table 3.4 S_{2p} peak fit data of deprotected **1** SAM on gold.^{a,b}

band	Energy (eV)	FWHM	% area
$S_{2p\ 3/2}$ bound	161.96	1.30	24.52
$S_{2p\ 1/2}$ bound	163.14	1.30	12.26
$S_{2p\ 3/2}$ unbound	163.46	1.30	42.15
$S_{2p\ 1/2}$ unbound	164.64	1.30	21.07

a $\chi^2 = 1.10$

b pass energy 58.70 eV

XPS analysis showed that the **1** molecules are bound with only one sulfur moiety to the gold, which could be expected and which is in agreement with previously reported results.¹⁰ As can be seen from Figure 3.10 and Table 3.4, the peaks corresponding to free sulfur are much bigger than those of bound sulfur. It should be noted that this is partly caused by the fact that the photoelectrons originating from atoms lying deeper within the SAM-layer are attenuated, thus giving rise to lower peaks. The thickness of a SAM of **1** is around 2.6 nm.

3.3 Insertion of *para*-di(phenylethynyl-4'-thioacetyl)benzene (**1**) in decanethiol SAMs

Mixed monolayers can be prepared in different ways. The insertion of molecules from solution in a preformed SAM and SAMs formed from a mixed solution are the most general ones. To obtain a low coverage of individual (single) molecules in a SAM matrix the insertion process is preferred. Adsorption from mixed (mM concentration) solutions with a 1:1000 ratio of compounds is difficult and differences in reactivity towards the surface might yield a SAM with a composition different than that of the solution.

For the insertion of molecules in SAMs, the SAMs have to be poorly ordered so that exchange with molecules from solution can occur. *Via* this method individual inserted molecules have been obtained for single molecule experiments.²⁶ An example is the study of coordination chemistry of individual metallo-pincer molecules assembled on the surface with organic ligands or with gold-colloids,²⁷ or the cage formation of individual cavitands (Chapter 7).

Thiols and sulfides can be inserted by immersing a SAM into a solution of these compounds in dichloromethane (Figure 3.11). Insertion can occur in existing pinholes but also the desorption of thiolates or disulfides from the SAM yields bare gold on which molecules can adsorb.²⁸

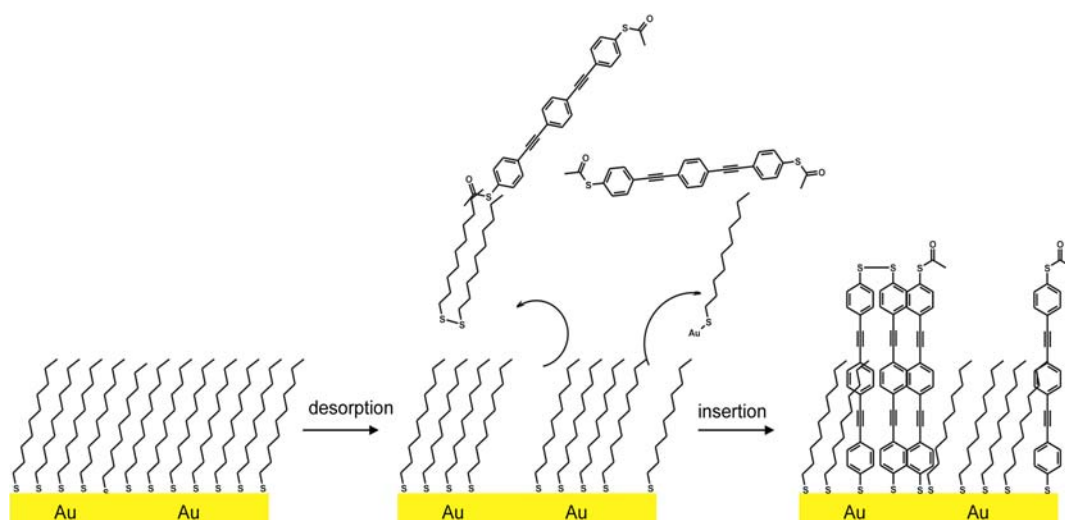


Figure 3.11 Schematic drawing of the insertion of dithioacetate **1** in a DT SAM.

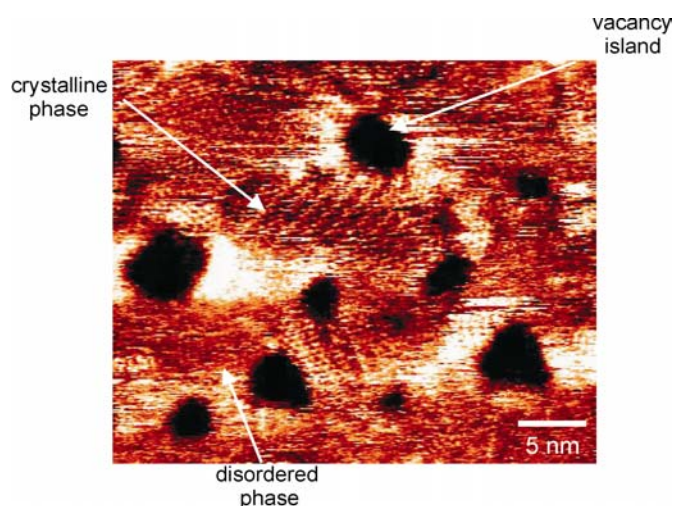


Figure 3.12 STM image of a DT SAM on a gold(111) surface. Measurement conditions: $V = +0.325$ V, $I_{tun} = 0.025$ nA, room temperature.²⁹

Figure 3.12 shows an STM image of a DT SAM. The black areas in the image correspond to the vacancy islands. Vacancy islands are one gold-atom deep patches created by the etching effect of thiol molecules in a solvent.³⁰ Part of the surface is covered with disordered thiolate patches and other areas are clearly crystalline.

It was attempted to insert dithioacetates into a decanethiol SAM without deprotecting both thiol groups with NH_4OH . In this way one thioacetate group can auto-deprotect at the gold surface while the other side stays protected. However, no inserted molecules could be detected with STM.

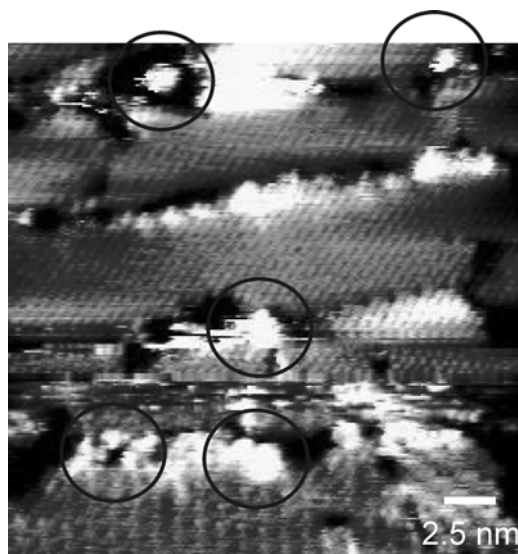


Figure 3.13 STM image of a DT SAM with inserted I molecules. Measurement conditions: ($V = +1.00$ V, $I_{tun} = 14$ pA, 77 K).

Deprotecting the thioacetates *in-situ* using 10 μL of an aqueous 25 % NH_4OH solution was performed according to literature procedures.^{31,32} After insertion the **1** molecules could be visualized with STM. Figure 3.13 shows an STM image of a DT SAM after insertion of **1**. The conductivity of these molecules makes them appear brighter in the STM image. The size of the bright spots and the instability of this spot suggest that they are not single inserted molecules but bundles of molecules. Whether these clusters are disulfide oligomers of **1** or several surface bound **1** molecules together (because of pi-pi interaction initiated clustering) is not clear yet.

3.4 Conclusions

Under the appropriate conditions (prepared from hexane purged with argon), NDT SAMs can be prepared in which one thiol group per molecule is bound to the gold surface and the other one is unbound, sticking outwards. This has been shown with XPS. Electrochemistry studies showed a reasonably ordered monolayer and contact angle measurements confirmed the thiol-terminated surface. Compared to an ODT SAM the order and charge transfer resistances are considerably lower.

The longer dithiol HDDT does not form well-packed SAMs bound with one sulfur group per molecule. This molecule is too long and binding with two thiol groups cannot be prevented.

para-Di(phenylethynyl-4'-thioacetyl)benzene (**1**) forms SAMs that are reasonably well packed and bound with one sulfur group to the surface. XPS indicates that the acetate groups are removed upon adsorption on the gold. EIS shows that the SAM is changing conformation when the experiment is repeated several times on the same sample. Dithioacetate **1** can be inserted in DT SAMs and imaged with STM. However, it is difficult to prevent oligomerisation, so that single inserted molecules are not obtained as the only insertion product.

NDT SAMs have been used in Chapter 4 for the deposition of gold islands to create Au-SAM-Au sandwich systems. HDDT SAMs are very badly packed, making them not useful in molecular electronics research. Possibly alternative assembly methods, like exchange with the molecules in an existing SAM, might give good HDDT SAMs. Another option might be the preparation of mixed SAMs with a long chain monothiol. *para*-Di(phenylethynyl-4'-thioacetyl)benzene (**1**) might be used for

the attachment of small metal clusters if individual inserted molecules can be obtained.

3.5 Experimental procedures

Chemicals: 1,9-Nonanedithiol (95 %, Acros), octadecanethiol (98 %, Janssen Chimica) and decanethiol (96 %, Aldrich) were used without further purification.

1, 1'-Biphenyl-4,-4'-dithiol: 5.99 g (32.1 mmol) biphenol, 21.64 g (193 mmol) DABCO (1,4-diazabicyclo[2.2.2]octane) and 23.86 g (193 mmol) N-N-dimethylthiocarbamoylchloride were dissolved in 200 ml DMF and stirred for 1.5 hours. The mixture was filtered over a Büchner funnel and washed with water, yielding 10.71 g (29.7 mmol, 93 %) of the O,O-bisthiocarbamate. ¹H-NMR (300 MHz, CDCl₃): δ 7.61 (d 4H), 7.18 (d 4H), 3.42 (d 12H). 1.88 g (5.2 mmol) of the bisthiocarbamate was heated to 285 °C for 30 minutes and the resulting solid was recrystallized from EtOH/CH₂Cl₂ yielding 1 g (53 %) of the rearranged S,S-bisthiocarbamate. ¹H-NMR (300 MHz, CDCl₃): δ 7.60 (m 8 H), 3.10 (s 12H). 1 g (2.8 mmol) was added to a solution of KOH (1.12 g, 16.6 mmol) in 45 ml ethylene glycol at 125 °C and stirred for 20 minutes. After cooling 1 M HCl solution was added and the precipitate was filtered off and purified using column chromatography over silica/dichloromethane, yielding 0.09 g (15 %) of biphenyldithiol. ¹H-NMR (300 MHz, CDCl₃): δ 7.40 (q 8H), 3.53 (s 2H).

1,16-Hexadecanedithiol: 0.95 g (3.68 mmol) 1,16-hexadecanediol was added to 30 ml 48 % HBr at 95° C in a three-neck round bottom flask, and 1 ml concentrated sulfuric acid was added. The mixture was refluxed for 5 hours until dibromide had formed. 0.9 g (63 %) of the crude 1,16-dibromohexadecane was obtained after separation of a DCM/water system. 0.9 g of the 1,16-dibromohexadecane was dissolved in 50 ml dioxane, 0.54 g (4.68 mmol) potassium thioacetate was added and the mixture was stirred for 72 hours. 0.49 g (1.31 mmol, 48 %) of hexadecane-1,16-dithioacetate was obtained after column chromatography (silica/hexane).

0.49 g (1.31 mmol) of hexadecane-1,16-dithioacetate was added to a degassed solution of 0.2 g (5 mmol) NaOH in 5 ml water and 14 ml methanol. The mixture was stirred under argon at 100° C for 2 hours. An excess of an aqueous 2 M HCl solution

was slowly added to the mixture. The solvent was evaporated and the solid was separated in a diethylether/water system. The diethylether layer was dried (MgSO_4), filtered and evaporated, yielding 0.24 g of the light-yellow dithiol (0.83 mmol, 63 %). $^1\text{H-NMR}$ (300 MHz., CDCl_3): δ 2.55 (m, 4H), 1.62 (m, 4H), 1.30 (m, 26H). MS (FAB-MS): m/z 289.2 ($[\text{M-H}]^-$) calculated $M = 290.21$ (EI-MS): m/z 290.3.

***para*-Di(phenylethynyl-4'-thioacetyl)benzene (1):** **1** was synthesized by Richard Egberink in the SMCT laboratory via a modified procedure as described by Tour *et al.*³³ 1-(S-acetylthio)-4-iodobenzene was synthesized following Lindsey *et al.*³⁴ from pipsyl chloride. Two equivalents 1-(S-acetylthio)-4-iodobenzene were reacted with *p*-bis-acetylene benzene, which was made via reduction of 1,4-bis(trimethylsilylacetylene)benzene.

SAM preparation: NDT and HDDT SAMs were made by immersing a cleaned gold substrate in an argon purged 1 mM NDT or HDDT in hexane solution overnight. Substrates were removed from solution and rinsed with dichloromethane, and stored under a nitrogen atmosphere to prevent oxidation of the top thiol moieties.

SAMs of **1** were prepared in two different ways: i) Cleaned gold substrates were immersed in a 1 mM solution of **1** in dichloromethane overnight. Substrates were rinsed with dichloromethane and blown dry in a nitrogen stream. ii) Cleaned gold substrates were immersed in a THF solution (0.5 mM) of deprotected **1** (deprotection of **1** was performed by adding 10 μl NH_4OH (25 % in water) to 20 ml of the THF solution of **1**). Substrates were rinsed with dichloromethane and blown dry in a nitrogen stream.

Insertion experiments: DT SAMs were prepared on annealed gold by immersing the substrate in a 1 mM ethanolic solution of DT for 14 hours. Samples were rinsed with dichloromethane, ethanol and water and blown dry in a nitrogen stream. Insertion of **1** was performed by immersing cleaned DT SAMs in a 1 mM solution of deprotected **1** in THF for 2 hours.

Electrochemistry: electrochemical measurements were performed in a three-electrode setup using the SAM as working electrode, a platinum disc as counter electrode and a Hg/HgSO_4 (MSE) as reference electrode. (0.62 V vs. normal hydrogen electrode (NHE)). An AUTOLAB PGSTAT10 equipped with a frequency response

analysis (FRA) module for EIS was used for the measurements. 0.1 mM K₂SO₄ in water was used for cyclic voltammetry. For EIS 1 mM K₃Fe(CN)₆ / K₄Fe(CN)₆ in 0.1 mM K₂SO₄ was used.

XPS: XPS measurements were performed on a Quantera Scanning X-ray Multiprobe instrument from Physical Electronics, equipped with a monochromatic Al_{Kα} X-ray source producing approximately 25 W of X-ray power. Spectra were referenced to the main C_{1s} peak set at 284.8 eV. Usually an area of the substrate of 1000 μm × 300 μm was scanned with the X-ray beam with a diameter of around 10 μm.

3.6 References

- ¹ (a) R. G. Nuzzo, D. L. Allara, *J. Am. Chem. Soc.* **1983**, 105, 4481-4483; (b) F. Schreiber, *Prog. Surf. Sci.* **2000**, 65, 151-256.
- ² C. M. Whelan, M. Kinsella, H. M. Ho, K. Maex, *J. Electron. Mater.* **2004**, 33, 1005-1011.
- ³ (a) A. Kumar, H.A. Biebuyck, N.L. Abbott, G.M. Whitesides, *J. Am. Chem. Soc.* **1992**, 114, 9188-9189; (b) A. Kumar, H.A. Biebuyck, G.M. Whitesides, *Langmuir* **1994**, 10, 1498-1511.
- ⁴ M. D. Porter, T. B. Bright, D. L. Allara, C. E. D. Chidsey, *J. Am. Chem. Soc.* **1987**, 109, 3559-3568.
- ⁵ A. Friggeri, F. C. J. M. van Veggel, D. N. Reinhoudt, *Chem. Eur. J.* **1999**, 5, 3595-3602.
- ⁶ U. Weckenmann, S. Mittler, S. Krämer, A. K. A. Aliganga, R. A. Fisher, *Chem. Mater.* **2004**, 16, 621-628.
- ⁷ B. de Boer, M. M. Frank, Y. J. Chabal, W. Jiang, E. Garfunkel, Z. Bao, *Langmuir* **2004**, 20, 1539-1542.
- ⁸ C. Winter, U. Weckenmann, R. A. Fischer, J. Käshammer, V. Scheumann, S. Mittler, *Chem. Vap. Deposition* **2000**, 6, 199-205.
- ⁹ (a) S. Chah, J. H. Fendler, J. Yi, *Chem. Commun.* **2002**, 18, 2094-2095. (b) P. Kohli, K. K. Taylor, J. J. Harris, G. J. Blanchard, *J. Am. Chem. Soc.* **1998**, 120, 11962-11968.
- ¹⁰ C. D. Bain, E. B. Troughton, Y.-T. Tao, J. Evall, G.M. Whitesides, R. G. Nuzzo, *J. Am. Chem. Soc.* **1989**, 111, 321-335.
- ¹¹ J. M. Tour, L. Jones II, D. L. Pearson, J. J. S. Lamba, T. P. Burgin, G. M. Whitesides, D. L. Allara, A. N. Parikh, S. V. Atre, *J. Am. Chem. Soc.* **1995**, 117, 9529-9534.
- ¹² D. L. Pugmire, M. J. Tarlov, R. D. van der Zee, *Langmuir* **2003**, 19, 3720-3726.
- ¹³ U. Weckenmann, S. Mittler, K. Naumann, R. A. Fischer, *Langmuir* **2002**, 18, 5479-5486.
- ¹⁴ B. de Boer, H. Meng, D. F. Perepichka, J. Zheng, M. M. Frank, Y. J. Chabal, Z. Bao, *Langmuir* **2003**, 19, 4272-4284.
- ¹⁵ D. G. Castner, K. Hinds, D. W. Grainger, *Langmuir* **1996**, 12, 5083-5086.
- ¹⁶ Values for the binding energy depend on the chosen reference. In this study a reference value of 284.8 eV for the C_{1s} peak was chosen. However, differently bound carbon atoms (alkyl, aromatic,

inorganic *etc.*) have different binding energies. For the fitting of the S_{2p} peaks the peak positions were chosen variable. The peak separations (between S_{2p 3/2} and S_{2p 1/2}) were kept the same for bound and unbound sulfur, as well as the FWHM values. Also the 2 to 1 area ratio (between S_{2p 3/2} and S_{2p 1/2}) was kept constant during fitting.

¹⁷ To calculate the exact amount of doubly bound dithiols the attenuation factors of the peaks resulting from electrons emitted from deeply inside the SAM should be taken into account. The peak attenuations (I_z) can be calculated with,

$$I(z) = I_0 e^{-\frac{z}{\lambda_i \cos \theta}}$$

where z is the excitation depth, θ the angle of emission with respect to the surface normal (45° in our case), and λ_i the inelastic electron mean free path. To calculate the attenuation the depth of all the atoms in the SAM must be known. (From: *Surface Analysis by Auger and X-Ray Photoelectron Spectroscopy*, Eds. D. Briggs, J. T. Grant, IM Publications, Charlton, UK, 2003, ISBN1901019047).

¹⁸ P. E. Laibinis, G. M. Whitesides, *J. Am. Chem. Soc.* **1992**, 114, 1990-1995.

¹⁹ M. D. Porter, T. B. Bright, D. L. Allara, C. E. D. Chidsey, *J. Am. Chem. Soc.* **1987**, 109, 3559-3568.

²⁰ (a) E. Sabatani, J. Cohen-Boulakia, M. Bruening, I. Rubinstein, *Langmuir* **1993**, 9, 2974-2981; (b) E. Sabatani, I. Rubinstein, *J. Phys. Chem.* **1987**, 91, 6663-6669; (c) S. G. J. Blankenburg, M. Sluyters-Rehbach, J. H. Sluyters, *J. Electroanal. Chem.* **1996**, 401, 3-19; (d) S. Flink, B. A. Boukamp, A. van den Berg, F. C. J. M. van Veggel, D. N. Reinhoudt, *J. Am. Chem. Soc.* **1998**, 120, 4652-4657; (e) S. Flink, F. C. J. M. van Veggel, D. N. Reinhoudt, *J. Phys. Chem. B* **1999**, 103, 6515-6520.

²¹ C. Henke, C. Steinem, A. Janshoff, G. Steffan, H. Luftmann, M. Sieber, H.-J. Galla, *Anal. Chem.* **1996**, 68, 3158-3165; the measurements were reproduced in the SMCT lab.

²² (a) J. H. Schön, H. Meng, Z. Bao, *Nature* **2001**, 413, 713-716 (retracted); (b) J. H. Schön, H. Meng, Z. Bao, *Science* **2001**, 294, 2138-2140 (retracted); (c) J. H. Schön, Z. Bao, *Appl. Phys. Lett.* **2002**, 80, 847-849 (retracted).

²³ B. de Boer, H. Meng, D. F. Perepichka, J. Zheng, M. M. Frank, Y. J. Chabal, Z. Bao, *Langmuir* **2003**, 19, 4272-4284.

²⁴ (a) D. K. James, J. M. Tour, *Chem. Mater.* **2004**, 16, 4423-4435; (b) F. Maya, A. K. Flatt, M. P. Stewart, D. E. Shen, J. M. Tour, *Chem. Mater.* **2004**, 16, 2987-2997.

²⁵ J. M. Tour, L. Jones, D. L. Pearson, J. J. S. Lamba, T. P. Burgin, G. M. Whitesides, D. L. Allara, A. N. Parikh, S. Atre, *J. Am. Chem. Soc.* **1995**, 117, 9529-9534.

²⁶ X. D. Cui, A. Primak, X. Zarate, J. Tomfohr, O. F. Sankey, A. L. Moore, T. A. Moore, D. Gust, G. Harris, S. M. Lindsay, *Science* **2001**, 294, 571-574.

²⁷ A. Friggeri, H.-J. van Manen, T. Auletta, X.-M. Li, S. Zapotoczny, H. Schönherr, G. J. Vancso, J. Huskens, F. C. J. M. van Veggel, D. N. Reinhoudt, *J. Am. Chem. Soc.* **2001**, 123, 6388-6395.

²⁸ J. B. Schlenoff, M. Li, H. Ly, *J. Am. Chem. Soc.* **1995**, 117, 12528-12536.

²⁹ A.-S. Hallböck, N. Oncel, J. Huskens, H. J. W. Zandvliet, B. Poelsema, *Nano Lett.* **2004**, 4, 2393-2395.

- ³⁰ (a) J. A. M. Sondag-Huethorst, C. Schönenberger, L. G. J. Fokkink, *J. Phys. Chem.* **1994**, 98, 6826-6834; (b) C. Schönenberger, J. A. M. Sondag-Huethorst, J. Jorritsma, L. G. J. Fokkink, *Langmuir* **1994**, 10, 611-614.
- ³¹ A. M. Rawlett, T. J. Hopson, L. A. Nagahara, R. K. Tsui, G. K. Ramachandran, S. M. Lindsay, *Appl. Phys. Lett.* **2002**, 81, 3043-3045.
- ³² F.-R. F. Fan, J. Yang, L. Cai, D. W. Price Jr., S. M. Dirk, D. V. Kosunkin, Y. Yao, A. M. Rawlett, J. M. Tour, A. J. Bard, *J. Am. Chem. Soc.* **2002**, 124, 5550-5560.
- ³³ J. M. Tour, A. M. Rawlett, M. Kozaki, Y. Yao, R. C. Jagessar, S. M. Dirk, D. W. Price, M. A. Reed, C.-W. Zhou, J. Chen, W. Wang, I. Campbell, *Chem. Eur. J.* **2001**, 7, 5118-5134.
- ³⁴ D. T. Gryko, C. Clausen, K. M. Roth, N. Dontha, D. F. Brocian, W. G. Kuhr, J. S. Lindsey, *J. Org. Chem.* **2000**, 65, 7345-7355.

Chapter 4

Fabrication of Arrays of Gold Islands on Self-Assembled Monolayers using Pulsed Laser Deposition through Nanosieves*

Sandwich structures of Au-SAM-Au were prepared by deposition of gold on alkylthiolate self-assembled monolayers (SAMs) on polycrystalline gold, using pulsed laser deposition (PLD) through a nanosieve. The arrays of sandwiches, around 700 nm in diameter, approximately 10 nm high and spaced 1.6 μm apart, were analyzed using atomic force microscopy. Electrochemical copper deposition experiments showed that about 15 % of the islands deposited on octadecanethiolate self-assembled monolayers were electrically insulated from the bottom gold electrode. This means that PLD is a suitable technique for the fabrication of metal-SAM-metal sandwich structures.

* Parts of this chapter have been published as: E. A. Speets, B. J. Ravoo, F. J. G. Roesthuis, F. Vroegindeweij, D. H. A. Blank, D. N. Reinhoudt, *Nano Lett.* **2004**, 4, 841-844 and F. Vroegindeweij, E. A. Speets, J. A. J. Steen, J. Brugger, D. H. A. Blank, *Appl. Phys. A* **2004**, 79, 743-745.

4.1 Introduction

A requirement for the development of devices that can be used to measure and exploit electronic properties of SAMs is the deposition of top electrodes on the SAM. Most of the methods used to electrically analyze SAMs use electrode/SAM/electrode systems that are not permanent, like a scanning tip or a mercury drop (Chapter 2). For the fabrication of working devices a permanent electrode on a SAM is of course necessary.

Deposition of metal electrodes on top of SAMs remains a bottleneck in the manufacturing of electronic devices. Due to the liquid crystalline like nature of a SAM on gold evaporated metal atoms diffuse to the S-Au interface, especially when noble metals are deposited on non-functionalized (inert, unreactive) SAMs. Often the substrate (SAM) is cooled down to liquid nitrogen temperature when the second electrode is deposited. In this way the SAM is not damaged because of overheating, while the SAM “crystallizes” making diffusion more difficult. Deposition results, however, are usually far from perfect. When electrodes larger than several tens of square nanometers are deposited the yield of devices without short circuits is generally low.¹

De Boer *et al.*² studied the metallic contact formation of vapor deposited metals and SAMs of conjugated mono and dithiols, using grazing incidence Fourier transform infrared (GI-FTIR) spectroscopy. They found that Au and Al penetrated into SAMs of the monothiol while Au and Al stayed on top of dithiol SAMs. This was caused by binding of the metal atoms with the top thiol groups of the SAM. Ti destroyed the SAM completely because of its reactivity towards organic compounds.

Allara *et al.* studied the interaction of vapor-deposited Al, Cu, Ag and Au atoms on a HS(CH₂)₁₆OCH₃ SAM on polycrystalline Au, using TOF-SIMS, IR-reflection spectroscopy and XPS.³ They found that Cu and Ag penetrated through the SAM and had a solvation-like interaction with the methoxy groups. Au diffused through the SAM, leaving the SAM in a kind of floating state (remaining on top of the gold). Al penetrated to the Au/S interface until a 1:1 Al/Au ratio was reached.⁴ The diffusion of Al probably occurs through the defects that arise because of the thermal

movement of metal-thiolate species. For aluminum these Al-thiolate species bind so strongly that the formation of transient defects is almost eliminated.

Czanderna *et al.* investigated the vacuum deposition of copper mercaptohexadecanoic acid (MHA) SAMs on gold.⁵ Submonolayer amounts of copper reacted with the COOH groups while the rest of the copper penetrated the SAM and formed adlayers at the Au-S interface. When deposition rates are fast and the temperature during deposition is lowered to 220 K the penetration of copper can be suppressed. When silver is deposited on these MHA SAMs no submonolayer reaction between the metal and acid groups takes place.⁶ Copper also interacts with SAMs terminated with CN⁷ or OH⁸ but in both cases the interaction is weak. For SAMs terminated with COOH, CN, OH, H₃COOC and CH₃ penetration to the Au-S interface is the dominant process.⁹

Organometallic vapor chemical deposition (OMCVD) was used to selectively deposit palladium on mixed biphenyldithiol (BDT) biphenylthiol (BT) SAMs on silver.¹⁰ Cp(allyl)Pd was employed as a precursor to deposit Pd(II) selectively on the BDT SAM over the BT SAM. The Pd(II) was bound to the BDT via a Pd-S bond. After prolonged deposition Pd starts to be deposited also on the BT parts.

Recently Rogers *et al.*^{11,12,13} developed so-called nanotransfer printing in which a poly-dimethylsiloxane (PDMS) stamp is used to transfer a layer of gold from the stamp onto a SAM. The advantage of this technique is that the gold is applied in bulk form and not as atoms like in vapor deposition techniques. Au is transferred from the PDMS stamp which has a limited interaction with the Au onto a thiol terminated SAM, on gallium arsenide (GaAs) or silicon-oxide (SiO₂), which acts as glue for the Au. To facilitate the transfer process an anti-sticking perfluoro-terminated SAM was deposited on the oxidized PDMS stamp.

Metzger *et al.* investigated rectification behavior of Langmuir-Blodgett (LB) films. To investigate whether the rectification is not caused by the asymmetric contacts, they prepared a gold/LB-layer/gold sandwich. Gold was deposited through a mask while the substrate was kept at liquid nitrogen temperature. Between the evaporation boat and the substrate a copper strip was placed to block the direct trajectory of the gold atoms.¹⁴ Besides that, the evaporation was done using a relatively high Ar pressure (between 8×10^{-4} and 3×10^{-3}), to make that the Au atoms would scatter off several Ar atoms before they reached the surface. When depositing

600 nm of Au *via* this method (measured using a Quartz Crystal Microbalance) only 17 nm was deposited on the sample.

In summary, metal deposition on SAMs on gold remains difficult because of the fragile nature of the SAMs and diffusion of the metal through the SAMs. In this Chapter a new method to deposit submicron sized gold islands on alkylthiolate SAMs is presented.

4.2 Pulsed laser deposition

In recent years PLD has been recognized as an excellent technique for the fabrication of inorganic thin films.^{15,16} The technique makes use of high intensity laser pulses to ablate small volumes of a target and bring them in a plasma phase. The plasma is directed perpendicularly from the target onto the substrate, which can be placed at a variable distance. In Figure 4.1 a schematic picture of a PLD (or laser ablation) setup is shown.

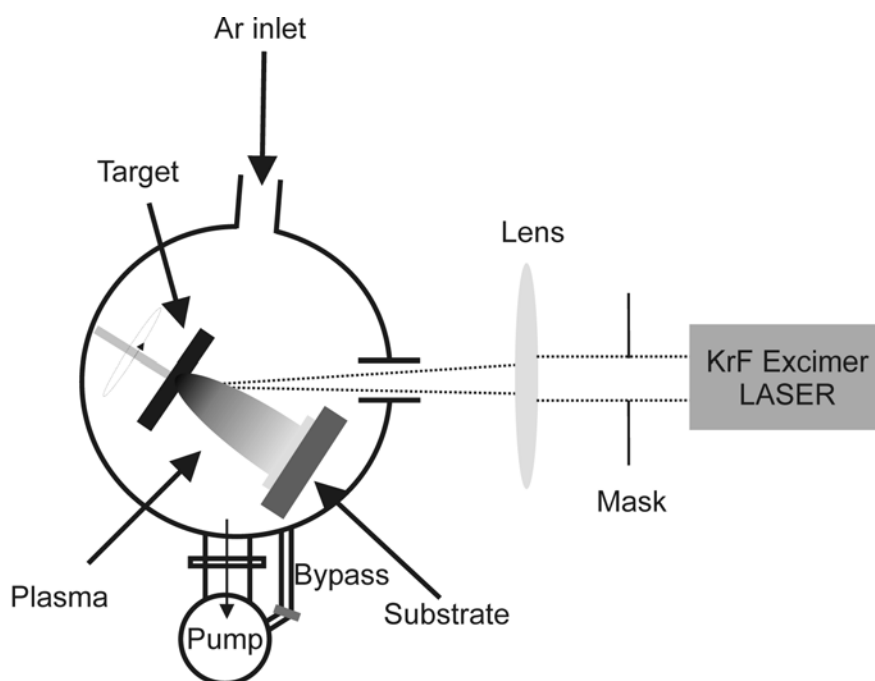


Figure 4.1 Schematic picture of a PLD system.

A gas inlet in the vacuum chamber facilitates the use of different background gases such as O₂ for the *in-situ* formation of oxides, or Ar as inert gas for the optimization of the deposition process, and a window to allow transmission of the laser pulses onto the target. An image of the laser passing through the mask is focused

on the target using a lens. The spot (image) size and intensity can be varied by moving the mask and moving the lens from and towards the target. The pump is connected to the system *via* a main valve and a bypass. By closing the main valve and regulating the bypass a broad range of gas-flow/pressure combinations can be used. The substrate is placed on a substrate holder/heater parallel to the target and can be moved in X, Y and Z directions. If necessary the substrate can be heated.

Differences between PLD and high vacuum (HV) gas phase deposition are the smaller distance between substrate and deposition material source in PLD, which is necessary for depositions at higher pressures, and the pulsed nature of the deposition. When using higher deposition pressures (by introducing a background gas) the ablated material will scatter and lose kinetic energy, but since the distance between target and substrate is in the order of a few centimeters, enough material will alight on the surface to facilitate high enough deposition rates.

PLD can be used to deposit a wide variety of inorganic compounds, and because of the ease of optimizing the deposition parameters it is a very versatile technique. Parameters that can be varied are the laser fluence (J cm^{-2}) which is the energy of the laser pulse per area on the target, the type of background gas, the background pressure (by pumping) and pressure of the gas (*via* the gas inlet, P (mbar)), the temperature of the substrate (T (K)), the distance between the target and the substrate (d (mm)), the spot size (mm^2) and the pulse frequency (f (Hz)). The pulse length is dependent on the laser used and cannot be changed from deposition to deposition. By varying the parameters the deposition speed as well as the kinetic energy of the particles and the nature of the particles as they land on the substrate can be changed. At lower pressures deposition takes place as atoms, like in conventional high vacuum (HV) gas phase deposition, while at higher pressures clusters can be formed because of the collisions of atoms. When depositing material on SAMs there are several restrictions in the deposition parameters. High substrate temperatures, usually necessary to obtain textured layers, cannot be used, because of the damage to the SAM, and also the kinetic energy of the ablated material should not be too high at the moment it reaches the substrate. This means that the distance of the target to the substrate cannot be too small and the background pressure cannot be too low.

4.2.1 Target ablation

PLD is based on ablation of a target material by interaction with laser pulses. The interaction of the UV light of the laser with the target material heats up a slab of the target and brings it in the gas phase. The plasma is an overheated gas, which will expand. Immediately after it is formed it has a temperature of several thousands Kelvin. Upon expansion the plasma will cool down rapidly, ensuring that after several centimeters (depending on pressure) the temperature has fallen approximately to ambient temperature. The ablation process is shown schematically in Figure 4.2. Because light with a given wavelength has a known depth of penetration in a given target material and because the spot size on the target is known, it can be estimated how much material is ablated in one pulse. The amount of ablated material also depends on the reflectivity of the material and the laser fluence.

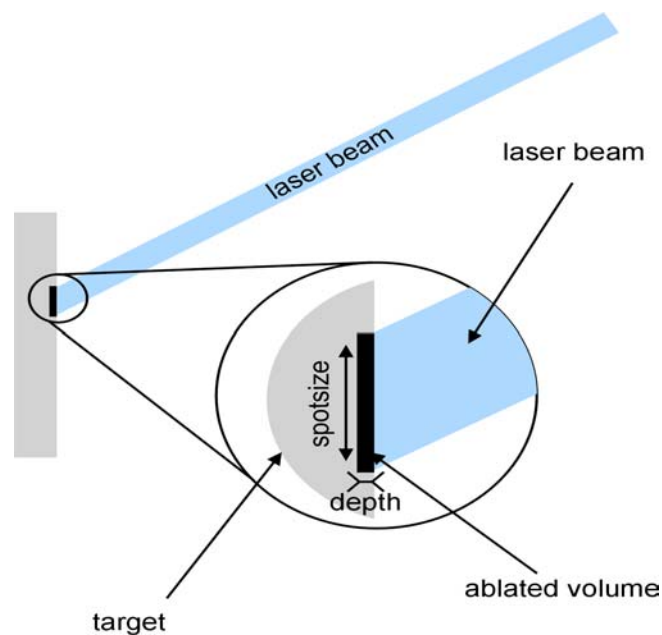


Figure 4.2 First step in the ablation of target material by a laser pulse.

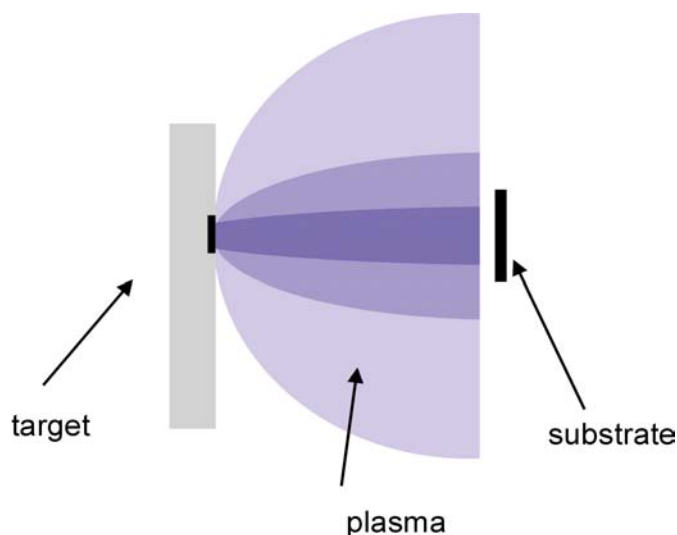


Figure 4.3 Plasma formation at different pressures after a laser pulse hits the target. The darker region corresponds to plasma at high pressure (scattering), lighter regions at lower pressures (less scattering).

Figure 4.3 shows how the plasma that is formed after the laser pulse expands towards the target. In the first part of the pulse, the volume of target is brought into the gas-phase, which is heated further into a plasma by the last part of the pulse. The plasma will then expand adiabatically, cooling down and emitting light. As shown in Figure 4.3 the plasma will be less broad at higher pressures because of scattering of the plasma caused by the gas atoms.

When the fluence is higher the kinetic energy of the ablated atoms in the plasma is higher. The correct position of the sample in the plasma is for this reason also dependent on the fluence. Since SAMs are easily damaged by the impact of the ablated particles and the heat of the plasma, the pressure during deposition cannot be too low and the distance between target and substrate should not be too small.

4.2.2 Nanosieves as shadow masks

The nanosieves used are thin silicon nitride (Si_3N_4) membranes that contain large arrays of holes of 300 nm minimum diameter.¹⁷ Nanosieves, which are commercially used for the filtration of beer,¹⁸ act as shadow masks that are placed directly on top of the substrate. During the deposition, the sieve will block the ablated material, except where the holes are present, thus replicating the pattern of the sieve on the substrate with the ablated material.

Besides the patterning, the nanosieve as shadow mask for PLD, has a secondary effect on the deposition. Because the pores are relatively narrow and deep the amount of material that reaches the substrate is lower than when no sieve is used. In other words the height of the islands is lower than the thickness of a layer prepared using the same parameters but without a sieve. Figure 4.4 A shows an SEM image of the sieve used as a mask for this deposition. The pores have a minimum diameter of 300 nm but the diameter of the opening of the pores, which are facing the SAM during the deposition, is 500 nm. The thickness of the silicon nitride membrane is 1.5 μm and the center-to-center spacing of the pores is 1.6 μm . The sieve consists of several silicon nitride membranes which span an area of $150 \times 1000 \mu\text{m}$ each. These membranes are supported by a $0.6 \times 0.6 \text{ cm}$ silicon chip (Figure 4.4 B). Hence, deposition of metal on a SAM through these nanosieves occurs only on the parts of the SAM directly below the pores. In this way, most of the surface remains unaffected and is available as internal control tool, making it possible to analyze both gold-SAM-gold structures and native SAM on one sample at the same time.

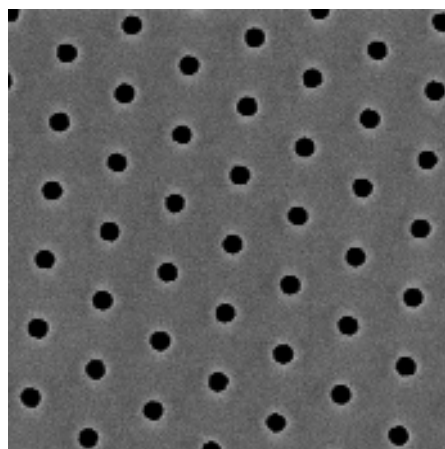


Figure 4.4 (A) SEM image of the silicon nitride membrane of the nanosieve ($10 \times 10 \mu\text{m}$). The distance between the pores is $1.6 \mu\text{m}$, the diameter is 500 nm at the opening and 300 nm inside the pores.

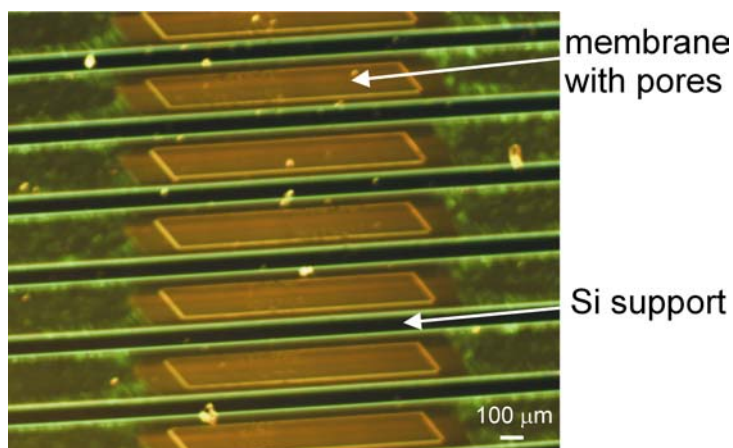


Figure 4.4 (B) Light microscopy image of the nanosieve chip. The thin (black) bands are the silicon support, the broad lines are the silicon nitride membranes. Only the center parts of the membranes contain pores.

The sieves were pressed directly on the SAM without spacers because of the high mobility of gold on SAMs and because of the diffuse character of the deposited material. In Figure 4.5 a schematic drawing of the sieve pressed on the substrate is shown. The sieve is glued onto a holder (made from metal sheet) using two-component glue. The sieve holder is gently screwed on the substrate holder with 3 screws, ensuring that the sieve is attached flat to the substrate.

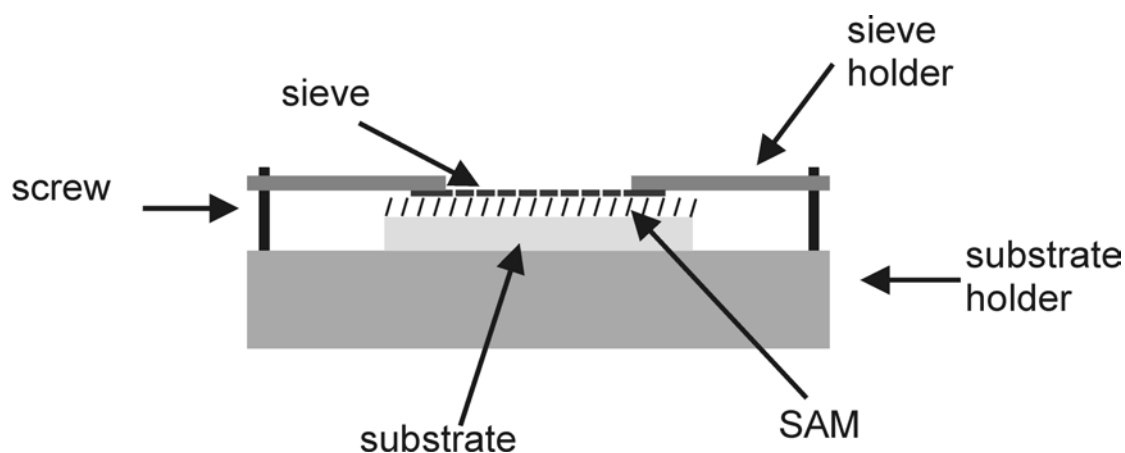


Figure 4.5 Substrate with SAM on substrate holder with sieve placed directly on top.

The contact between the substrate and the sieve is never perfect in this experimental system. Two solid objects can not be brought in conformal contact at the micro- or nanoscale so easily. Also the handling of the substrate, *i.e.* the placing and removing of the sieve, causes local damage to the SAM. After depositing gold for some time the pores of the nanosieves can become clogged.¹⁹ To clean the sieves they

are immersed in an aqueous gold-etch solution.²⁰ After etching the sieves were rinsed with water and ethanol and could be used again without a problem.

4.3 Deposition of gold islands on SAMs

Two candidate molecules for SAMs were chosen on which gold was to be deposited, *viz.* octadecanethiol (ODT), which is known to form very well packed SAMs,²¹ and 1,9-nonanedithiol (NDT), which forms SAMs with less order than ODT but which has a thiol group pointing upwards, which can act as glue for deposited gold (Chapter 3).²² Figure 4.6 illustrates fabrication of Au islands on SAMs.

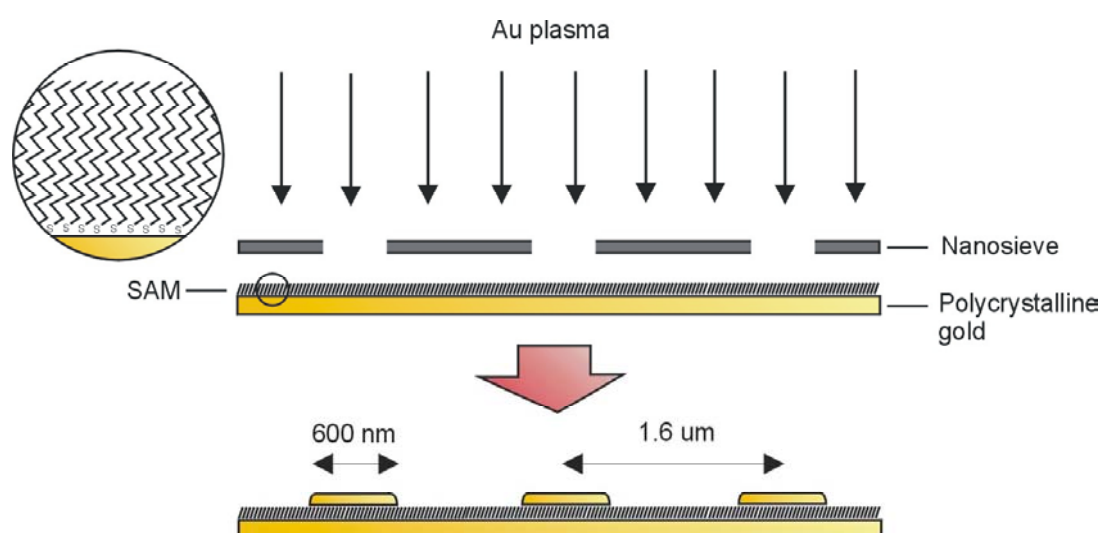


Figure 4.6 Schematic representation of gold deposition through a nanosieve on an alkanethiolate SAM on gold.

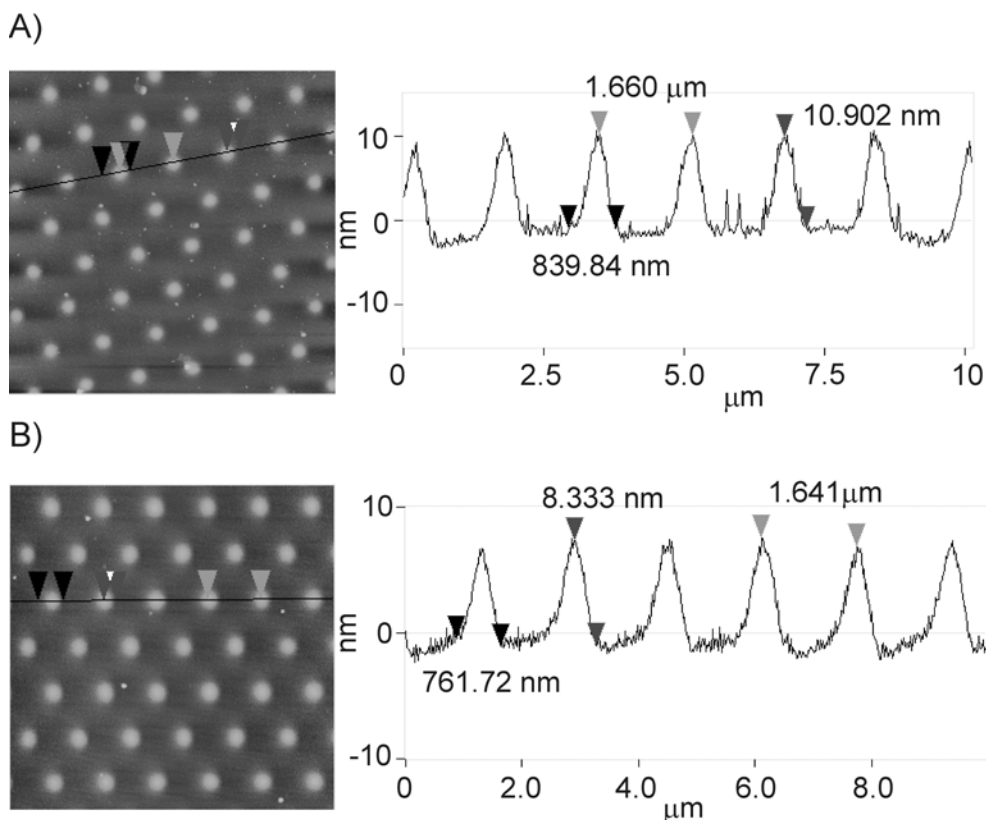


Figure 4.7 AFM height images ($10 \times 10 \mu\text{m}$) and section analyses of (A) an ODT SAM and (B) an NDT SAM, with gold islands deposited via PLD through a nanosieve.

Figure 4.7 shows that the hexagonal pattern of circular holes of the nanosieve has been replicated on the SAM. As can be seen from the section analysis of Figure 4.7 the deposited islands have a diameter of around 800 nm, which is considerably larger than the size of the holes in the sieve. Probably the contact between the sieve and the SAM had been not optimal, and diffusion of Au over the SAM surface as well as expansion of the ablated Au via scattering has taken place. The center-to-center distance of the islands is however 1.6 μm, which is the same as for the holes in the sieve. Because the distance of the holes in the sieve is large enough the islands do not touch each other. Furthermore it can be seen that the type of SAM that is used does not influence the pattern formation on the surface.

4.3.1 Insulation of the gold islands from the gold substrate by the SAM

To demonstrate that the deposited gold islands were not covered by the SAM (as a result of diffusion of Au through the SAM) a new SAM was prepared on the gold islands. The sample was immersed for 5 minutes in a 1H,-1H,-2H,-2H-

perfluorodecanethiol solution (~ 5 mM in CH_2Cl_2), after which XPS analyses were performed to measure the relative fluorine concentration on the islands, compared to the reference SAM. This is possible because of the design of the nanosieve, which gives a pattern of islands only on a limited part of the surface. Due to the spot size of the X-ray beam used in XPS (~ 10 μm minimum diameter) the islands cannot be analyzed individually. The XPS measurement is averaged over an area of several tens to hundreds of square microns, *i.e.* on the islands together with the native SAM in between the islands (Figure 4.8). The analyses showed that the concentration of fluorine in the areas with islands was much higher than on the reference areas outside the patterned part of the sample (Table 4.1). It can be concluded that the surface of the gold islands remains exposed after PLD and that a SAM of fluorinated thiols can be readily prepared on top of these islands. Some fluorine is also detected in the reference areas of the samples where no islands were deposited as a result of the insertion of fluorinated thiol molecules from solution into the existing SAM. The higher content of fluorine on the islands compared to the reference SAM measured for the ODT SAM compared to that for the NDT SAMs is in agreement with this. Insertion and replacement of thiolates is slower in SAMs that are well packed.²³

Table 4.1 Elemental ratio of fluorine to carbon of samples after immersion in a fluorinated thiol solution, as calculated from XPS measurements.^a

SAM	[F]/[C] islands	[F]/[C] SAM	[F]/[C] islands / [F]/[C] SAM
NDT	0.88	0.19	4.6
ODT	0.15	0.006	25

^a The fluorine to carbon ratio is given for areas of the SAM where gold islands were deposited ([F]/[C] islands) and for areas of the SAM where no gold islands were deposited ([F]/[C] SAM).

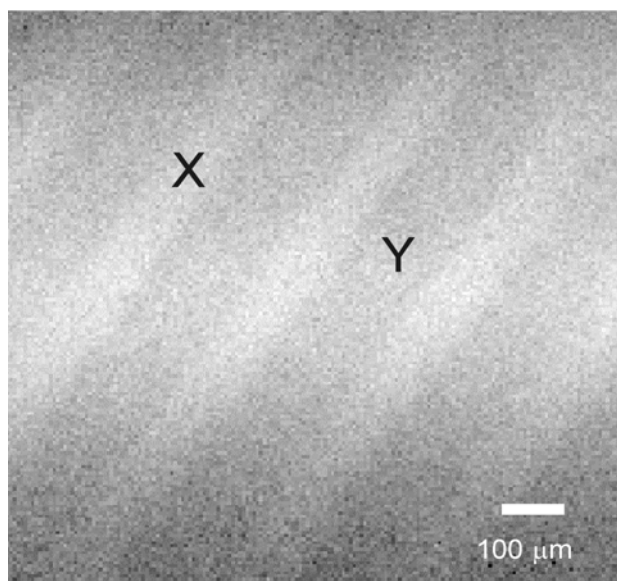


Figure 4.8 Scanning X-ray image which shows dark lines (gold islands) and light lines (only SAM). X (native SAM) and Y (gold islands and SAM) mark the spots where XPS analyses were done (Scale 1000 × 1000 μm).

The scanning X-ray image (SXI) shows a pattern of dark and light lines, which corresponds to the freestanding membrane parts with pores (see Figure 4.4 B) of the nanosieve. Dark areas indicate the presence of Au islands, which are absent from the light areas. The individual Au islands are not resolved by SXI.

4.3.2 Electrochemical investigation of the insulation of the gold islands

A quick method to investigate if thousands of islands are electrically insulated from the underlying gold substrate by the SAM in a parallel way is electrochemical copper deposition. At a slight overpotential²⁴ Cu^{2+} is reduced from an aqueous CuSO_4 solution on the substrate. Provided that modest potentials are used, islands without short circuits behave as electrically insulated objects, while islands with short circuits to the bottom electrode behave as small electrodes and hence copper will “grow” on them (Figure 4.9). The bare SAM acts as internal reference to see if the SAM shields the gold substrate and copper deposition does not take place everywhere. The substrate after PLD of Au was used as working electrode and an aqueous solution of CuSO_4 (10 mM) and H_2SO_4 (10mM) as the electrolyte. A Pt disc was used as a counter electrode and placed close to the working electrode in a parallel geometry.

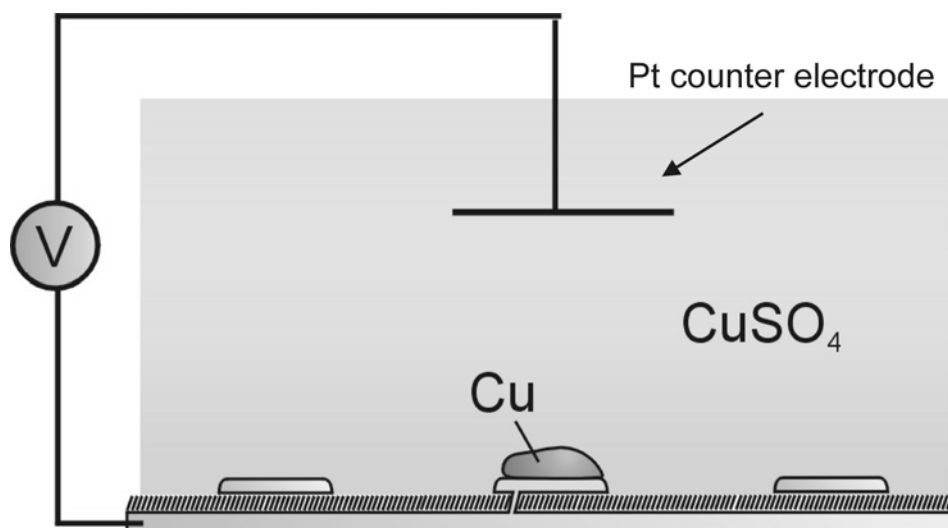


Figure 4.9 Schematic representation of electrochemical copper deposition on insulated and non-insulated gold islands.

One cycle from -0.7 to -0.75 V (vs. Hg/HgSO₄, at 0.01 V s⁻¹) was used to reduce Cu(II) from solution on the non-insulated islands. With ODT SAMs part of the Au islands deposited at 10^{-2} mbar showed Cu deposition while others remained unaffected (Figure 4.10).

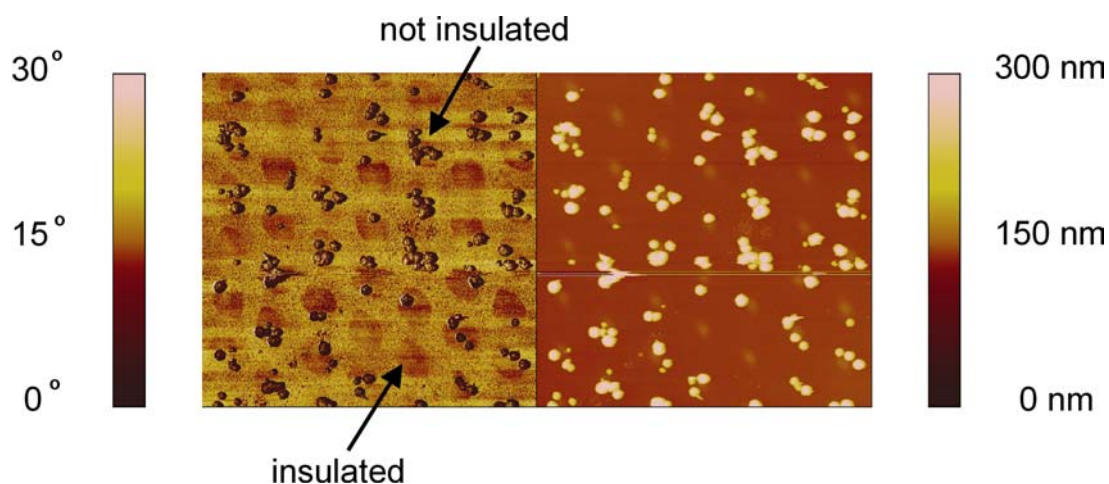


Figure 4.10 AFM phase and height images of an ODT SAM on Au after subsequent pulsed laser deposition of Au islands and electrochemical copper deposition. (Scale of both scans: 10×10 μm).

When a deposition pressure of 10^{-3} mbar or lower was used no insulated islands were obtained: electrochemical experiments showed that all the islands showed Cu deposition. When higher deposition pressures were used the islands grew together laterally and could no longer be distinguished as individual “electrodes”.

With NDT SAMs no insulated islands were found, *i.e.* all islands showed Cu growth, even when lower deposition pressures were used (10^{-2} mbar).

Figure 4.10 shows that on 15 % of the Au-islands on the ODT SAM Cu did not grow, which indicates that these islands are insulated from the bottom electrode by the ODT SAM. It also shows that no Cu did not grow on the SAM itself, indicating that there are no significant defects in the monolayer.²⁵ This observation demonstrates that Cu deposition can only take place on areas where there is electrical contact with the Au-substrate. From these electrochemical experiments it can further be concluded that the islands are not connected. The height of the Cu clusters is constant, in this experiment around 80 nm, indicating that the deposition starts simultaneously on all the non-insulated islands. Cu growth has been confirmed by XPS analyses of the patterned substrate: when analyzing the islands a considerable amount of Cu (Cu/C = 0.13) was detected, confirming that the material on the islands is Cu. Outside of the electrode region no Cu could be found (Cu/C = 0).

When the electrochemical deposition experiment was performed on a sample on which a monolayer of fluorinated thiols had been formed on the islands no Cu growth took place at all. The fluorinated SAM that has formed on top of the exposed islands shields the surface from Cu deposition in the same way as the SAM around the islands does.

To check whether Au islands deposited on inert ODT SAMs were stable such a sample was sonicated in an ethanol/water mixture. As can be seen in Figure 4.11 the gold islands remain attached even after 1 minute of sonication. This means that for islands with these dimensions SAMs with reactive SH surface groups (such as NDT), are not necessary to attach the gold islands on the surface.

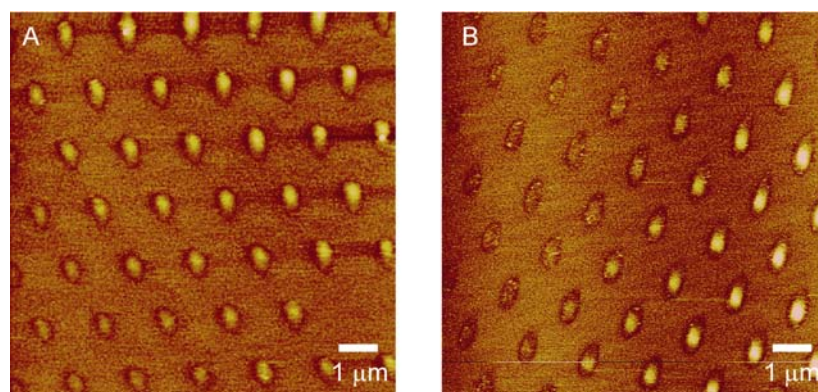


Figure 4.11 AFM height images of (A) Au islands deposited on an ODT SAM (deposition conditions: $P=0.01$ mbar, 4 min at 8 Hz, 40 mm, 4 J cm^{-2}) and (B) same sample after 1 minute sonication in water/ethanol (height scale ranges from 0-10 nm).

4.4 Conclusions

PLD in combination with nanosieve shadow masks is a useful tool to deposit arrays of gold electrodes on top of SAMs of ODT. Electrochemical copper deposition experiments and AFM show that around 15 % of the islands is not in electrical contact with the bottom electrode. NDT SAMs gave no insulated islands so it seems that the packing of the SAM is more important than the head group, when depositing metal islands on SAMs. The fact that it is possible to deposit a new fluorinated thiol SAM on the gold islands shows that bare gold is available on top of the islands and that the islands are not buried under the ODT SAM.

4.5 Experimental procedures

General: All glassware used was cleaned in Hellmanex detergent. The glass was immersed in a 2 % solution of Hellmanex in Millipore Q2 water and sonicated for 45 minutes, then rinsed with large amounts of MilliQ water. Gold substrates were obtained from Ssens (Hengelo the Netherlands) and consisted of 20 nm of evaporated gold on silicon with a 2 nm titanium adhesion layer. Before use, the substrates were immersed in HPLC grade dichloromethane for 15 minutes. Octadecanethiol (ODT) (98 %, Janssen Chimica) and nonanedithiol (NDT) (95 %, Acros) were used without further purification. The gold was immersed in mM solutions of ODT in ethanol *p.a.* and NDT in hexane (Acros, HPLC grade).

SAM preparation: ODT SAMs were prepared from ~ 1mM solutions in ethanol *p.a.* NDT SAMs were prepared from ~ 1 mM solutions in hexane (Acros, HPLC grade). A description of the preparation and analysis is given in Chapter 3.

Pulsed laser deposition: A Compex 205 KrF excimer laser of Lambda Physik emitting 25 ns pulses at 248 nm was used. Deposition pressures of 10^{-1} mbar to 10^{-7} mbar were used with argon as background gas, an argon flow was used from 0.2 mbar $l\ min^{-1}$ to $7.5\ ml\ min^{-1}$ depending on the working pressure. A laser fluence of $4\ J\ cm^{-2}$ was used, with a spot size of $\sim 3\ mm^2$. The laser beam entered the vacuum chamber at an angle of 45° with respect to the target normal. The substrate was placed parallel to the target at a distance of 40 mm. The pulse frequency was 8 Hz. The Au target was 4N (99.99 % pure) and obtained from Engelhard-CLAL (Drijfhout B.V.) Netherlands.

XPS: XPS analyses were performed on a Quantera SXM, from Physical Electronics equipped with monochromator. The X-ray source is Al with $K\alpha$ of 1486.6 eV. The spot size could be varied between 10 and 100 μm in diameter. The bundle was scanned over a surface in order not to damage the SAM by staying for a long time on one spot. C_{1s} (284.8 eV), $Cu\ 2p_{3/2}$ (932.5 eV) and F_{1s} (689.5 eV) peaks were used for concentration measurements. C_{1s} was chosen as reference and set at 284.8 eV.

Cu deposition: Electrochemistry was performed using an Autolab PGSTAT10 potentiostat, in a custom built electrochemical cell equipped with a platinum counter electrode, a mercury sulfate (MSE) reference electrode ($V_{MSE} = + 0.61\ vs.\ V_{NHE}$) and using the substrate as working electrode, attached to the bottom of the cell closed with an O ring. An aqueous solution of 10 mM H_2SO_4 and 10 mM $CuSO_4$ was purged with nitrogen for 10 minutes before the experiments. 1 cycle of -0.70 to -0.75 V vs. MSE at a scan-speed of 0.01 V/s was used to deposit copper. After the experiment the samples were washed very gently with water and ethanol.

AFM: AFM was performed on a Nanoscope III multimode AFM (Digital Instruments, Santa Barbara, Ca., USA) in the *tapping mode* using the J-scanner. Silicon cantilevers (Nanosensors, Neufchatel Switzerland) with stiffness between 37

and 56 N m^{-1} were used. Measurements were performed at frequencies slightly lower than the natural resonance frequency of the cantilever in air ($\sim 300 \text{ kHz}$). All AFM analyses were performed at room temperature and ambient pressure. Samples were attached to a magnetic holder using double-sided stickers and removed from the holder for every single experiment.

4.6 References

- ¹ (a) M. D. Austin, S. Y. Chou, *Nano Lett.* **2004**, 4, 535-535; (b) J.-O. Lee, G. Lientschnig, F. Wiertz, M. Struijk, R. A. J. Janssen, R. Egberink, D. N. Reinhoudt, P. Hadley, C. Dekker, *Nano Lett.* **2003**, 3, 113-117.
- ² B. de Boer, M. M. Frank, Y. J. Chabal, W. Jiang, E. Garfunkel, Z. Bao, *Langmuir* **2004**, 20, 1539-1542.
- ³ A. V. Walker, T. B. Tighe, O. M. Cabarcos, M. D. Reinard, B. C. Haynie, S. Uppili, N. Wiongrad, D. L. Allara, *J. Am. Chem. Soc.* **2004**, 126, 3954-3963.
- ⁴ G. L. Fisher, A. V. Walker, A. E. Hooper, T. B. Tighe, K. B. Bahnk, H. T. Skriba, M. D. Reinard, B. C. Haynie, R. L. Opila, N. Winograd, D. L. Allara, *J. Am. Chem. Soc.* **2002**, 124, 5528-5541.
- ⁵ L. S. Dake, D. E. King, A. W. Czanderna, *Solid State Sci.* **2000**, 2, 781-789.
- ⁶ G. C. Herdt, A. W. Czanderna, *J. Vac. Sci. Technol. A* **1995**, 13, 1275-1280.
- ⁷ D. R. Jung, D. E. King, A. W. Czanderna, *J. Vac. Sci. Technol. A* **1993**, 11, 2382-2386.
- ⁸ D. R. Jung, D. E. King, A. W. Czanderna, *Appl. Surf. Sci.* **1993**, 70/71, 127-132.
- ⁹ G. C. Herdt, A. W. Czanderna, *J. Vac. Sci. Technol. A* **1993**, 11, 2382-2386.
- ¹⁰ U. Weckenmann, S. Mittler, S. Krämer, A. K. A. Aliganga, R. A. Fisher, *Chem. Mater.* **2004**, 16, 621-628.
- ¹¹ Y.-L. Loo, R. L. Willet, K. W. Baldwin, J. A. Rogers, *J. Am. Chem. Soc.* **2002**, 124, 7654-7655.
- ¹² Y.-L. Loo, D. V. Lang, J. A. Rogers, J. W. P. Hsu, *Nano Lett.* **2003**, 3, 913-917.
- ¹³ E. Menard, L. Bilhaut, J. Zaumseil, J. A. Rogers, *Langmuir* **2004**, 20, 6871-6878.
- ¹⁴ T. Xu, I. R. Peterson, M. V. Lakshminantham, R. M. Metzger, *Angew. Chem. Int. Ed.* **2001**, 40, 1749-1752 (and references therein).
- ¹⁵ D. B. Chrisey, G. K. Hubler (Eds.), *Pulsed Laser Deposition of Thin Films*, Wiley, New York, **1994**.
- ¹⁶ (a) P. R. Willmott, J. R. Huber, *Rev. Mod. Phys.* **2000**, 72, 315-328; (b) M. Strikovski, J. H. Miller Jr., *Appl. Phys. Lett.* **1998**, 73, 1733-1735; (c) L. M. Doeswijk, G. Rijnders, D. H. A. Blank, *Appl. Phys. A* **2004**, 78, 263-268; (d) G. Rijnders, Ph.D. Thesis, University of Twente, Netherlands **2001**, ISBN 90-365-1657-9, p. 13-18.
- ¹⁷ (a) J. Brugger, J. W. Berenschot, S. Kuiper, W. Nijdam, B. Otter, M. Elwenspoek, *Microelec. Eng.* **2000**, 53, 403-405; (b) M. Kolbel, R. W. Tjerkstra, J. Brugger, C. J. M. van Rijn, W. Nijdam, J. Huskens, D. N. Reinhoudt, *Nano Lett.* **2002**, 2, 1339-1343; (c) Nanosieves (trade name is microsieve) were bought from Aquamarijn Micro Filtration B.V., Hengelo (Gld.), The Netherlands.

- ¹⁸ S. Kuiper, C. van Rijn, W. Nijdam, O. Raspe, H. van Wolferen, G. Krijnen, M. Elwenspoek, *J. Membr. Sci.* **2002**, 196, 159-170.
- ¹⁹ M. Kölbl, R. W. Tjerkstra, G. Kim, J. Brugger, C. J. M. van Rijn, W. Nijdam, J. Huskens, D. N. Reinhoudt, *Adv. Funct. Mater.* **2003**, 13, 219-224.
- ²⁰ Y. N. Xia, G. M. Whitesides, *Angew. Chemie. Int. Ed.* **1998**, 37, 551-575.
- ²¹ M. D. Porter, T. B. Bright, D. L. Allara, C. E. D. Chidsey, *J. Am. Chem. Soc.* **1987**, 109, 3559-3568.
- ²² (a) S. Chah, J. H. Fendler, J. Yi, *Chem. Commun.* **2002**, 18, 2094-2095; (b) P. Kohli, K. K. Taylor, J. J. Harris, G. J. Blanchard, *J. Am. Chem. Soc.* **1998**, 120, 11962-11968.
- ²³ (a) J. B. Schlenoff, M. Li, H. Ly, *J. Am. Chem. Soc.* **1995**, 117, 12528-12536; (b) J. A. M. Sondag-Huethorst, C. Schönenberger, L. G. J. Fokkink, *J. Phys. Chem.* **1994**, 98, 6826-6834.
- ²⁴ Potential used was based on Pourbaix diagrams and previous experiments on bare SAMs.
- ²⁵ J. A. M. Sondag-Huethorst, L. G. J. Fokkink, *Langmuir* **1995**, 11, 4823-4831.

Chapter 5

Pulsed Laser Deposition of Noble Metal Clusters on Self-Assembled Monolayers*

Nanometer-size noble metal clusters on top of alkylthiolate self-assembled monolayers (SAMs) on annealed gold were fabricated using pulsed laser deposition in the presence of a background gas. Size distributions of the clusters depended on the metal and on the pressure during deposition. Conducting probe atomic force microscopy (CP-AFM) and scanning tunneling microscopy (STM) showed that the clusters were insulated from the substrate by the SAM. Room temperature Coulomb blockades could be measured with STM for Pd clusters on decanethiol SAMs.

* Part of this chapter has been accepted for publication: E. A. Speets, B. Dordi, B. J. Ravoo, N. Oncel, A.-S. Hallbäck, H. J. W. Zandvliet, B. Poelsema, G. Rijnders, D. H. A. Blank, D. N. Reinhoudt, *Small* **2005**, 1, 395-398.

5.1 Introduction

The electronic parameters of single immobilized molecules cannot be derived straightforwardly from systems as described in Chapter 4, which have junction areas containing many thousands of molecules. Inhomogeneities and pinholes in the SAM influence the “bulk” measurements so that a measured value is a combination of multiple electronic effects.

For single molecule studies the size of the top electrodes should be in the order of nanometers.^{1,2,3} Small metal clusters placed on top of a SAM can be used for this purpose. Ohgi *et al.* investigated the difference between Au evaporation on “reactive” dithiol and “unreactive” monothiol SAMs by STM.⁴ They found that with monothiols Au penetrated through the SAM to form monoatomic height islands under the SAMs while with dithiols Au particles were formed on top of the SAM. Earlier STM measurements were performed on Au clusters deposited *via* a cluster beam source⁵ on short dithiol SAMs.^{6,7} Cluster beam evaporation uses a cold gas flow to aggregate gas phase metal atoms into clusters. Henderson *et al.* deposited Au clusters with a cluster beam source on SAMs of dithiols and diisocyanides and analyzed them with STM.⁸

Stabilized Au colloids can be attached from solution to thiol groups on a surface.^{9,10} This protocol does not work for non-sticky surfaces and the organic stabilizer of the metal clusters might interfere with the electronic measurements. Small noble metal clusters were also deposited on SAMs *via* evaporation of Au,¹¹ chemical reduction of silver nitrate¹² or *via* self-assembly of hexanethiol stabilized Au clusters.¹³

In this Chapter a new fabrication method for nanometer size metal clusters on top of SAMs is reported. Clusters were deposited on SAMs by PLD. Depositions are carried out without using a nanosieve as described in Chapter 4 for reasons of simplicity, and a much lower number of pulses was used (10 *vs.* ~1000) to prevent formation of larger aggregates. The main goal of this investigation was the deposition of clusters on SAMs in such a way that they are electrically insulated from the Au substrate and without destroying the SAM. These small metal clusters are an excellent tool for the analysis of surface bound molecules with scanning probe techniques.¹⁴

5.2 Preparation of nanometer size metal clusters

Metal was deposited first on TEM grids in order to see whether clusters are formed and to investigate the dependence of the cluster size on the deposition parameters. PLD of Au using 10 laser pulses, at a repetition rate of 4 Hz, gave a reasonable surface coverage without creating large aggregates of metal. TEM (Figure 5.1) showed that the Au is present as small clusters.

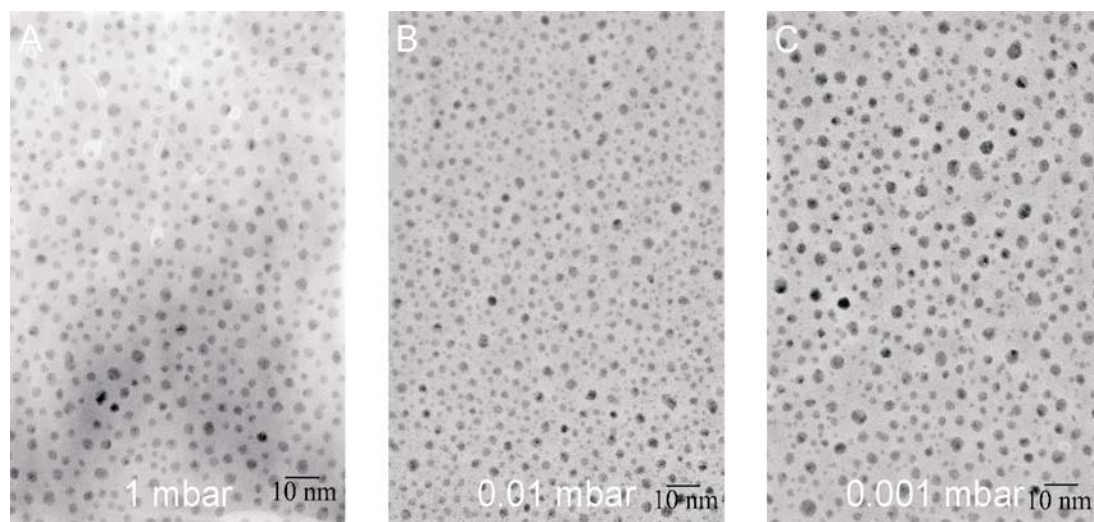


Figure 5.1 TEM images of Au clusters made with 10 pulses at 40 mm target/substrate separation (laser fluence 4 J cm^{-2} , spot size 3 mm^2). The Ar-pressure is indicated in white. The average sizes of the clusters are (A) $2.67 \pm 0.60 \text{ nm}$, (B) $2.40 \pm 0.50 \text{ nm}$, (C) $2.30 \pm 0.94 \text{ nm}$.

The average diameter of the clusters at different deposition pressures is comparable. Clusters formation probably takes place on the surface and aggregation in the plasma does not seem to be important at these pressures. The size distribution is narrower at higher pressures than at lower pressures. A possible reason for this might be that small clusters on the surface aggregate to form larger clusters. From the clusters coverage on the surface measured by TEM it can be estimated that around 0.2 \AA of Au is deposited per pulse. This value does not depend significantly on the pressure. The surface coverage (calculated using grey scale analysis) of the clusters is roughly 20 % for pressures ranging from 0.001 to 1 mbar. The line structure of the Au crystal planes (Figure 5.2) indicates that the Au clusters are crystalline.

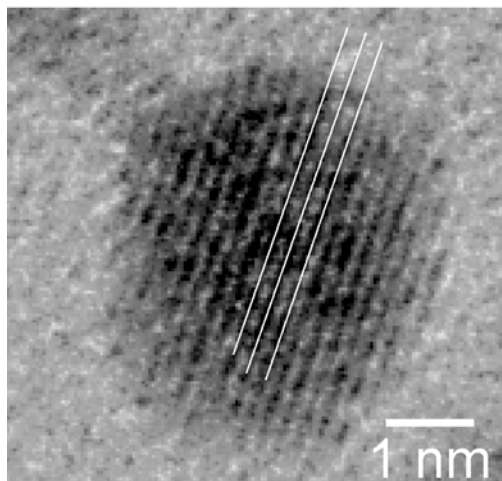


Figure 5.2 Zoomed in TEM image of a Au cluster deposited at 0.01 mbar Ar pressure on a TEM grid (10 pulses) $d = 0.23$ nm (Au(111)), white lines indicate crystal planes.

Figure 5.3 shows TEM images of Au clusters deposited at different target/substrate distances. Because of the directionality of PLD and the relatively high pressures that are used the position of the substrate relative to the target is important. The distance between the target and the substrate also influences the cluster size. Figure 5.3 shows that Au clusters deposited on TEM grids that were placed 60 mm away from the target are significantly smaller than when the grid was placed at a distance of 40 mm. Which indicates that surface growth is the most important cluster formation regime. The surface coverage at 60 mm distance (~ 10 %) was also significantly lower than at 40 mm distance (~ 20 %).

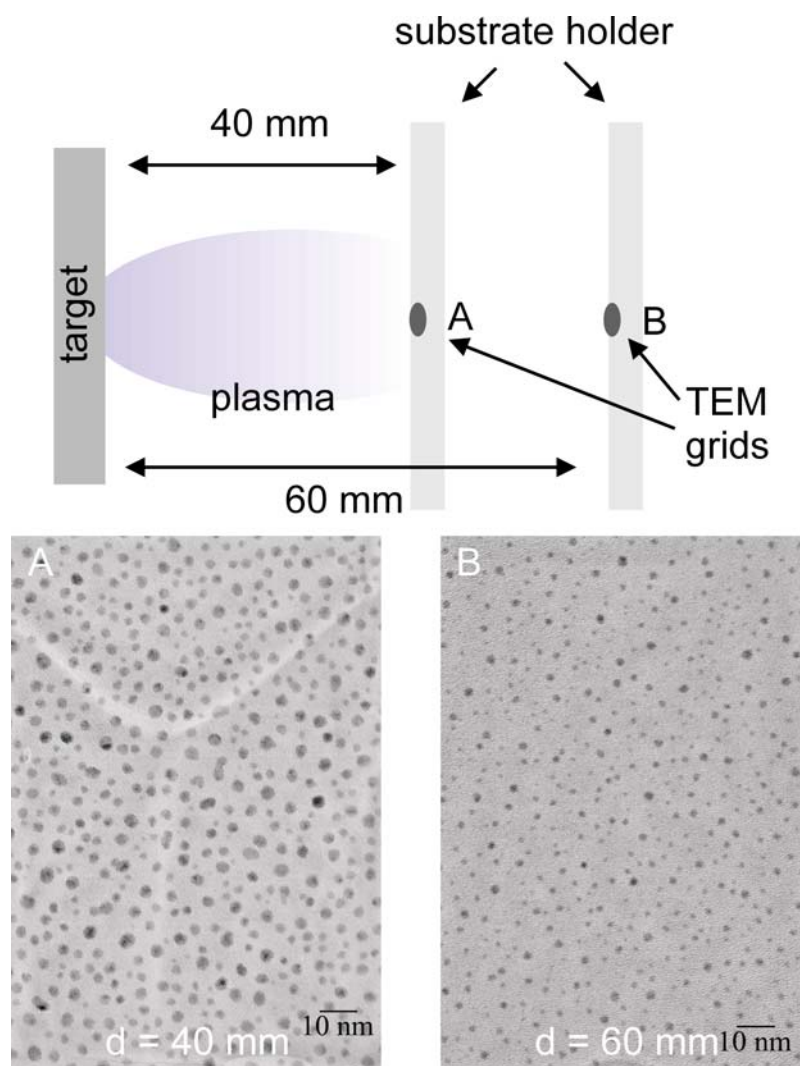


Figure 5.3 Schematic experimental setup and TEM images of Au clusters deposited on TEM grids at varying distances from the target, (10 pulses at $p = 0.5$ mbar) The average size of the clusters is (A) 2.66 ± 0.67 nm (B) 1.71 ± 0.37 nm.

Samples made by deposition on TEM grids placed 1.5 cm away from the normal of the plasma on the substrate holder show a much lower surface coverage as well as smaller clusters. In Figure 5.4 two TEM-images of clusters made using 10 pulses at 0.01 mbar are shown.

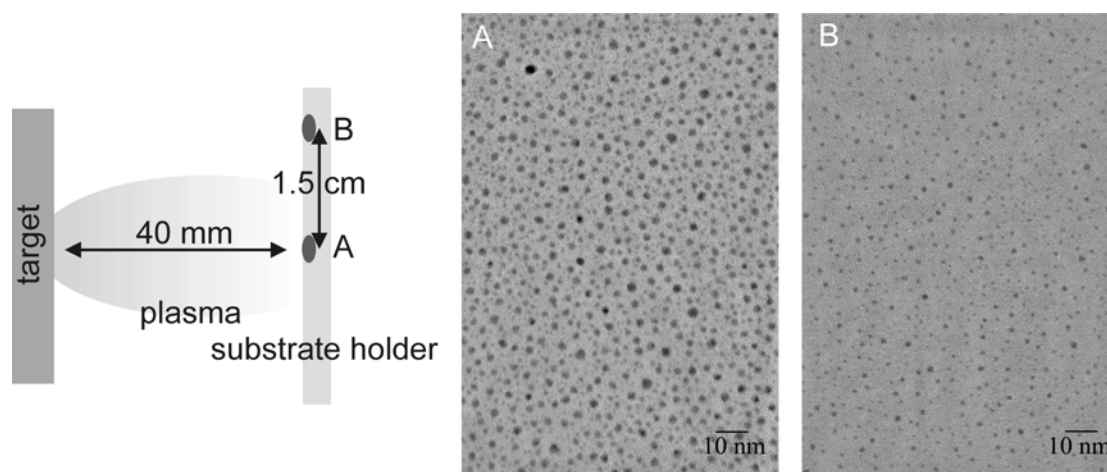


Figure 5.4 TEM images of Au clusters deposited on TEM grids during the same deposition (10 pulses, $p = 0.01$ mbar), on a different location on the substrate holder. The average size of the clusters is (A) 2.35 ± 0.58 nm, (B) 1.44 ± 0.26 nm.

It can be seen from Figure 5.4 that the alignment of the plasma with the substrate is very important when depositing on small substrates. The distance between point B and the laser spot on the target is not significantly larger than that of spot A (43 mm vs. 40 mm). The difference between the two samples is caused by the fact that the centre of the plasma arrives straight at point A while only the outer, most diffuse part of the plasma arrives at point B.

When more pulses are used to form metal clusters aggregation of clusters occurs. This can be seen in Figure 5.5 A and B. The clusters in Figure 5.5 B are much larger and often have irregular shapes, indicating that they have formed by the fusion of two or more clusters.

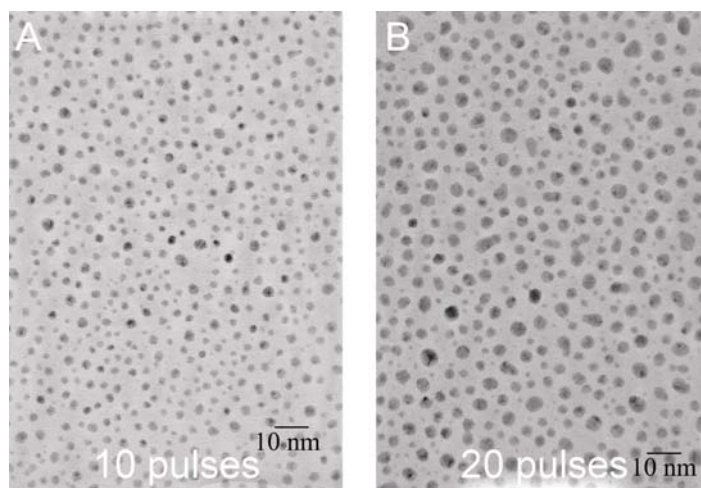


Figure 5.5 TEM images of Au clusters deposited using different number of pulses ($p = 0.1$ mbar, fluence = 4 J cm^{-2}). The average size of the clusters is (A) $2.40 \pm 0.50 \text{ nm}$ (B) $3.11 \pm 0.79 \text{ nm}$.

Figure 5.5 B shows that besides the large aggregates also smaller clusters are present on the surface. The larger clusters seem to be the result of aggregation of several smaller clusters.

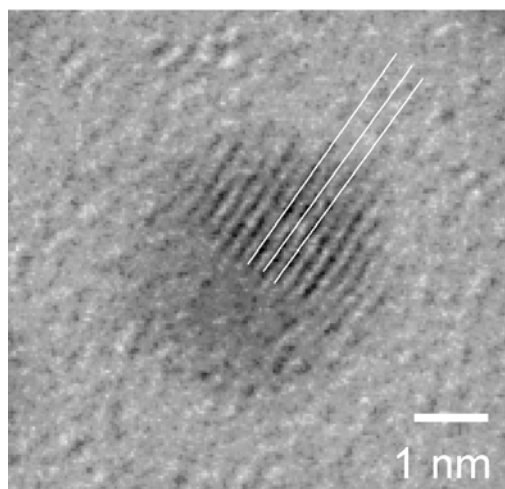


Figure 5.6 Close-up TEM image of a cluster after deposition of 20 laser pulses Au at $p = 0.1$ mbar (Figure 5.5 B), $d = 0.24 \text{ nm}$ (Au(111)), white lines indicate crystal plane.

The cluster shown in Figure 5.6 has a crystalline part (right side) and an amorphous part (left side) indicating that it might have been formed by aggregation of several clusters.

Pd and Pt were also deposited on grids and analyzed by TEM (Figure 5.7). While Au and Pd clusters are of comparable sizes the Pt clusters are substantially

smaller, probably due to the higher reflectivity of Pt for the laser light (wavelength of 248 nm). This reflectivity reduces the efficiency of the ablation so that less plasma is formed and fewer collisions can take place in the plasma. With a fluence of 5 J cm^{-2} larger clusters are formed.

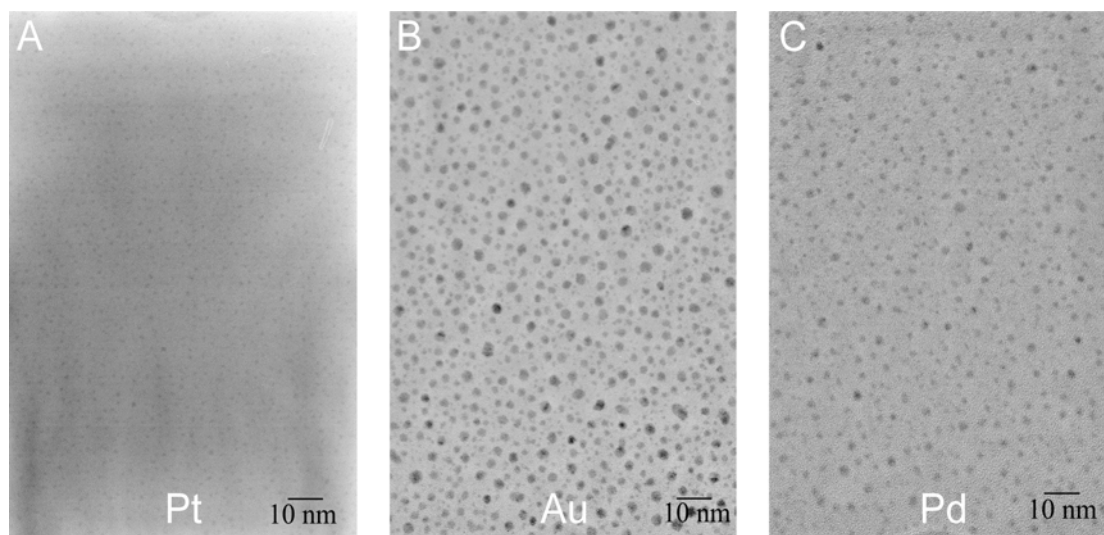


Figure 5.7 Clusters of (A) Pt (B) Au and (C) Pd made with 10 laser pulses, at 0.01 mbar with a target-substrate separation of 40 mm and a fluence of 4 J cm^{-2} . The average cluster sizes are (A) $1.06 \pm 0.21 \text{ nm}$ (B) $2.40 \pm 0.50 \text{ nm}$ (C) $2.29 \pm 0.50 \text{ nm}$.

In summary, Pd, Pt and Au can be deposited on carbon TEM grids using PLD. All three metals form nm size clusters when 10 laser pulses are used. The deposition pressure, the distance between target and substrate, the alignment of the target and the number of pulses all influenced the cluster size and/or cluster coverage. It seems that cluster growth takes place on the surface as well as in the plasma.

5.3 Deposition of metal clusters on SAMs

Depositions were performed directly on alkylthiolate SAMs on flame-annealed Au. AFM measurements showed that also on SAMs metal clusters were present. Conducting probe AFM (CP-AFM) measurements in parallel with conventional AFM height measurements were performed to investigate if the metal clusters were insulated on top of the SAM or buried in the SAM. CP-AFM was performed on samples of Au clusters on octadecanethiol (ODT) SAMs. Au was deposited using 6 laser pulses (fluence 4 J cm^{-2} , spot size 3 mm^2) on a Au target at

0.01 mbar argon pressure at a distance of 40 mm from the substrate. Since the AFM tip has to be able to distinguish between single clusters less pulses were used in order to obtain a lower cluster coverage on the surface.

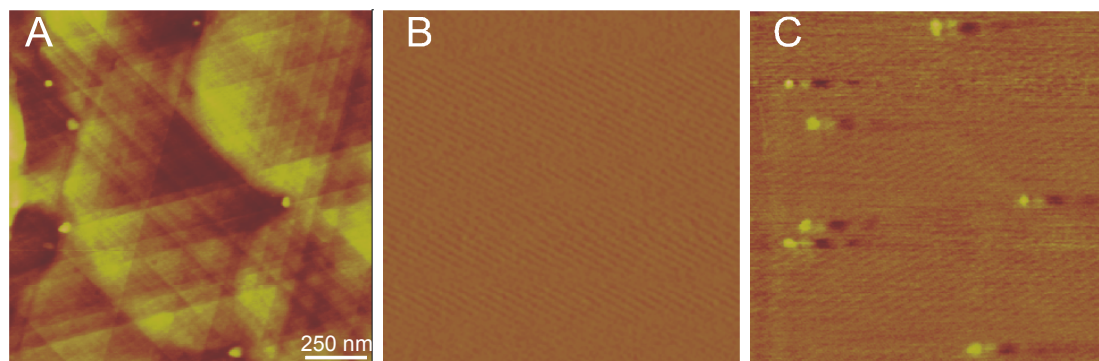


Figure 5.8 Simultaneous measurements of topography and current of an ODT SAM with deposited Au clusters obtained by CP-AFM, acquired in air. (A) height image (z -scale = 10 nm), (B) and (C) current images at a bias of 3 V and 7 V, respectively (z -scale = 0.5 pA). Light region: conducting, dark region: dielectric.

The number of clusters on the SAM (Figure 5.8 A) is lower than on the TEM images. On flame-annealed Au substrates deep ($\sim 20 - 50$ nm) trenches between the Au(111) islands are present. AFM indicates the presence of clusters in these trenches. This is likely to be caused by the mobility of clusters on the hydrophobic SAM. The accumulation of deposited material in these trenches is responsible for the lower number of clusters visible on SAMs when compared to TEM grids. The clusters in Figure 5.8 are stable and are not moved by the AFM tip despite not being chemically attached to the surface. The clusters only became visible in the current image if the bias over the tip and the sample was raised to ~ 5 V (Figure 5.8 B and C). If the clusters would be buried in the SAM, making contact with the Au substrate, they would be visible at much lower voltages. The fact that they are only visible at higher voltages indicates that these clusters are insulated on the SAM. The images were reproducible upon changing the bias from high to low voltage. Au clusters deposited on a shorter chain thiol SAM showed the same behavior when measured using CP-AFM (Figure 5.9). Au was also deposited on a decanethiol (DT) SAM using 10 laser pulses (fluence 4 J cm^{-2} , spot size 3 mm^2) on a Au target at 0.01 mbar Ar pressure at a distance of 40 mm from the substrate. As expected for this thinner SAM, the clusters

became visible in the current image at a lower applied bias compared to clusters on the ODT SAM.

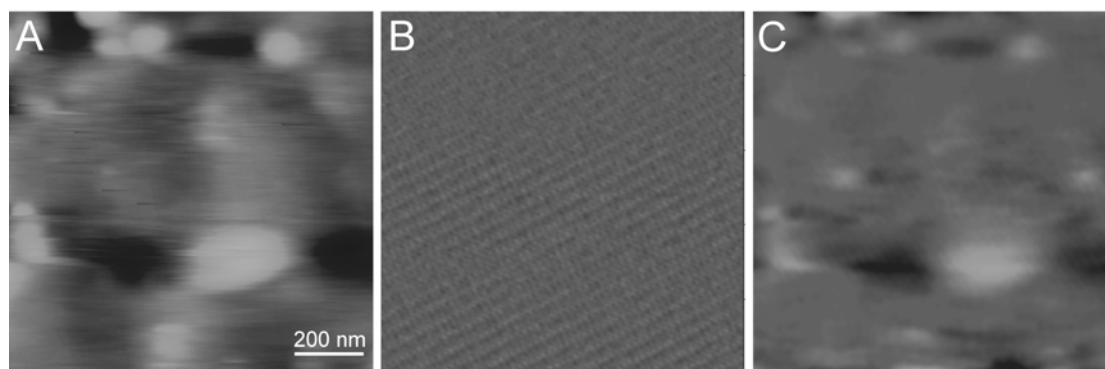


Figure 5.9 Simultaneous measurements (acquired in air) of topography and current of a DT SAM by CP-AFM. (A) Height image (z -scale = 10 nm), (B) and (C) current images at a bias of 1 V and 3 V respectively (z -scale = 0.3 pA). Light region: conducting, dark region: dielectric.

Pd clusters were deposited on DT SAMs using 10 laser pulses (fluence 4 J cm^{-2} , spot size 3 mm^2) on a Pd target at 0.01 mbar at a distance of 40 mm from the substrate. The samples were measured in a high vacuum STM directly after preparation. Figure 5.10 shows a typical STM image of a DT SAM with Pd clusters.

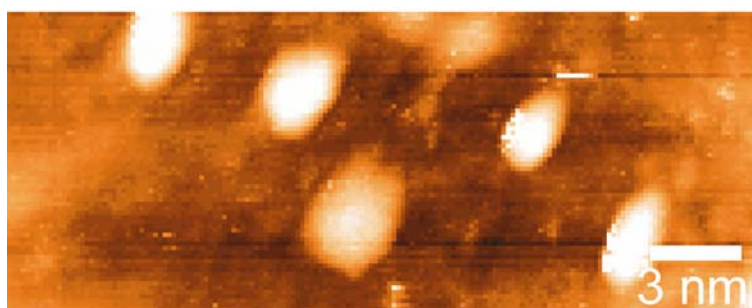


Figure 5.10 STM image ($25 \times 10 \text{ nm}$) of Pd clusters on top of a DT SAM taken at 300 K. The typical diameter of the Pd clusters is about 2 nm ($V = 0.5 \text{ V}$, $I = 0.1 \text{ nA}$).

It is quite clear from the STM image (Figure 5.10) that Pd clusters are present on top of the SAM. Moreover, the Pd clusters are distributed over the entire substrate and are not aggregated. The typical diameter of these Pd clusters is around 2 nm, which is in good agreement with the TEM measurements (Figure 5.7). I/V curves taken on the Pd clusters show Coulomb blockade behavior proving the insulated position of the clusters. In order to observe Coulomb blockade the total capacitance of

the Pd cluster should be smaller than $e^2 / 2kT$ and the resistances of the tunnel junctions should be larger than the resistance quantum $h / 2e^2$.¹⁵

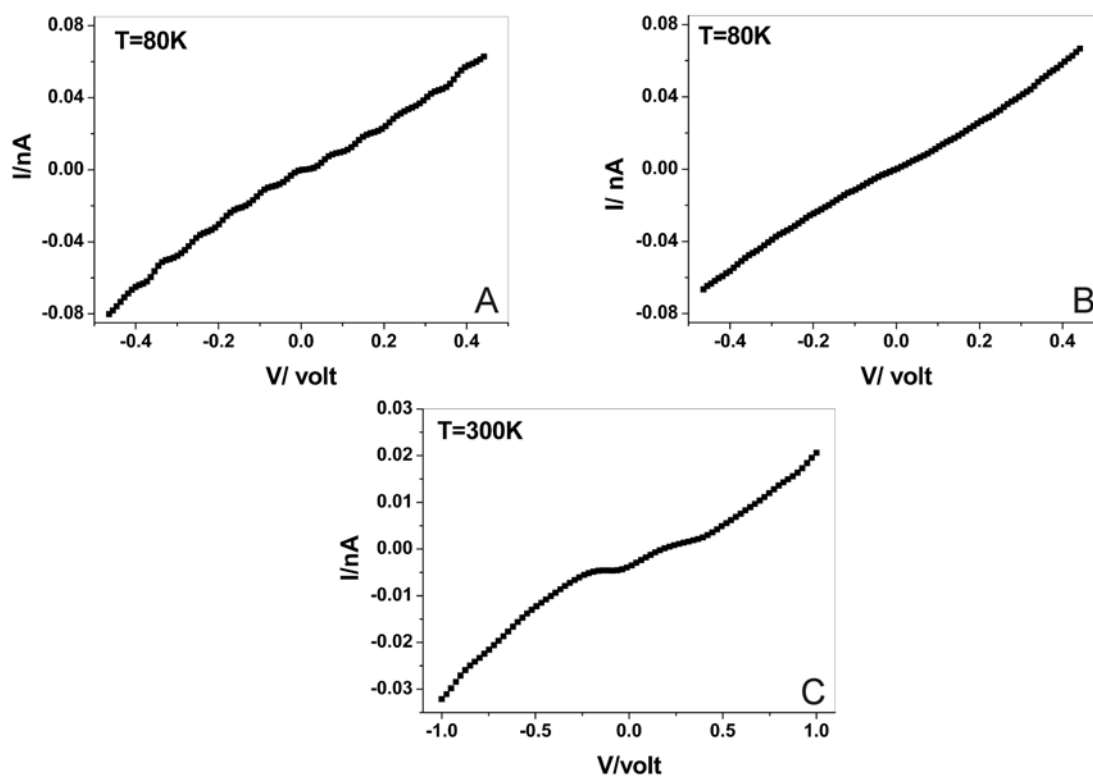


Figure 5.11 I/V curves taken on the Pd clusters on the SAM and in between the Pd clusters on the SAM at different temperatures. Curve (A) is taken on a Pd cluster at 80 K. Curve (B) shows the I/V curve of the bare SAM at 80 K. Curve (C) is taken on a Pd cluster at room temperature (298 K).

If it is assumed that the Pd clusters are insulated from the surface by the DT SAM, the system can be modeled as a double junction circuit. The first junction is composed of the STM tip and the Pd cluster separated by vacuum, whereas the second junction consists of the Pd cluster and the Au substrate separated by the monolayer. Each junction is modeled by a resistor in parallel with a capacitor. At extremely low capacitance values (e.g. $\sim 10^{-18}$ Farad) and very large resistance values (e.g. $\sim 10^9 \Omega$), one can measure the Coulomb gap and the Coulomb staircase, even at elevated temperatures. The latter observation, however, requires an asymmetric double junction, *i.e.* both junctions should have different RC values.

In Figure 5.11 several I/V curves taken both on the Pd clusters on the DT SAM and the uncovered SAM substrate at different temperatures are shown. I/V

curves taken on the individual Pd clusters always exhibit the characteristic Coulomb staircase and Coulomb gap. Although the Coulomb staircase is also faintly present at room temperature, equidistantly spaced steps in the I/V curve are clearly resolved at 80K. I/V curves taken on the bare SAM have typical ohmic characteristics and do not show any evidence for Coulomb blockade effects. These STM observations clearly prove that individual Pd clusters are electrically insulated from the underlying Au substrate.¹⁵

5.4 Conclusions

Pulsed laser deposition of the noble metals Au, Pt and Pd was used to fabricate nanometer size metal clusters. TEM analyses showed clusters of Pd, Pt and Au which were deposited on carbon TEM grids, with sizes in the order of 1 to 3 nm. The cluster size and size distribution could be influenced by the deposition parameters, such as number of pulses and target-substrate distance. CP-AFM performed on samples of Au clusters on ODT and DT SAMs showed that on the SAM covered Au (111) surface only insulated clusters were present. It seems that the clusters are relatively mobile on the SAMs. However, insulated clusters that were observed with CP-AFM did not move during the measurement nor were they influenced by the applied bias.

Small Pd clusters were also deposited directly on DT SAMs, and STM showed that they were indeed insulated on top of the SAM. Room temperature Coulomb blockade confirmed the small size of the clusters as well as the insulated position of these particles, in lateral sense from one another and also from the substrate. At 80 K, I/V curves showed a very clear Coulomb blockade and staircase behavior again indicating the excellent insulation of these particles. The SAM itself showed Ohmic I/V characteristics.

5.5 Experimental procedures

SAM preparation: decanethiol (96 %, Aldrich) and octadecanethiol (98 %, Janssen Chimica) SAMs were made from 1 mM solutions of the thiol in ethanol (*p.a.*, Merck). Au substrates (200 nm Au, on 5 nm chromium on glass) were obtained from Metallhandel Schroer GmbH, Lienen, Germany. Substrates were rinsed with dichloromethane (*p.a.*, Biosolve) and directly flame annealed in a hydrogen flame

(purity 6). After annealing substrates were cooled down slowly in air (5 minutes) after which they were immersed in the ethanolic solution. Substrates were kept overnight in solution after which they were removed and rinsed with dichloromethane *p.a.*, ethanol *p.a.*, and water (Q2 millipore)

PLD of clusters: a Compex 205 KrF excimer laser of Lambda Physik emitting 20 ns pulses at 248 nm was used. Deposition pressures of 1 to 10^{-3} mbar were used with argon as background gas; an argon flow was used from 0.2 ml min^{-1} to 26 ml min^{-1} depending on the working pressure. A laser fluence of 4 J cm^{-2} was used, with a spot size of $\sim 3 \text{ mm}^2$. The laser beam entered the vacuum chamber at an angle of 45° with respect to the target normal, the substrate was placed parallel to the target at a distance of 40 mm. The pulse frequency was 4 Hz. Gold target was 4N (99.99 % pure) and obtained from Engelhard-CLAL/Drijfhout B.V., The Netherlands. Palladium was obtained from Goodfellows, Cambridge, UK (99.95 % pure). Platinum was obtained from Engelhard-CLAL/Drijfhout B.V. The Netherlands (99.99 % pure). Depositions were done on carbon coated Cu TEM grids and freshly prepared decanethiol and octadecanethiol self-assembled monolayers.

Transmission electron microscopy: TEM images were collected on a Philips CM 30 Twin/STEM, operated at 300 kV. The TEM was equipped with a Kevex EDX detector with BN window and a Thermo Noran System Six Analyzer. Samples were deposited directly on carbon coated 200 mesh copper grids. Average particle sizes, size distributions and coverages were determined from the TEM images, using analySIS software.

Conducting probe AFM: CP-AFM was performed by Dr. Barbara Dordi on a Nanoscope IV Multimode (Digital Instruments, Santa Barbara, Ca., USA) with tunA extension, capable of measuring picoampere currents. Gold coated silicon cantilevers with stiffness of 0.12 N m^{-1} (before coating) were obtained from Veeco Instruments.

Scanning tunneling microscopy: STM measurements (performed by Nuri Oncel, Ann-Sofie Hallbäck and Dr. Harold Zandvliet of the solid state physics group, MESA⁺ Institute for Nanotechnology) under UHV conditions using an Omicron Low

Temperature STM. Samples were introduced in the STM *via* a loadlock within 30 minutes after preparation.

5.6 References

- ¹ B. Xu, N. J. Tao, *Science* **2003**, 301, 1221-1223.
- ² Y. Selzer, M. A. Cabassi, T. S. Mayer, D. L. Allara, *J. Am. Chem. Soc.* **2004**, 126, 4052-4053.
- ³ X. D. Cui, A. Primak, X. Zarate, J. Tomfohr, O. F. Sankey, A. L. Moore, D. Gust, G. Harris, S. M. Lindsay, *Science* **2001**, 294, 571-574.
- ⁴ T. Ohgi, H.-Y. Sheng, H. Nejoh, *Appl. Surf. Sci.* **1998**, 130-132, 919-924.
- ⁵ T. Castro, Y. Z. Li, R. Reifenger, E. Choi, S. B. Park, R. P. Andres, *J. Vac. Sci. Technol. A* **1989**, 7, 2845-2849.
- ⁶ M. Dorogi, J. Gomez, R. Osifchin, R. P. Andres, R. Reifenger, *Phys. Rev. B.* **1995**, 9071-9077.
- ⁷ R. P. Andres, T. Bein, M. Dorogi, S. Feng, J. I. Henderson, C. P. Kubiak, W. Mahoney, R. G. Osifchin, R. G. Reifenger, *Science* **1996**, 272, 1323-1325.
- ⁸ J. I. Henderson, S. Feng, G. M. Ferrence, T. Bein, C. P. Kubiak, *Inorg. Chim. Acta.* **1996**, 242, 115-124.
- ⁹ G. K. Ramachandran, J. K. Tomfohr, J. Li, O. F. Sankey, X. Zarate, A. Primak, Y. Terazono, T. A. Moore, A. L. Moore, D. Gust, L. A. Nagahara, S. M. Lindsay, *J. Phys. Chem. B* **2003**, 107, 6162-6169.
- ¹⁰ A. M. Rawlett, T. J. Hopson, L. A. Nagahara, R. K. Tsui, G. K. Ramachandran, S. M. Lindsay, *Appl. Phys. Lett.* **2002**, 81, 3043-3045.
- ¹¹ T. Ohgi, D. Fujita, *Surf. Sci.* **2003** 523-535, 294-299.
- ¹² U.-W. Grummt, M. Geissler, Th. Schmitz-Huebsch, *Chem. Phys. Lett.* **1996**, 263, 581-584.
- ¹³ A. W. Snow, M. G. Ancona, W. Kruppa, G. G. Jernigan, E. E. Foos, D. Park, *J. Mater. Chem.* **2002**, 12, 1222-1230.
- ¹⁴ A. M. Rawlett, T. J. Hopson, L. A. Nagahara, R. K. Tsui, G. K. Ramachandran, S. M. Lindsay, *Appl. Phys. Lett.* **2002**, 81, 3043-3045.
- ¹⁵ A detailed analysis of the Coulomb blockade is presented in: N. Oncel, A. S. Hallbäck, H. J.W. Zandvliet, E. A. Speets, B. J. Ravoo, D. N. Reinhoudt, B. Poelsema, *Phys. Rev. B*, submitted.

Chapter 6

Scope of Pulsed Laser Deposition of Metals on Self-Assembled Monolayers

In this chapter the deposition of several metals via pulsed laser deposition through nanosieves on self-assembled monolayers is described. The focus is on the pattern replication and the morphology of the deposited metal islands. Au, Pt, Pd and Cu have been deposited on various SAMs on various substrates to investigate the influence of the SAM thickness, surface functionality and substrate (Au vs. SiO₂) on the properties of the deposited islands. Furthermore the pattern enhancement of metal clusters deposited through shadow masks is described. Patterns of Cu were obtained by depositing metal clusters through shadow masks followed by electroless deposition from a Cu²⁺ plating bath.

6.1 Introduction

The use of pulsed laser deposition (PLD) through nanosieves on self-assembled monolayers (SAMs) would be more attractive when different combinations of materials and substrates could be used. Different metals and SAMs could be useful for applications in molecular electronics, in order to identify the optimal electrode material, and to improve contacts between electrode and molecule.

The metal deposition has to be controlled precisely if sieves with smaller feature sizes have to be used. Enlargement of the patterns of the deposited material leads to coalesced features if these features are too close together. For example, shadow mask evaporation of Au (on Ti) yielded a borderline of clusters on the edges of structures.¹ E-beam evaporation of Al through shadow masks on Si₃N₄ gave a slight enlargement of the pattern, nevertheless, lines with a width of only 128 nm could be fabricated.² PLD performed at higher pressures on SAMs generally leads to enlargement of features (Chapter 4). The enlargement of the pattern can be minimized by placing the sieve as close as possible to the substrate and by depositing the metal at lower pressure to minimize scattering of atoms in the gas phase. However, as was shown in Chapter 4, depositions on SAMs can not be performed at too low pressures, because of damage to the SAM and the creation of short circuits.

An alternative method to prepare metal electrodes on SAMs is to combine the short deposition of metal clusters (Chapter 5) through a nanosieve with selective electroless deposition (ELD) of metals on the template of patterned clusters. ELD is a technique that can develop metal patterns on surfaces. ELD uses a pre-existing pattern of a catalytic species to form the corresponding metal pattern.³ It has been used in combination with several patterning techniques such as microcontact printing,⁴ photolithography⁵ and e-beam lithography.⁶

Metal(0) is a catalyst for the initiation of ELD.^{7,8} Chelated metal ions are reduced on a metal(0) surface by a reductor present in solution. Metal(0) is often created by chemically reducing metal ions bound to a surface.⁷ The use of a gas phase deposition technique that can deposit metal(0) particles directly on surfaces could improve this process.

In this chapter the PLD of various metals (Au, Pt, Pd, Cu) through nanosieves on SAMs on SiO₂ and Au is described. Furthermore, thick and thin SAMs are used as substrates for PLD and SAMs with and without reactive head groups. The pattern

replication and morphology of different systems is analyzed using SEM, light microscopy and AFM. Finally, it is investigated whether small metal clusters fabricated by PLD through nanosieves and microsieves on SAMs could act as a selective template for ELD, in order to minimize the gas phase deposition, and develop the pattern by a chemical deposition from an aqueous phase.

6.2 Variations of substrate, SAM and deposited metal in PLD on SAMs

6.2.1 Deposition of various metals

6.2.1.1 Pattern replication in shadow mask deposition

An important issue in the use of PLD on SAMs in combination with nanosieves is the faithful replication of the pattern. In Chapter 4 it has already been shown that Au islands could be deposited in patterns in such a way that the islands are not in contact laterally. Here the deposition of islands of Pd, Cu and Pt under different deposition conditions is described

Pd was deposited on SAMs through a nanosieve. Figure 6.1 shows an AFM height image and section analysis of Pd islands on an octadecanethiol (ODT) SAM. The hexagonal pattern of the islands can be clearly seen. The height of the islands is approximately 5 nm (dark section) and the diameter is approximately 900 nm. From the light section, taken between the islands, it can be seen that the islands are not touching each other. The flat baseline corresponds to the SAM's surface.

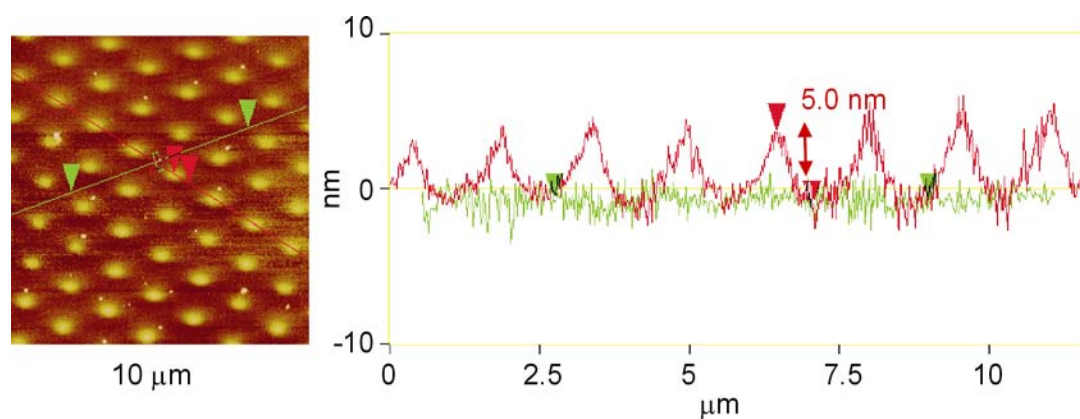


Figure 6.1 AFM height image and section analysis of Pd islands made by PLD through nanosieve on an ODT SAM. ($p = 0.001$ mbar, $d = 40$ mm, $t = 4$ min at 8 Hz, spot size ~ 1.76 mm², fluence ~ 5 J cm⁻²).

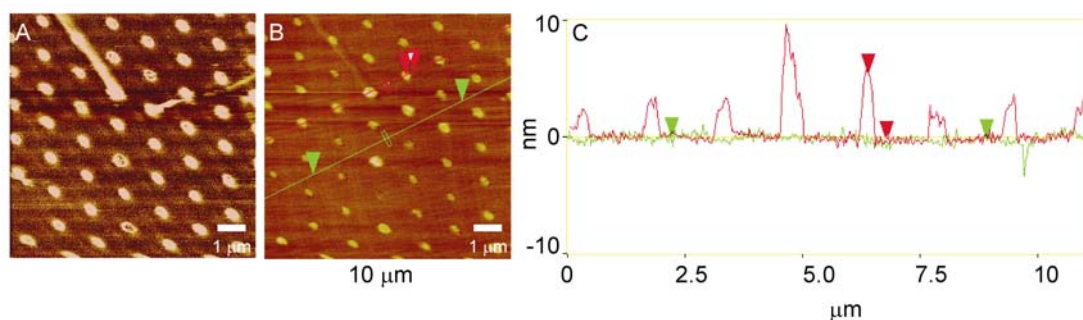


Figure 6.2 (A) AFM friction and (B) height image and (C) section analysis of Cu islands made by PLD through nanosieve on an ODT SAM. ($p = 0.001$ mbar, $d = 40$ mm, $t = 4$ min at 8 Hz, spot size ~ 2.97 mm², ~ 3.5 J cm⁻²).

Figure 6.2 B shows an AFM image of Cu islands on an ODT SAM. As can be seen in the section analysis (Figure 6.2 C), the islands have irregular heights, ranging from 2.5 to 8.5 nm. From the light section it can be seen that the islands are not touching each other laterally. The corresponding AFM friction image (Figure 6.2 A) shows a much more homogeneous pattern, where all islands look the same.

Figure 6.2 illustrates clearly the complementarity of topography and friction images. There is a clear distinction between missing islands (left bottom of Figures 6.2 A and B, no contrast in friction and in height) and islands that are present but have a lower height (just below the middle in Figure 6.2 A and B an island that is missing in the height image shows up very clearly in the friction image, indicating the presence of deposited Cu). The reason for this difference in shape between the islands

is not clear yet, but it might originate from defects or clogging of the nanosieve used for the deposition.

Figure 6.3 shows Pt islands deposited on an ODT SAM. In this image it can be seen clearly that the islands are not in contact with each other. Besides that, these islands are much better defined than the previous ones.

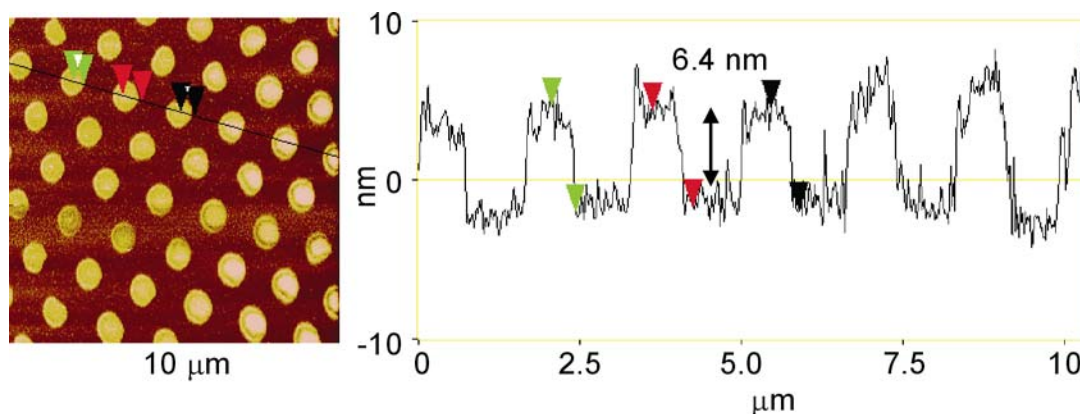


Figure 6.3 AFM height image and section of Pt islands deposited on an ODT SAM ($p = 0.001$ mbar, $t = 2$ min. at 8 Hz, fluence 5.0 J cm^{-2} , $d = 40$ mm).

From Figures 6.1 to 6.3 it is clear that several metals can be deposited with PLD through nanosieves, yielding patterns of islands that do not touch each other. No further conclusions can be drawn from the islands' heights and shapes. The contact of the sieve with the substrate, the alignment of the plasma with the substrate, and the kinetic energy of the plasma can differ from deposition to deposition. This can cause blurring of the pattern, because of merging of the islands, and a reduction of the deposited amount of metal. If there is a large gap between the sieve and the substrate, caused by dust or 'bad' positioning of the sieve, a pattern is not reproduced accurately on the surface.

6.2.1.2 Morphology of deposited metal islands on SAMs

In order to use metal components in electronic devices they must be homogenous and free of defects. This issue is most obvious in the case of submicron metal wires on surfaces. The chance that such wires are discontinuous increases as the dimensions get smaller. Figure 6.4 shows an AFM image of a single Au island on an ODT SAM. The morphology of the deposited Au islands resembles the morphology of the Au substrate (covered by the SAM).

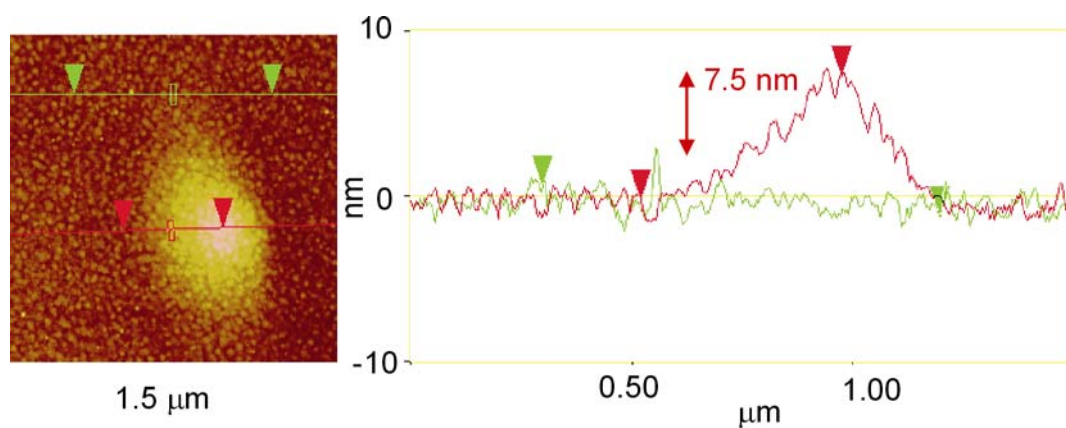


Figure 6.4 AFM height image and section analyses of a Au island deposited via PLD on an ODT SAM on 20 nm Au ($p = 0.01$ mbar, $d = 40$ mm, fluence 4 J cm^{-2} , $t = 4$ min. at 8 Hz).

Apparently, the Au-island (Figure 6.4) consists of a collection of small Au clusters that together form the larger structure. It is difficult to say anything about the size of these clusters from AFM images, but this size will probably range between 2 nm (as was shown for clusters in Chapter 5) and ~ 10 nm. The structure of Au deposited on a SAM using PLD looks very much like Au evaporated in high vacuum (HV) on solid substrates at room temperature. The shape of the island is not perfectly circular, which is likely caused by incorrect (manual) positioning of the sieve on the substrate and/or wrong alignment of the plasma with the substrate. Figure 6.5 shows an AFM height image and section analyses of a Pd island on an ODT SAM.

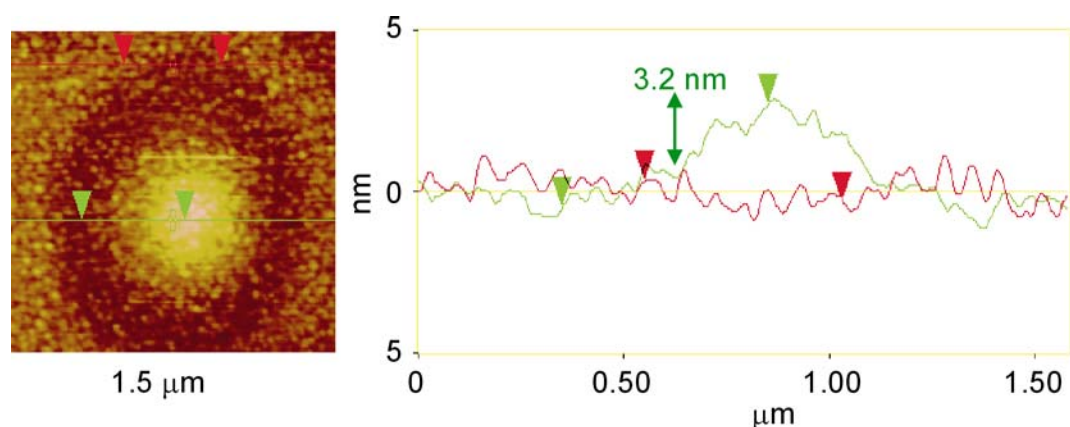


Figure 6.5 AFM height image and section analyses of Pd island deposited via PLD on an ODT SAM on 20 nm Au ($p = 0.01$ mbar, $d = 40$ mm, fluence 4 J cm^{-2} , $t = 2$ min. at 8 Hz).

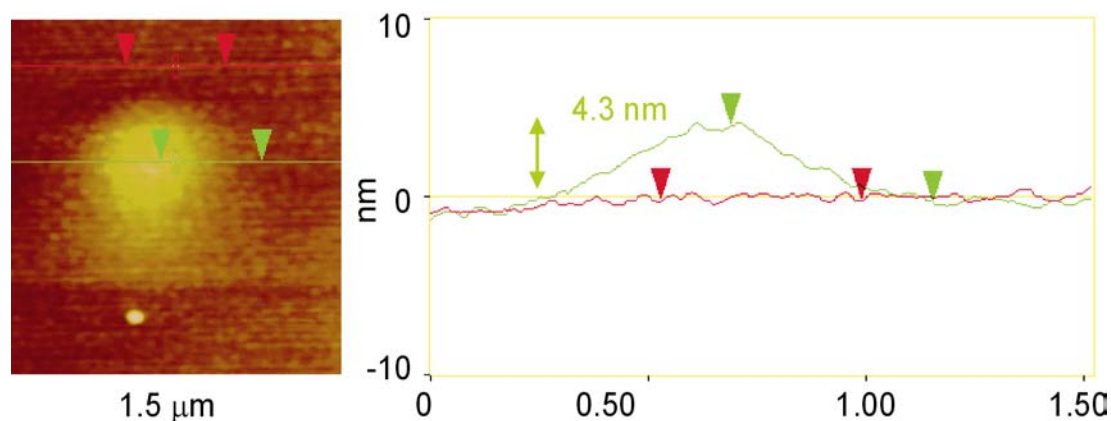


Figure 6.6 AFM height image and section analyses of Pt island deposited via PLD on an ODT SAM on 20 nm Au. ($p = 0.01$ mbar, $d = 40$ mm, fluence 4.5 J cm^{-2} , $t = 2$ min. at 8 Hz).

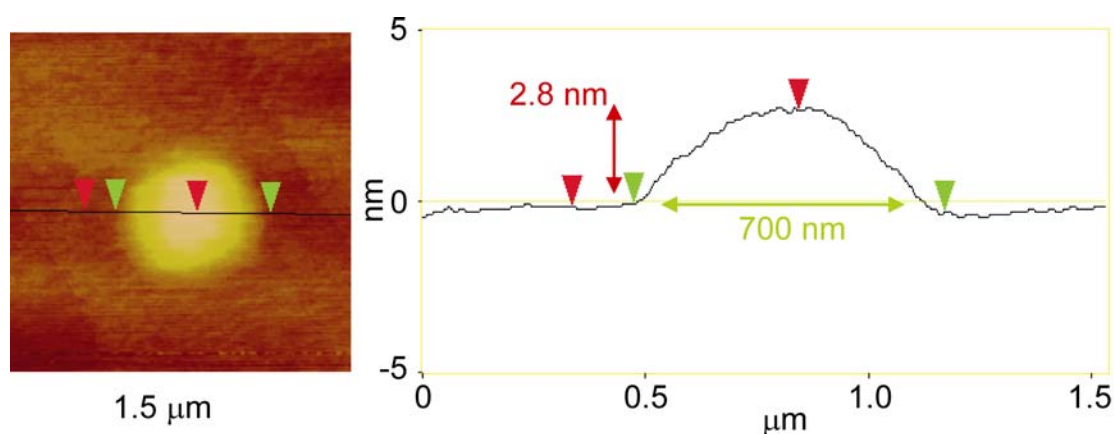


Figure 6.7 AFM height image and section analyses of Cu island deposited via PLD on an ODT SAM on 20 nm Au ($p = 0.001$ mbar, $d = 40$ mm, fluence 4 J cm^{-2} , $t = 4$ min. at 8 Hz).

In summary, isolated Au, Pd, Pt (Figure 6.6) and Cu (Figure 6.7) islands were fabricated with PLD through nanosieves. The diameter of the islands is always larger than that of the holes in the sieves. Whether the enlargement of the islands is caused by surface diffusion on the SAM or *via* the gas phase could not be determined. The island structure is grain-like just as is the case for metal films evaporated at low substrate temperatures.⁹

AFM is not a very suitable technique to analyze the cluster size of the deposited metal. Because of the large size of the tip compared to the average cluster size no reliable measurements can be obtained. From the previous images it can be concluded that PLD through nanosieves yields homogeneous islands that are more or

less flat without large height differences (< 0.5 nm). For metal islands to be homogeneous, a minimum thickness of several nm is necessary.

6.2.2 Deposition on various substrates

For the conventional silicon-based semiconductor chip industry metal depositions on SiO_2 are of great interest because in principle such depositions could be directly integrated in the standard technology.¹⁰ SiO_2 -SAM-metal systems might be used in SAMFETs or other devices. SAMs on SiO_2 are bound *via* silicon-oxygen bonds and formed by condensation of chlorosilanes or alkoxy silanes with surface silanol groups,¹¹ in combination with the adsorbed water film on the SiO_2 -substrate.¹² SAMs on silicon (especially long-chain alkyl SAMs) are stable towards hydrolysis and withstand immersion in organic solutions.¹³ In this section the deposition of metal on siloxane SAMs on SiO_2 was using PLD is described. Au depositions on sticky and non-sticky SAMs on SiO_2 yielded very regular islands (Figure 6.8 and 6.9). Depositions on the inert octadecyltrichlorosilane (ODTS) SAMs (Figure 6.9) show no significant diffusion of metal over the surface when compared to SAMs with sticky head groups such as SAMs made from 11-cyano-undecanetrichlorosilane (CUTS) (Figure 6.8). The results are consistent with the observations in Chapter 4 (Au on ODT on Au *vs.* Au on NDT on Au) and indicate that for the island shape as well as for the stability, sticky thiol or cyanide groups are not a necessity. The electronic properties of SAMs on SiO_2 , before and after PLD of Au, were not investigated.

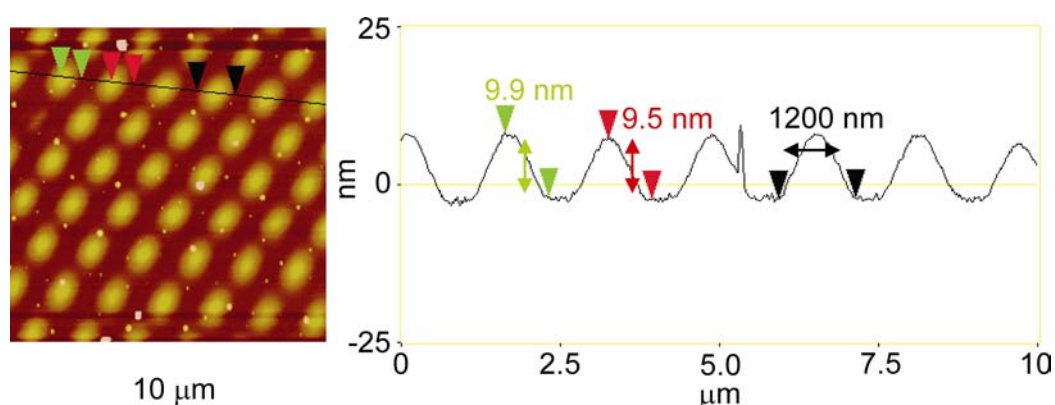


Figure 6.8 AFM image and section of Au deposited ($d = 40$ nm, $t = 2$ min. at 8 Hz, $p = 0.01$ mbar, fluence 4 J cm^{-2}) on a CUTS SAM on SiO_2 .

However, diffusion of metal through the SAM will not likely take place on SiO₂ surfaces. Reports of high vacuum (HV) deposition of gold on SAMs on siliconitride show that the SAM is not damaged by the deposition.¹⁴ The height differences between the islands in Figure 6.8 and 6.9 are mainly caused by the difference in deposition pressure. Higher pressures result in lower deposition rates (Chapter 4).

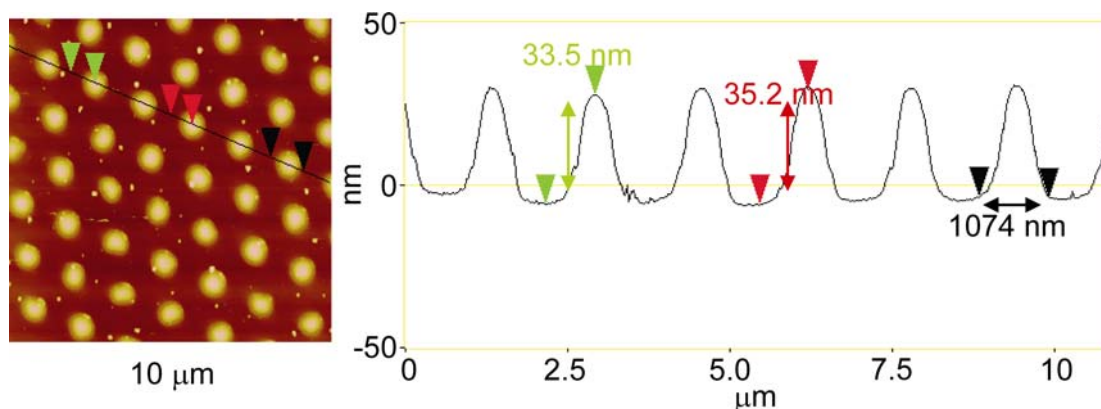


Figure 6.9 AFM image and section of Au deposited ($d = 40$ mm, $t = 2$ min. at 8 Hz, $p = 0.001$ mbar, fluence 4 J cm⁻²) on an ODTS SAM on SiO₂.

Au islands deposited on SAMs on SiO₂ can be investigated by scanning electron microscopy (SEM). The contrast between metal and SiO₂ is large enough to visualize the Cu islands (Figure 6.10). The hexagonal pattern can also in Figure 6.10 be clearly distinguished, but in this case no information about the height of the islands can be obtained. The diffuse edges of the islands as generally observed in AFM further reduce the contrast in SEM images so that the lateral size cannot be measured with great precision.

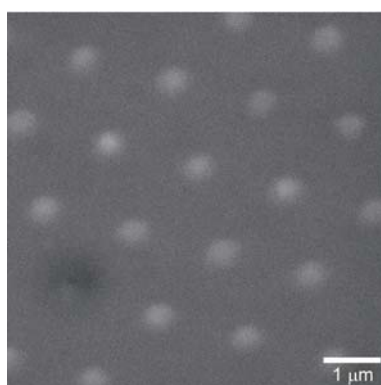


Figure 6.10 SEM image of Cu islands deposited on a CUTS SAM on SiO₂ ($d = 40$ mm, $t = 4$ min. at 8 Hz, $p = 0.001$ mbar, fluence 3 J cm⁻²).

6.2.3 Other sieves

To investigate the versatility of shadow mask PLD depositions on SAMs various shadow masks were used. Shadow masks with a total area of 19×19 mm made from 500 nm thick silicon nitride membranes were obtained from the Brugger group.¹⁵ These masks contain many different features with sizes ranging from 200 nm to several hundreds of μm (detail shown in Figure 6.11).¹⁶ Through this sieve Au was deposited on ODT SAMs.

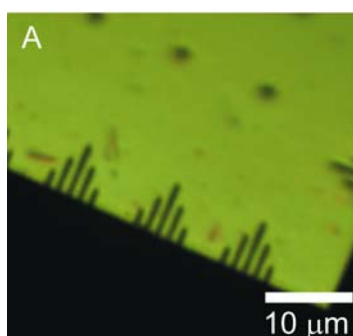


Figure 6.11 Light microscope image of a small part of a shadow mask.

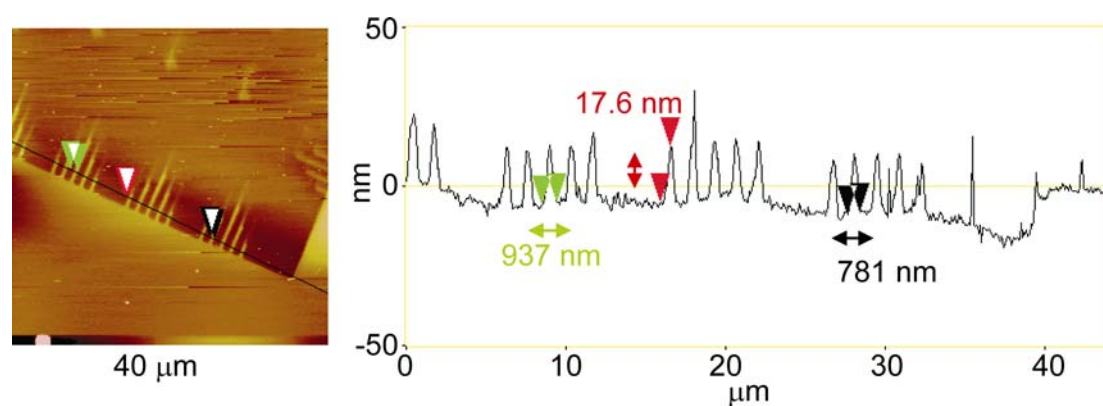


Figure 6.12 AFM image and section analysis of Au deposited on an ODT SAM through a microsieve shadow mask ($d = 40$ mm, $t = 2$ min. at 8Hz, $p = 0.01$ mbar, fluence 4 J cm^{-2}).

Figure 6.12 shows an AFM image of a small part of an ODT surface after PLD through this shadow mask. The pattern of the sieve could be replicated reasonably well, even over several cm^2 of the surface. Also this sieve was placed directly on the substrate, which caused some damage to the Si_3N_4 membrane. Because of the large feature sizes and spacing these samples were difficult to analyze with AFM. When

thicker layers were deposited, or different materials that contrast more, light microscopy could be used to analyze these samples.

6.3 Pattern enhancement of pulsed laser deposited metal patterns using electroless deposition

Patterns of metal clusters on SAMs were obtained by short PLD through nanosieves and microsieve shadow masks. The pattern of clusters on the SAM was then used as a template for ELD of Cu. A schematic drawing of the cluster deposition and enhancement of the pattern with ELD is shown in Figure 6.13. Using this method the potentially damaging gas phase deposition step can be minimized. It is also possible to easily obtain structures made from mixed metals after a gas phase deposition of one metal followed by ELD of another metal. Samples containing metal island or cluster patterns were immersed in a Cu ELD solution for several minutes. The results were analyzed using AFM and light microscopy.

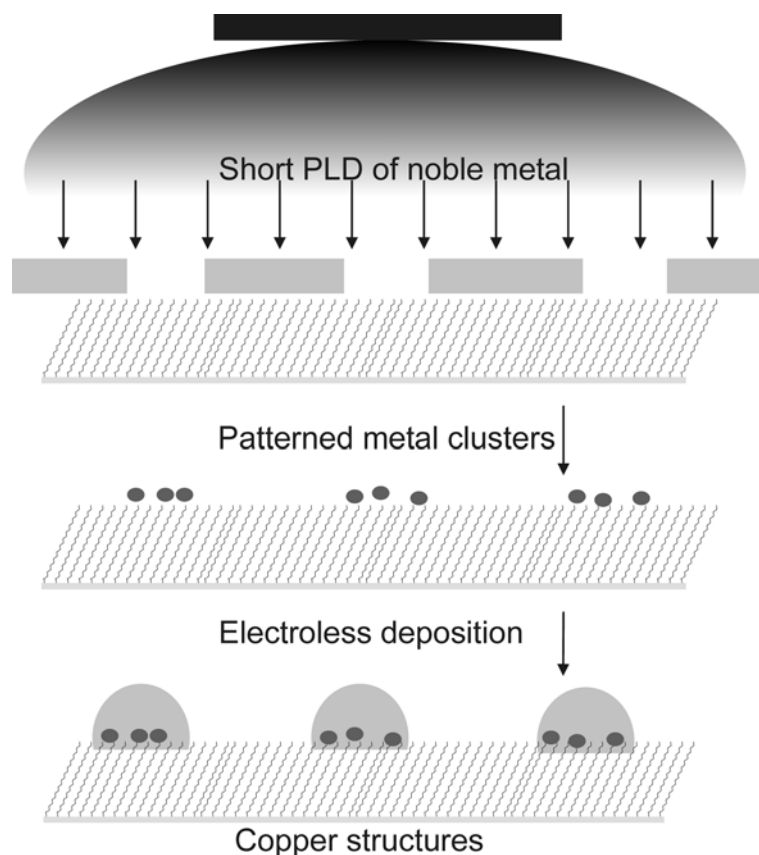


Figure 6.13 Schematic representation of PLD on a SAM followed by pattern enhancement with Cu ELD.

6.3.1 PLD and ELD on SAMs on SiO₂

To prevent ELD on pinholes and damaged parts of SAMs on Au, siloxane SAMs on SiO₂ were used. Sieves of 19 × 19 mm were used as shadow masks for the deposition of metal. The structures deposited through these sieves can, because of their size, be visualized with a light microscope, provided that they are thick enough and the material contrasts sufficiently with the Au substrate. Pd was deposited through microsieve shadow masks (Figure 6.14 A) on octadecyltrichlorosilane (ODTS) SAMs on SiO₂,¹⁷ after which the sample was immersed in an ELD solution. The small amount of deposited Pd could in this case not be visualized with a light microscope. By depositing only 40 pulses of Pd on the SAM enough metal is present to catalyze the ELD process very specifically, and enhance the pattern (Figure 6.14 B). The bottom part of the feature in the upper right of Figure 6.14 B is not visible with the light microscope, only the edges show.

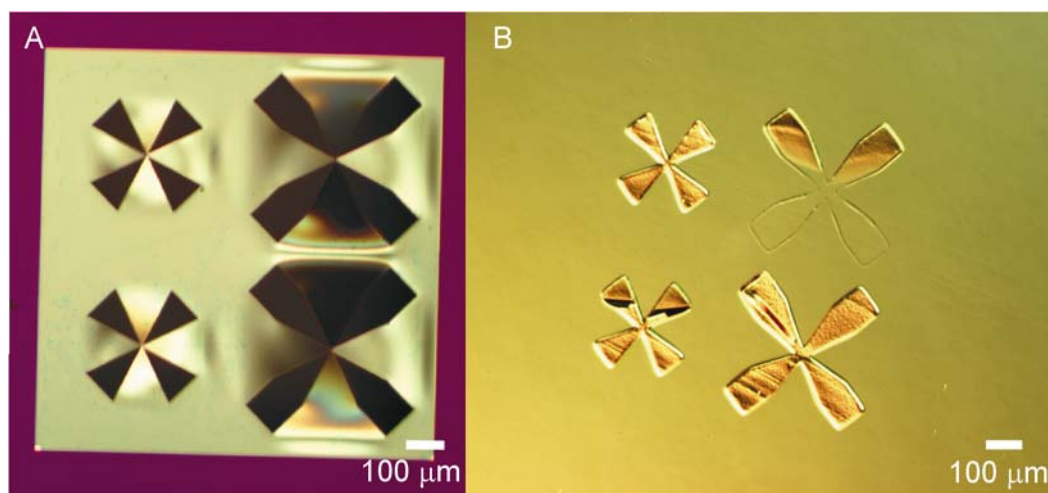


Figure 6.14 Light microscope images of (A) siliconnitride shadow mask and (B) ODTs SAM on SiO₂ after 40 pulses Pd PLD through shadow mask at $p = 0.001$ mbar, fluence 4 J cm^{-2} , followed by 5 minutes ELD.

A pattern of Au islands prepared by PLD through a nanosieve on an ODTs SAM on SiO₂ was immersed in an ELD solution as well. The Au islands made using PLD at 0.001 mbar are a good catalyst for ELD. Figure 6.15 A shows the pattern of ~5 nm high gold islands deposited with PLD on an ODTs SAM. In Figure 6.15 B, the spectacular growth of the islands by ELD can be seen. It is also clear that the island pattern is retained, demonstrating the selective nature of the ELD process.

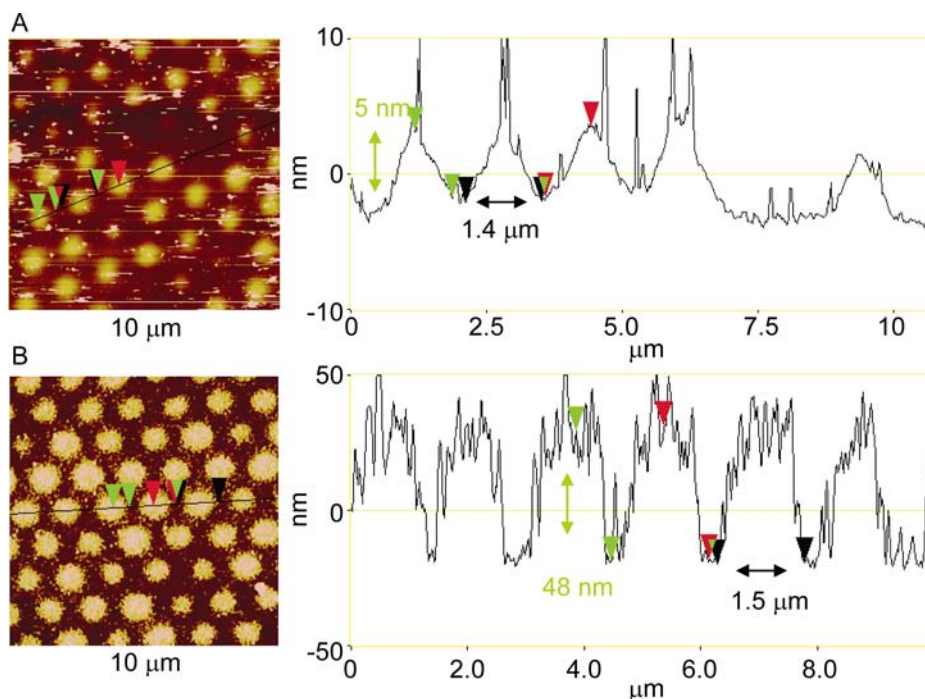


Figure 6.15 AFM height images and section analyses of (A) pattern of Au islands on ODTs SAM on SiO₂ ($d = 40$ nm, fluence 4 J cm⁻², $t = 2$ min. at 8 Hz, $p = 0.001$ mbar, ~ 4 J cm⁻²), (B) after 5 min. Cu-ELD.

6.3.2 PLD and ELD on SAMs on Au

ELD pattern enhancement on SAMs on Au substrates was also studied with different metals. In Figure 6.16 B a light microscope image of an ODT SAM with 120 pulses Au deposited *via* PLD through a microsieve (Figure 6.16 A), after 2 minutes Cu-ELD is shown. The original pattern of Au clusters could not be imaged with the light microscope due to the lack of contrast of the small amount of Au. However the structures after ELD are clearly visible. No ELD occurred outside the desired pattern indicating the suitability of this method and the stability of the SAM in this multistep process.

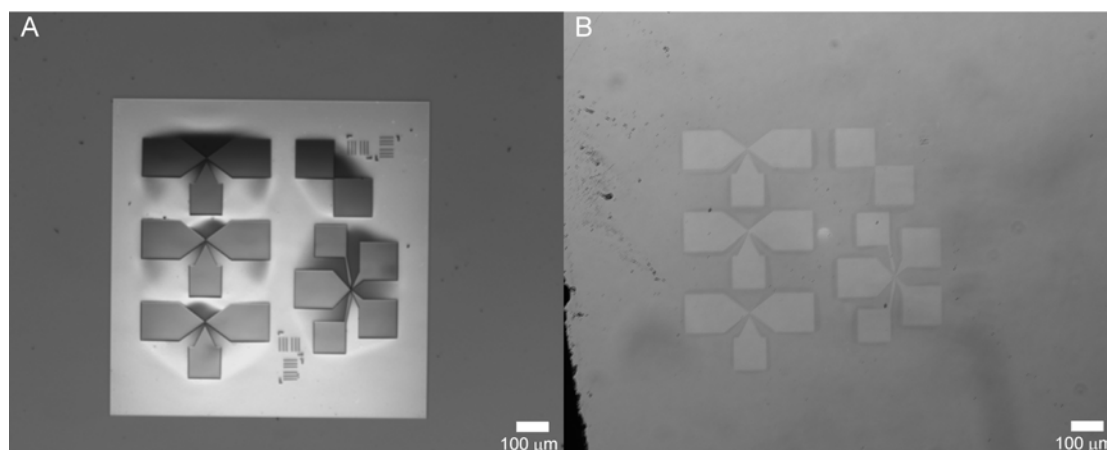


Figure 6.16 Light microscope images of (A) detail of microsieve shadow mask (B) ODT SAM with 120 pulses of Au deposited through corresponding part of microsieve via PLD ($p = 0.01$ mbar, $d = 40$ mm, fluence 4 J cm^{-2}) after 2 minutes ELD of Cu.

Pt was also used as Cu ELD catalyst. In Figure 6.17 AFM height images of a sample containing Pt islands before and after Cu-ELD are shown. After 240 pulses Pt islands are present, as can be seen with AFM (Figure 6.17 A). The sample was immersed in an ELD solution for 1 minute, which was sufficient to see the deposited copper by eye.

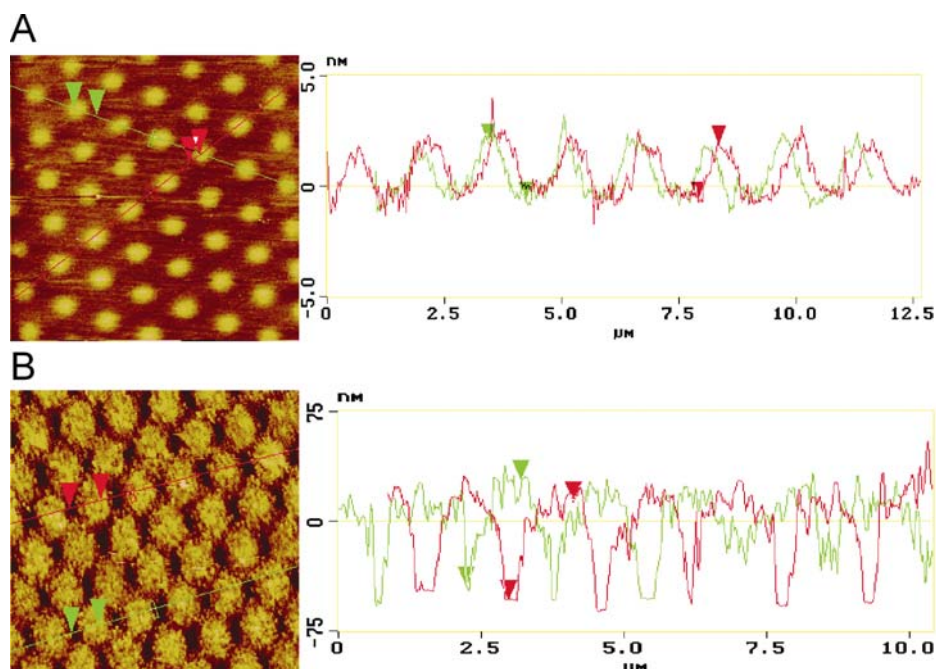


Figure 6.17 AFM height images and section analyses of (A) ODT SAM on Au with 240 pulses of Pt ($d = 40$ mm, $p = 0.001$ mbar, fluence 5 J cm^{-2}), (B) same sample after 1 minute Cu-ELD. ($10 \times 10 \mu\text{m}$).

The height of the islands before ELD was approximately 3 nm while after ELD it had grown to 75 nm (Figure 6.17 B). As can be seen from the section analysis, the islands did hardly coalesce (the diameter of the islands did not increase by more than ~ 100 nm) and the pattern is still clearly visible. This is another indication that between the islands no significant amount of metal is present, which implies that almost no diffusion of metal over the SAM surface takes place.

Figure 6.18 shows two light microscope images of a pattern of Pt clusters on an ODT SAM before and after ELD of Cu. Only 120 pulses of Pt, deposited through a microsieve (Figure 6.18 A), were sufficient to create a visible pattern (Figure 6.18 B) on the SAM/Au substrate.

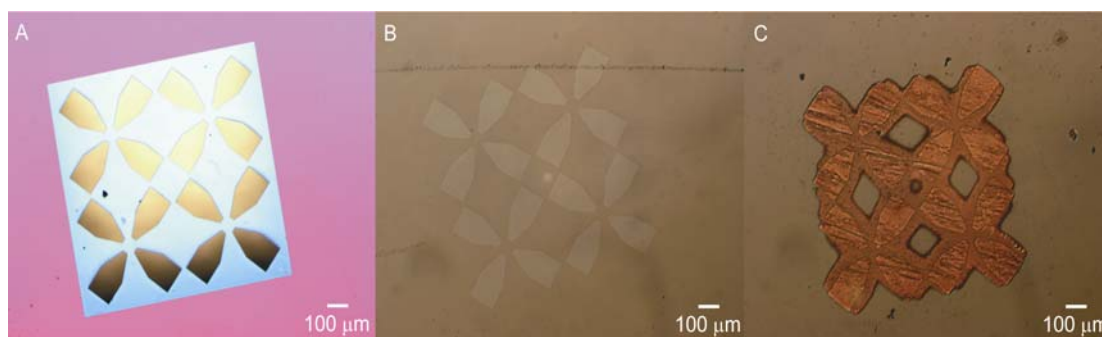


Figure 6.18 Light microscope images of (A) detail of microsieve shadow mask (B) 120 pulses of Pt ($p = 0.01$ mbar, $d = 40$ mm, fluence 5 J cm^{-2}) deposited through the microsieve on an ODT SAM on Au (20 nm) and (C) after 5 minutes ELD of Cu.

As can be seen in Figure 6.18 C, the Cu growth also expanded to outside of the area with Pt clusters. This can be simply overgrowth or a result of the diffusion of Pt clusters over the SAM, leading to enlargement of the patterns. The feature-size is still clearly visible in the image after ELD. No growth takes place on other parts of the substrate, indicating that the ODT SAM protects the Au substrate against ELD growth. This means that the ODT SAM is well ordered and withstands exposure to the alkaline ELD solution.

6.4 Conclusions

Several metals could be deposited *via* PLD through Si_3N_4 nanosieves on SAMs. Besides Au (Chapter 4) also Pd, Pt and Cu form islands on SAMs in the hexagonal pattern replicated from the nanosieve. The island shape, height and lateral

isolation were investigated by AFM friction and height measurements. The morphology of the deposited islands seems not to depend on the use of a sieve. The grain structures resemble the structure of evaporated material. Metals were deposited on different SAMs and on different substrates, (ODT/Au, ODTS/SiO₂, CUTS/SiO₂). These results indicate the versatility and flexibility of PLD in substrate and material use.

Patterns of metal clusters deposited through shadow masks by a small number of pulses (down to 40) on ODT/Au and ODTS/SiO₂ SAMs could be enhanced *via* electroless Cu deposition. Cu structures form on the places where metal(0) particles are present and not on the places where the SAM protects the surface. Deposited Au, Pd and Pt particles all function as ELD catalysts.

6.5 Experimental procedures

SAMs on SiO₂: ODTS SAMs on silicon oxide were prepared as follows: p-type silicon chips were immersed in piranha solution for 15 minutes. The samples were rinsed thoroughly with milliQ water and dried in a nitrogen flow. Directly after drying the chips were immersed in a 0.1 % solution of octadecyltrichlorosilane (ODTS), decyltrichlorosilane (DTS) or 11-cyanoundecyltrichlorosilane (CUTS) in distilled toluene for 2 hours under a nitrogen atmosphere. SAMs were rinsed with toluene. ODTS SAMs had advancing contact angles of 114° and receding angles of 101°, which correspond to a hydrophobic SAM. CUTS SAMs had contact angles of 77° / 57°, which are in agreement with previously reported results.¹⁸

Pulsed Laser Deposition: Patterns of metal clusters were made by performing PLD through nanosieves (as described in Chapter 4 and 5) and microsieves.

Shadow masks: Shadow masks with varying sizes were fabricated by Marc van den Boogaart and Jürgen Brugger from the LMIS1 group at the EPFL in Switzerland. They consisted of silicon nitride membranes supported on a silicon chip.

Electroless deposition: SAM substrates with patterned metal particles were immersed in an ELD solution for 2 to 5 minutes. The ELD plating bath consisted of

an aqueous solution of 40 mM CuSO₄, 140 mM Na₂SO₄, 120 mM Na₄EDTA, 300 mM HC(O)ONa and 30 mM formaldehyde. After dissolving all compounds the solution was brought to a pH value of around 13 using NaOH. The rate of ELD depends on the pH and is higher at higher pH values. After ELD, substrates were gently washed with water and ethanol and carefully dried in a nitrogen stream.

Atomic force microscopy: AFM-analyses were performed on a Nanoscope III multimode AFM (Digital Instruments, Santa Barbara, CA) in tapping mode as described Chapter 4. Contact mode AFM was performed using silicon nitride cantilevers with a spring constant of 0.12 N m⁻¹, and using both E and J-scanner.

Light microscopy: light microscopy was performed using an Olympus BHSM-NL-2 stereo microscope equipped with a colorview 12 CCD camera. AnalySIS software from Soft Imaging System GmbH., Germany was used for capturing images.

6.6 References

- ¹ S. A. Levi, A. Mourran, J. P. Spatz, F. C. J. M. van Veggel, D. N. Reinhoudt, M. Möller, *Chem. Eur. J.* **2002**, 8, 3808-3816.
- ² G. M. Kim, M. A. F. van den Boogaart, J. Brugger, *Microelectron. Eng.* **2003**, 67-68, 609-614.
- ³ (a) C. S. Dulsey, J. H. Georger Jr., V. Krauthammer, D. A. Stenger, T. L. Fare, J. M. Calvert, *Science* **1991**, 252, 551-554; (b) C. D. Zangmeister, R. D. van Zee, *Langmuir* **2003**, 19, 8065-8068.
- ⁴ T. B. Carmichael, S. J. Vella, A. Afzali, *Langmuir* **2004**, 20, 5593-5598.
- ⁵ L. A. Porter Jr., H. C. Choi, J. M. Schmeltzer, A. E. Ribbe, L. C. C Elliot, J. M. Buriak, *Nano Lett.* **2002**, 2, 1369-1372.
- ⁶ D. W. Carr, M. J. Lercel, C. S. Whelan, H. G. Craighead, K. Seshadri, D. L. Allara, *J. Vac. Sci. Technol. A* **1997**, 15, 1446-1450.
- ⁷ H. Kind, A. M. Bittner, O. Vavalleri, K. Kern, T. Greber, *J. Phys. Chem. B* **1998**, 102, 7582-7589.
- ⁸ P. C. Hidber, W. Helbig, E. Kim, G. M. Whitesides, *Langmuir* **1996**, 12, 1375-1380.
- ⁹ H. T. G. Hentzell, C. R. M. Grovenor, D. A. Smith, *J. Vac. Sci. Technol. A* **1984**, 2, 218-219.
- ¹⁰ (e.g.) C. A. Richter, C. A. Hacker, L. J. Richter, E. M. Vogel, *Solid-State Electron.* **2004**, 48, 1747-1752.
- ¹¹ L. T. Zhuravlev, *Langmuir* **1987**, 3, 316-318.
- ¹² H. O. Finklea, L. R. Robinson, A. Blackburn, B. Richter, D. Allara, T. Bright, *Langmuir* **1986**, 2, 239-244.
- ¹³ (a) N. Tilman, A. Ulman, J. S. Schildkraut, T. L. Penner, *J. Am. Chem. Soc.* **1988**, 110, 6136-6144; (b) N. Tilman, A. Ulman, T. L. Penner, *Langmuir* **1989**, 5, 101-111.

- ¹⁴ M. Kölbl, R. W. Tjerkstra, G. Kim, J. Brugger, C. J. M. van Rijn, W. Nijdam, J. Huskens, D. N. Reinhoudt, *Adv. Funct. Mater.* **2003**, 13, 219-224.
- ¹⁵ J. Brugger, M. van den Boogaard, Microsystems Laboratory (LMIS1), EPFL, Lausanne, Switzerland.
- ¹⁶ M. A. F. van den Boogaart, G. M. Kim, R. Pellens, J.-P. van den Heuvel, J. Brugger, *J. Vac. Sci. Technol. B* **2004**, 22, 3174-3177.
- ¹⁷ (a) J. Sagiv, *J. Am. Chem. Soc.* **1980**, 102, 92-98; (b) L. Netzer, J. Sagiv, *J. Am. Chem. Soc.* **1983**, 105, 674-676; (c) S. R. Cohen, R. Naaman, J. Sagiv, *J. Phys. Chem.* **1986**, 90, 3054-3056; (d) A. Ulman, *Chem. Rev.* **1996**, 96, 1533-1554.
- ¹⁸ S. Onclin, A. Mulder, J. Huskens, B. J. Ravoo, D. N. Reinhoudt, *Langmuir* **2004**, 20, 5460-5466.

Chapter 7

Surface-Confined Single Molecules: Assembly and Disassembly of Nanosize Coordination Cages on Gold (111)*

A cavitand, functionalized with four alkylthioether groups at the lower rim and four tolylpyridine groups at the upper rim is able to bind to a gold surface via its thioether groups and forms a coordination cage with Pd(dppp)(OTf)₂ via its pyridine groups. Both the cavitand and the cage complex can be inserted from solution into a self-assembled monolayer (SAM) of 11-mercaptoundecanol on gold. The inserted molecules can be individually detected by AFM as they protrude from the SAM. The cages can be reversibly assembled and disassembled on the gold surface. AFM can distinguish between single cavitand and cage molecules of 2.5 and 5.8 nm height respectively.

*The research described in this Chapter has been published in: E. Menozzi, R. Pinali, E. A. Speets, B. J. Ravoo, E. Dalcanale, D. N. Reinhoudt, *Chem. Eur. J.* **2004**, 10, 2199-2206.

7.1 Introduction

Single molecule experiments are important for bottom-up nanotechnology. The ability to position, to detect and to address individual molecules plays a crucial role in the search for smaller information storage devices. A single molecule would be one of the smallest possible data units (bits) and with a suitable readout technique could lead to terabit inch⁻² storage capacities. Assuming the area occupied by one molecule (bit) to be 1 nm², one square inch could contain 6×10^{14} of these bits. Bottom-up techniques would then lead to the formation of usable devices from single molecules. The controlled assembly of molecules into larger complexes is therefore very important.

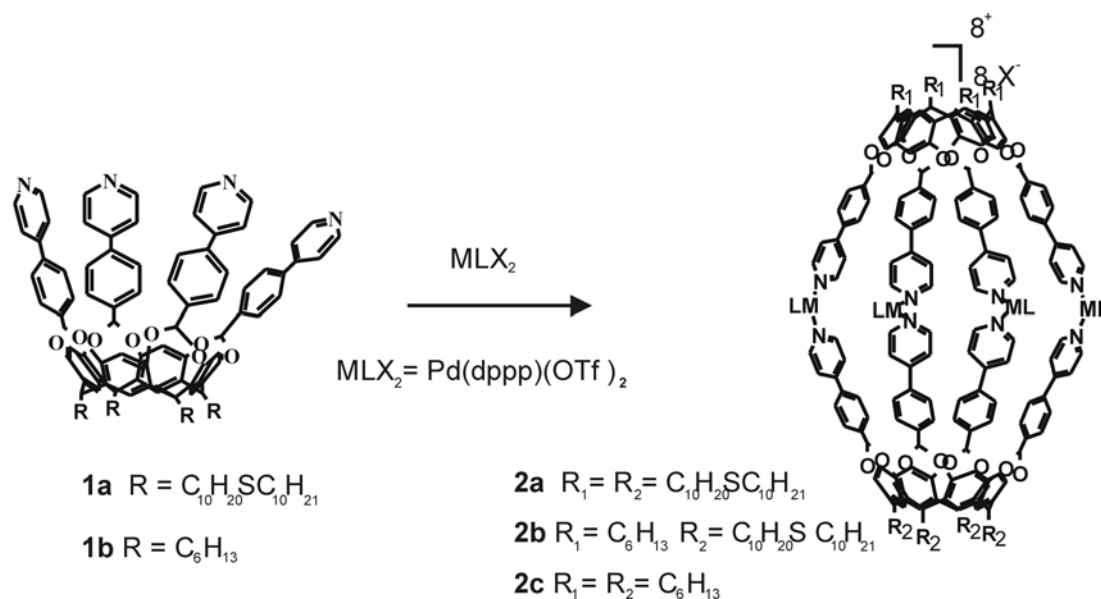
Self-assembly, in its various forms, is emerging as a key technology for the formation of two- or three-dimensional structures.¹ The appeal of self-assembly resides in the thermodynamic control of the process, which leads to the exclusive formation of the desired molecular architecture under a given set of conditions. The reversibility of the process conveys interesting properties such as self-repairing ability and responsiveness to external stimuli. Of the various self-assembly protocols, metal-directed self-assembly is particularly appealing because of the large number of different structural motifs and bond energies that are available through coordination chemistry.² There have been only few attempts so far to transfer self-assembly protocols from the solution phase to surfaces.³ In collaboration with the Dalcanale group our group has recently reported the attachment of thioether functionalized coordination cages to gold substrates in micrometer-size patterned self-assembled monolayers (SAMs),⁴ created by soft lithographic techniques.⁵ The attachment of *single* molecular containers, able to encapsulate ions and neutral molecules on solid surfaces is attractive for single-molecule addressing.⁶

In this Chapter the use of a cavitand, functionalized with four alkylthioether groups at the lower rim and four tolylpyridine groups at the upper rim for single molecule experiments on gold surfaces is described, as well as the use of the cage-complex⁷ assembled from this cavitand. These cavitands were inserted into a mercapto-undecanol (MU) SAM as individually detectable molecules. The self-assembly of coordination *heterocages* from these surface-immobilized cavitands with Pd(dppp)(OTf)₂ is shown. Pre-assembled *homocages* were inserted into MU SAMs on

gold from solution, and could subsequently be disassembled, leaving the individual cavitands embedded in the MU SAM. The insertion and assembly processes were monitored by tapping mode atomic force microscopy (AFM) by measuring the height of individual cavitands and cages.

7.2 Large cavitands and cages

A large cavitand (**1a**) (shown in Scheme 7.1) was used to study the insertion process of these tetrathioether-functionalized molecules and to study the assembly of these cavitands with the palladium complex $\text{Pd}(\text{dppp})(\text{OTf})_2$ on gold surfaces. Cages are formed in solution when cavitand **1a** or **1b** is mixed in equimolar amounts with the palladium complex $\text{Pd}(\text{dppp})(\text{OTf})_2$.⁸ This “cage self-assembly” (CSA) is a highly selective dimerization of two cavitands using four equivalents of transition metal complex, which means that no polymer but only cages are formed. The formation of cages **2** from cavitands **1** in solution is shown in Scheme 7.1.



Scheme 7.1 CSA of nanosized coordination cages **2a**, **2b** and **2c** from 2 equivalents of cavitand **1a** and **1b** and 4 equivalents of $\text{Pd}(\text{dppp})(\text{OTf})_2$.

These cages can also be formed using a platinum salt like $\text{Pt}(\text{dppp})(\text{OTf})_2$. Cage **2** has a very large internal volume of around 1800 \AA^3 . This value has been calculated from a crystal structure obtained for the platinum-coordinated cage.⁸ The crystal structure also shows two ethanol molecules inside the cavity, whereas the eight triflate anions are assembled outside the cavity. In this study the thioether-

functionalized cavitand **1a** is used to investigate the attachment to gold surfaces using the thioether functional groups.

7.3 Surface assembly of cages

The dialkylsulfide groups on the bottom of cavitand **1a** facilitate attachment to gold surfaces as observed for calixarenes⁹ and cyclodextrines.¹⁰ The assembly of ordered self-assembled monolayers (SAMs) of cavitand **1a** on gold surfaces was however not possible for steric reasons. The cross-sectional area of the phenylpyridine-bridged upper rim is much larger than the cross-sectional area of the sulfide chains at the lower rim, making a well-ordered packing on the surface impossible. Self-assembly results in disordered monolayers, on which it was not possible to perform CSA. ‘Molecular ruler’ experiments, as described before⁴ indicated no height difference after the cage assembly step.

In Figure 7.2 the insertion of the cavitand **1a** into an MU SAM on gold is shown. MU SAMs were prepared on flame annealed gold surfaces. Flame annealing of gold layers results in micrometer sized gold terraces which show a Au(111) crystal plane. The use of these atomically flat islands enables single molecule detection by AFM. Hydroxy-terminated SAMs are favoured over methyl-terminated alkylthiolate SAMs because they cause less physisorption of hydrophobic cavitand molecules.⁴

An MU SAM is hydrophilic and is reasonably well ordered. If an MU SAM is immersed in a solvent *e.g.* dichloromethane (DCM) desorption of thiolates (as disulfides¹¹) or gold thiolates¹² might occur, leaving exposed gold available for chemisorption of excess adsorbates from solution. Together with the existing pinholes these exposed gold parts are used for the surface assembly of cavitands *via* insertion. When a MU SAM is immersed in a 1 mM solution of cavitand **1a** in DCM insertion of the thioether functionalized cavitand will take place (see Figure 7.2). Extensive washing (DCM, ethanol and finally water) ensures the removal of all physisorbed material. The samples were analysed by tapping mode AFM.

As can be seen in Figure 7.2, features with heights of approximately 1.87 nm (see Table 7.1 for measured and calculated heights of inserted cages and cavitands) protrude out of the MU-SAM matrix. Determined from X-ray and CPK models it was found that the total height of cavitand **1a** is about 2.5 nm. Considering that the molecules are inserted into a SAM of 0.8 nm height,¹³ they are expected to protrude

from the SAM by approximately 2 nm. This means that individual cavitant molecules protruding from the SAM can be observed. The heights of the features are not always the same. This is mainly caused by the resolution of the section analysis, and might also be caused by the influence of the size of the AFM tip compared to the molecule. Furthermore, the molecule is not necessarily attached with all four thioether feet, so it may be tilted relative to the gold surface. The surface shown in Figure 7.2 displays the triangular structure of the gold (111) surface.

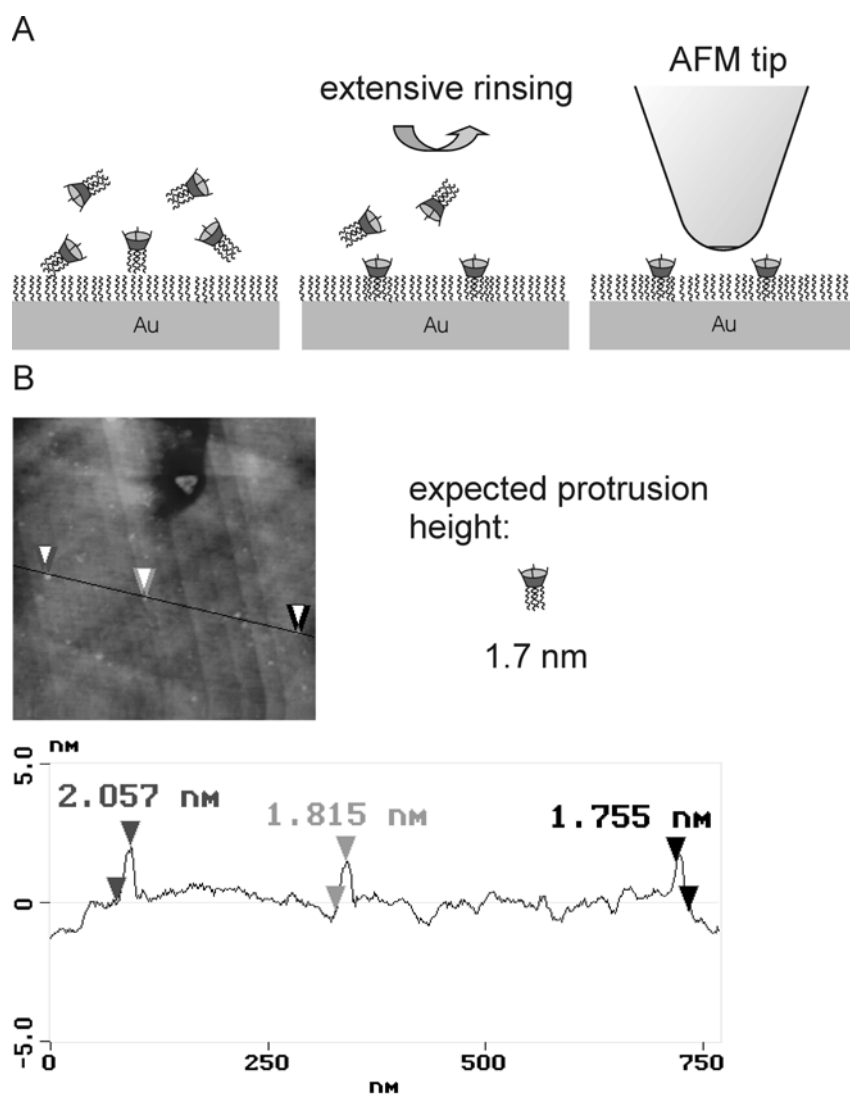


Figure 7.2 (A) Schematic representation of cavitant **1a** insertion and AFM analysis on MU SAM; (B) AFM image (750×750 nm) and section analysis of an MU SAM with inserted phenylpyridine functionalized thioether-footed cavitant **1a**.

The same insertion experiment was performed using the pre-assembled cage complex **2a**. The homocage insertion process of thioether-footed cage **2a** is

schematically shown in Figure 7.3 A. A clean MU SAM was soaked in a 0.25 mM solution of cage **2a** in DCM for 1h at room temperature. After extensive rinsing with DCM, EtOH and finally H₂O, the sample surface was analysed by AFM (see Figure 7.3 B). Here as well the conclusion is that these objects are individual cages inserted into and protruding from the SAM. The average height of the cage is 5.27 nm, which is consistent with the dimensions obtained from the X-ray structure.⁸ In addition to the factor mentioned above, the variations in height can be attributed to the flexible conformation of the sulphide chains at the lower rim of the cages.

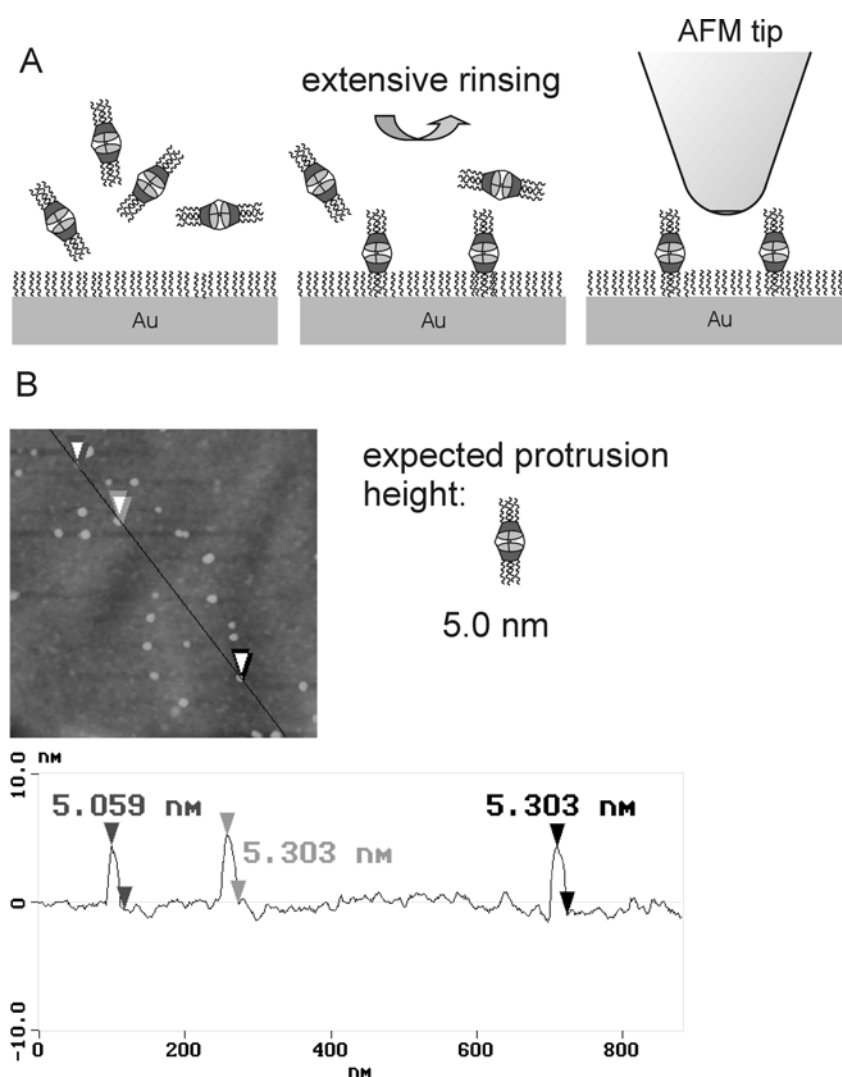


Figure 7.3 (A) Schematic representation of the insertion of homocage **2a** into a MU SAM; (B) AFM height image and section analysis of an MU SAM with inserted homocages **2a**.

Besides the direct insertion of cavitands and *homocages*, cages can also be assembled on the surface from already attached cavitands with cages in solution. An

example is the assembly of the *heterocage* **2b** (Scheme 7.1). Using the cavitands **1** already attached to the surface, nanosize cages **2b** could be assembled on the gold surface.

Upon exposing a SAM with inserted **1a** to a 0.25 mM solution of cage **2c**, with eight hexyl chains at the lower rim of the resorcinarene skeleton, the assembly of *heterocage* **2b** on gold was effected. The formation of cages **2b** on gold requires ligand exchange with cages **2c** present in solution. Ligand exchange between cages has already been proven in solution.^{7g} Our experiments were performed using the cage **2c** of the cavitands without thioether chains to make sure that the cages seen on the surface were assembled in two steps on the surface, and not directly inserted from solution (see control experiments below).

Extensive rinsing with DCM, EtOH and finally H₂O ensured the removal of all physisorbed material. AFM experiments (see Figure 7.4) and section analysis showed the presence of two different features: (i) objects with a height of approximately 4-5 nm (ii) objects with a height of approximately 2 nm. The different heights of the objects suggest that both uncapped cavitands and *heterocages* are present. Partial success of the capping reaction is not surprising considering that very dilute conditions do not favour complete ligand exchange. In order to verify the correctness of the experimental AFM data X-ray data from alkyl-footed cavitands were used to estimate the height of cavitand **1a** (2.5 nm) and cage **2a** (5.8 nm), also taking into consideration the contribution of the thioether chains in a backfolded conformation to the total length (see Table 7.1). The MU molecules in the SAM are tilted to optimise Van der Waals interactions and packing stability. The thickness of the MU monolayer is approximately 0.8 nm, due to this tilted orientation.¹⁴ Based on of these considerations *homocage* **2a** is expected to protrude beyond the OH-terminated surface by at least 5.0 nm and cavitand **1a** by approximately 1.7 nm. Table 7.1 shows the calculated heights and the average heights measured by AFM of the inserted cavitands and cages. Heights were calculated using CPK data for the cavitands and cages.

Table 7.1 Calculated and measured protrusion heights of cavitands and cages.

Cavitand and Cages	Height from x-ray data (nm)	Calculated height ^a (nm)	Measured height (AFM) (nm)
cavitand 1a	2.5	1.7	1.87 ± 0.18
homocage 2a	5.8 ^b	5.0	5.27 ± 0.59
heterocage 2b	4.8 ^c	4.0	3.96 ± 0.32

^a The expected data are calculated by subtracting the thickness of the MU SAM (0.8 nm) from CPK data

^b Value calculated for the upper thioether chains in the backfolded conformation (1.8 nm)

^c Value calculated for the hexyl chains in the *all-trans* conformation (0.8 nm)

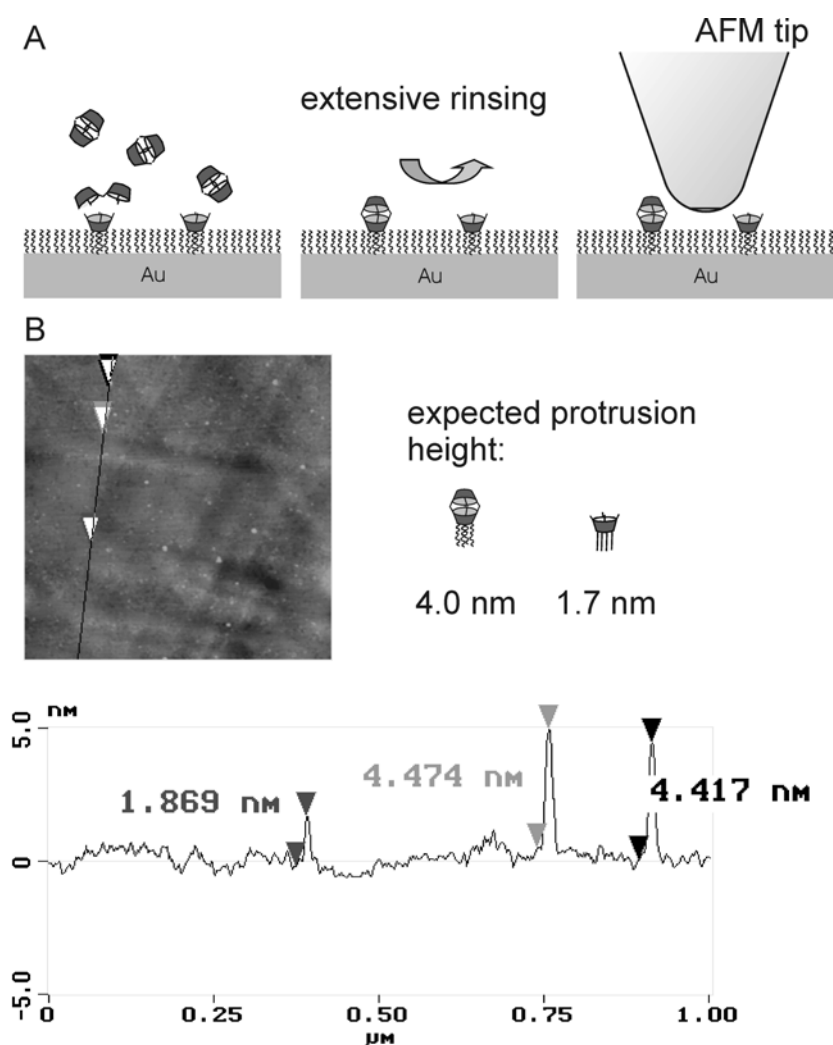


Figure 7.4 (A) Schematic representation of the surface assembly of heterocages **2b** from surface bound cavitands **1a** with cages **2c** in solution. (B) AFM image and section analysis of an MU SAM with randomly scattered heterocages **2b** and cavitands **1a**.

The cages assembled on the surface can also be disassembled again using triethylamine (Et_3N). Et_3N competes with the pyridine functionalities of the cavitands to bind Pd centres. Because of the higher concentration of Et_3N compared to the surface assembled cages, the cages are disassembled, shown schematically in Figure 7.5.

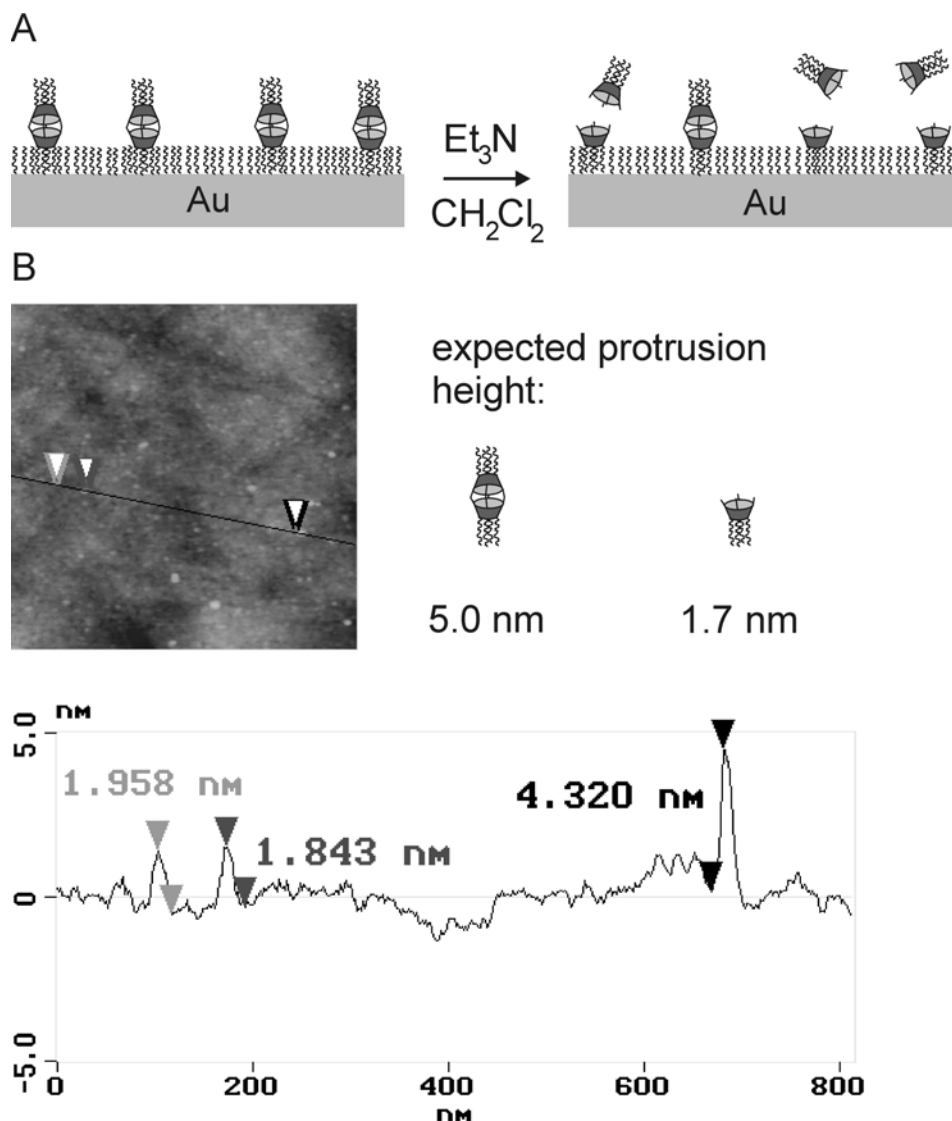


Figure 7.5 (A) Schematic representation of the disassembly of the surface bound cages **2a**. (B) AFM height image and section analysis of partly disassembled cages **2a** in an MU SAM.

A substrate with the in the MU SAM inserted *homocage 2a* was immersed in a 5 mM solution of Et_3N in ethanol for one hour. In Figure 7.5 B features of different heights can be seen. Most of the features have sizes corresponding to the inserted cavitands, but also features corresponding to the intact inserted cages are present.

Et₃N was able to shift the equilibrium towards the formation of [Pd(dppp)(Et₃N)₂(OTf)₂] and free cavitand.

Since the MU SAMs were clean and had been extensively rinsed prior to the insertion experiments in order to remove physisorbed material, it was assumed that the features observed in AFM are inserted cavitands or cages. To confirm these results and to exclude artefacts, control experiments have been carried out.

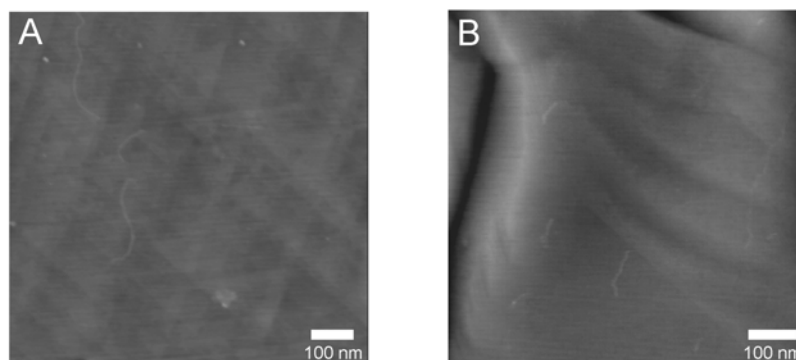


Figure 7.6 AFM height images of MU SAMs after (A) immersion in **1b** solution and (B) immersion in **2c** solution. (height scale from 0 to 20 nm from dark to light)

These control experiments were performed using cavitand **1b** and cage **2c** with inert hexyl tails instead of thioethers at the lower rim (Scheme 7.1). An MU SAM was immersed in a 0.25 mM DCM solution of cavitand **1b** or cage **2c** for 1 hour. After extensive rinsing with solvents the substrates were analyzed by TM-AFM (Figure 7.6). The analyses clearly show that no detectable features are present on the gold surface. Hence, no insertion or adsorption of molecules occurs in absence of a functional group with affinity for gold and the thioether groups in cavitand **1a** and cage **2a** are required for binding to the gold substrate.

7.4 Conclusions

Individual molecular containers of nanosize dimensions have been assembled in a controlled fashion on gold. The insertion into MU SAMs on gold, the assembly in two steps after cavitand insertion and the disassembly of the Pd-coordinated cage compounds were monitored by TM-AFM. TM-AFM clearly showed the single molecules and complexes protruding from the MU SAM. Because of their large sizes

the cavitands and cages could be clearly distinguished, making it possible to monitor the assembly and disassembly processes. The reversibility of the system might be exploited to reversibly encapsulate guest molecules in the cages on the surface. Also the potential to generate *heterocages* with different substituents in the upper and lower part opens new possibilities. The top half of *heterocages* might be equipped with further functionalities for specific interaction with molecules or nanoparticles. The assembly and disassembly of the cages could be used as a write, read and erase circle.

7.5 Experimental procedures

General methods: cavitands **1a** and **1b** and Pd(dppp)(Otf)₂ were prepared by E. Menozzi and R. Pinali as described in ref ¹⁵. For monolayer preparation and rinsing *p.a.* grade solvents were used as received. Water was purified by a Millipore (MilliQ, Q2) system. 11-mercapto-undecanol (MU, 97 %, Aldrich) was used as received.

Gold substrates were obtained from Metallhandel Schroer GmbH., Lienen, Germany. Samples consisted of an 11 × 11 mm glass substrate with a 5 nm chromium adhesion layer and on top of that 200 nm gold. Prior to use substrates were rinsed with dichloromethane, dried in an N₂ flow and annealed in a hydrogen (purity 6) flame. After annealing the slightly cooled substrates were first immersed in ethanol. After 5 minutes the substrates were rinsed with ethanol and immersed in the MU solution.

AFM-analyses were performed on a Nanoscope III multimode AFM (Digital Instruments, Santa Barbara, Ca., USA) in the *tapping mode* using the E-scanner (~12 micron), as described in Chapter 4.

SAM preparation: All glassware used was cleaned in fresh piranha solution (3 parts sulfuric acid, 1 part 30 % hydrogen peroxide) for at least 15 minutes. **Warning: Piranha solution should be handled with caution. It has been reported to detonate unexpectedly. Contact with organic solvents must be avoided.** After removal from the piranha solution the glass was rinsed extensively with MilliQ water to remove all acid. Gold substrates for AFM measurements were flame annealed using a H₂ flame (grade 6) and, after cooling, kept in ethanol solution for 5 minutes. Substrates were immersed with minimal delay in a 1.0 mM solution of MU in ethanol, for 14 hours at room temperature. The substrates were removed from the solution and

extensively rinsed with pure water, ethanol and dichloromethane. Before insertion experiments, the MU SAMs were checked for the presence of nm-size features by TM-AFM. To exclude that pollution particles on the SAM are mistaken for inserted cavitands, only SAMs with less than ~ 3 features per $1 \mu\text{m}^2$ were used.

Insertion of cages and cavitands was obtained by soaking the MU monolayer in a 0.25 mM solution of cage **2a** or cavitand **1a** in dichloromethane for 1 hour at room temperature. Self-assembly of *heterocage* **2b** was effected by exposing a SAM of cavitand **1a** to a 0.25 mM solution of cage **2c** in dichloromethane for 1 hour. *Homocage* disassembly was achieved by soaking the MU SAMs with inserted cage **2a** with a ~ 5 mM solution of Et_3N in CH_2Cl_2 for 1 hour. Control experiments using cavitand **1b** and cage **2c** were performed in the same way as the insertion of **1a** and **2a**.

All monolayers with inserted molecules were extensively rinsed with *p.a.* ethanol and dichloromethane and dried in a nitrogen flow before AFM analyses.

7.6 References

¹ (a) J.-M. Lehn, *Science* **2002**, 295, 2400-2403; (b) D. N. Reinhoudt, M. Crego-Calama, *Science* **2002**, 295, 2403-2407; (c) G.M. Whitesides, B. Grzybowski, *Science* **2002**, 295, 2403-2407.

² (a) M. Fujita, J. Yazaki, K. Ogura, *J. Am. Chem. Soc.* **1990**, 112, 5645-5647; (b) M. Fujita, K. Umemoto, M. Yoshizawa, N. Fujita, T. Kusukawa, K. Biradha, *Chem. Commun.* **2001**, 509-518; (c) S. Leininger, B. Olenyuk, P.J. Stang, *Chem. Rev.* **2000**, 100, 853-908.

³ (a) I. Weissbuch, P. N. W. Baxter, S. Cohen, H. Cohen, K. Kjaer, P. B. Howes, J. Als-Nielsen, G. S. Hanan, U. S. Schubert, J.-M. Lehn, L. Leiserowitz, M. Lahav, *J. Am. Chem. Soc.* **1998**, 120, 4850-4860; (b) A. Hatzor, T. Moav, H. Cohen, S. Matlis, J. Libman, A. Vaskevich, A. Shanzer, I. Rubinstein, *J. Am. Chem. Soc.* **1998**, 120, 13469-13477; (c) A. Hatzor, T. Moav, S. Yochelis, A. Vaskevich, A. Shanzer, I. Rubinstein, *Langmuir* **2000**, 16, 4420-4423.

⁴ S. A. Levi, P. Guatteri, F. C. J. M. van Veggel, G. J. Vancso, E. Dalcanale, D. N. Reinhoudt, *Angew. Chem. Int. Ed.* **2001**, 40, 1892-1896.

⁵ Y. Xia, G. M. Whitesides, *Angew. Chem. Int. Ed.* **1998**, 37, 550-575.

⁶ A. Friggeri, H.-J. van Manen, T. Auletta, X.-M. Li, S. Zapotoczny, H. Schönherr, G. J. Vancso, J. Huskens, F. C. J. M. van Veggel, D. N. Reinhoudt, *J. Am. Chem. Soc.* **2001**, 123, 6388-6395.

⁷ For cavitand-based coordination cages see: (a) P. Jacopozzi, E. Dalcanale, *Angew. Chem. Int. Ed.* **1997**, 36, 613-615; (b) O. D. Fox, N. K. Dalley, R. G. Harrison, *J. Am. Chem. Soc.* **1998**, 120, 7111-7112; (c) O. D. Fox, N. K. Dalley, R. G. Harrison, *Inorg. Chem.* **1999**, 38, 5860-5863; (d) O.D. Fox, M. G. M. Drew, P.D. Beer, *Angew. Chem. Int. Ed.* **2000**, 39, 136-140; (e) F. Fochi, P. Jacopozzi, E. Wegelius, K. Rissanen, P. Cozzini, E. Marastoni, E. Fiscaro, R. Fokkens, E. Dalcanale, *J. Am. Chem.*

Soc. **2001**, 123, 7539-7552; (f) N. Cuminetti, M. H. K. Ebbing, P. Prados, J. de Mendoza, E. Dalcanale, *Tetrahedron Lett.* **2001**, 42, 527-530; (g) L. Pirondini, F. Bertolini, B. Cantadori, F. Ugozzoli, C. Massera, E. Dalcanale, *Proc. Natl. Acad. Sci. USA* **2002**, 99, 4911-4915; (h) R.G. Harrison, O.D. Fox, M.-O. Meng, N.K. Dalley, L.J. Barbour, *Inorg. Chem.* **2002**, 41, 838-843.

⁸ R. Pinalli, V. Cristini, V. Sottili, S. Geremia, M. Campagnolo, A. Caneschi, E. Dalcanale, *J. Am. Chem. Soc.* **2004**, 126, 6516-6517.

⁹ E. U. Thoden van Velzen, J. F. J. Engbersen, P. J. de Lange, J. W. G. Mahy, D. N. Reinhoudt, *J. Am. Chem. Soc.* **1995**, 117, 6853-6862.

¹⁰ (a) M. W. J. Beulen, J. Bügler, B. Lammerink, F. A. J. Geurts, E. Biemond, K. G. C. van Leerdam, F. C. J. M. van Veggel, J. F. J. Engbersen, D. N. Reinhoudt, *Langmuir* **1998**, 14, 6424-6429; (b) M. W. J. Beulen, J. Bügler, M. R. de Jong, B. Lammerink, J. Huskens, G. J. Vancso, B. A. Boukamp, H. Wieder, A. Offenhäuser, W. Knoll, F. C. J. M. van Veggel, D. N. Reinhoudt, *Chem. Eur. J.* **2000**, 6, 1176-1183; (c) T. Auletta, B. Dordi, A. Mulder, A. Sartori, S. Onclin, C. M. Bruinink, M. Péter, C. A. Nijhuis, H. Beijleveld, H. Schönherr, G. J. Vancso, A. Casnati, R. Ungaro, B. J. Ravoo, J. Huskens, D. N. Reinhoudt, *Angew. Chem. Int. Ed.* **2004**, 43, 369-373

¹¹ (a) J. B. Schlenoff, M. Li, H. Ly, *J. Am. Chem. Soc.* **1995**, 117, 12528-12536; (b) E. Cooper, G. J. Legget, *Langmuir* **1999**, 15, 1024-1032; (c) A. Friggeri, H. Schönherr, H.-J. van Manen, B.-H. Huisman, G. J. Vancso, J. Huskens, F. C. J. M. van Veggel, D. N. Reinhoudt, *Langmuir* **2000**, 16, 7757-7763; (d) C. E. D. Chidsey, C. R. Bertozzi, T. M. Putvinski, A. M. Muijsce, *J. Am. Chem. Soc.* **1990**, 112, 4301.

¹² J. A. M. Sondag-Huethorst, C. Schönenberger, L. G. J. Fokkink, *J. Phys. Chem.* **1994**, 98, 6826-6834.

¹³ S. Levi, Supramolecular chemistry at the nanometer level, *Ph.D. Thesis*, University of Twente, The Netherlands **2001**.

¹⁴ A. Ulman, *Chem. Rev.* **1996**, 96, 1533-1554.

¹⁵ E. Menozzi, R. Pinali, E. A. Speets, B. J. Ravoo, E. Dalcanale, D. N. Reinhoudt, *Chem. Eur. J.* **2004**, 10, 2199-2206.

Summary

The central topic of this thesis is the deposition of metals on Self-Assembled Monolayers (SAMs). Metals are deposited in the form of submicron scale islands, nanometer scale clusters, and as supramolecular, organometallic coordination cages. Several SAMs on various substrates were prepared and analyzed for their quality and usefulness as metal deposition platform. Pulsed laser Deposition (PLD) is used as metal deposition technique in combination with nanosieve shadow masks for patterning. The combination can be used to deposit metal on organic SAMs in submicron patterns without damaging the SAM. Small clusters could be deposited on SAMs using PLD. The clusters were proven to be insulated from the substrate by the SAM using scanning tunneling microscopy (STM) and conducting probe atomic force microscopy (CP-AFM). Thin patterns of Pt, Pd and Au could be enhanced by electroless deposition (ELD) of Cu. Large cavitands, with thioether functionalities could be assembled on surfaces and analyzed as single molecules. Via organometallic coordination cage complexes could be assembled and disassembled on a single molecule scale, and monitored by atomic force microscopy (AFM).

In Chapter 2 a literature overview of the field of molecular electronics is given. The focus is on the use of SAMs in electronic devices and the electronic analysis of SAMs and surface-immobilized single molecules. The most important device architectures and measurement setups are discussed. Molecular electronic devices like SAM field-effect transistors (SAMFETs), diodes, switches and capacitors are described. Most recently the focus is on correct and reproducible measurements of electronic properties of molecules, *i.e.* a form of ‘benchmarking’ of the field of molecular electronics.

In Chapter 3 the preparation and analysis of SAMs made from difunctional molecules is described. SAMs of 1,9-nonanedithiol (NDT) seem suitable for the incorporation into nanoscale electronic devices. XPS, electrochemistry (cyclic voltammetry and electrochemical impedance spectroscopy) and contact angle measurements indicate that the molecules are in an upright position on the surface and expose a free thiol group. 1,16-Hexadecanedithiol did not form ordered SAMs and

most molecules were bound to the surface with both thiol groups. Biphenyldithiol and 1,4-di(phenylethynyl-4'-thioacetyl)benzene formed SAMs with a lower order although the molecules were only bound with one S-group to the surface. The insertion of conjugated molecules into decanethiol (DT) SAMs was investigated.

Chapter 4 describes the preparation of Au-SAM-Au sandwiches by Pulsed Laser Deposition (PLD) of Au through silicon nitride nanosieves on SAMs. Patterns of islands with submicron diameters could be made over areas of several square millimeters. Electrochemical Cu-deposition showed that on octadecanethiol (ODT) SAMs, roughly 15 % of these islands deposited at a pressure of 0.01 mbar are electrically insulated from the gold surface. If lower deposition pressures were used no insulated islands were obtained. On the thinner NDT SAMs no insulated islands could be obtained irrespective of what deposition pressure was used.

In Chapter 5 the deposition with PLD of nm size Au, Pd and Pt clusters is described. Clusters, with sizes depending on the deposition conditions were prepared on carbon membranes and analyzed with transmission electron microscopy (TEM). These clusters were also deposited on SAMs. Pd clusters were deposited on top of DT SAMs and it was shown with scanning tunneling microscopy (STM) that these particles were insulated from the Au substrate. A Coulomb blockade was observed for this system even at room temperature. Conducting probe atomic force microscopy (CP-AFM) also showed that gold clusters deposited on ODT and DT SAMs were insulated from the Au substrate by the SAM. The bias necessary to visualize the clusters in the current (I) images was higher for the thicker ODT SAM than for the DT SAM.

Chapter 6 shows AFM analyses of islands made from various metals, deposited on various SAMs on Au and SiO₂. The versatility of the PLD technique in combination with nanosieves and SAMs is demonstrated. The use of patterns of deposited metal clusters made by PLD through nanosieves and microsieves on SAMs for pattern replication by electroless deposition (ELD) of Cu is described. Patterns that were made using short PLD can be selectively enhanced with Cu. This method reduces the potentially damaging gas phase deposition step.

In Chapter 7 large cavitand molecules and Pd-containing cage complexes that are functionalized with thioether groups are inserted into mercaptoundecanol (MU) SAMs on gold. The inserted molecules and complexes can be detected by AFM as they protrude from the SAM. Inserted cage complexes can be disassembled using

triethylamine as competing ligand for the Pd centers. Cages in solution can exchange with single surface bound cavitands forming a new “mixed” cage on the surface.

The results of the work described in this thesis show that PLD can be a valuable technique that can be used for the fabrication of metal-molecule contacts on SAMs. For larger electrode sizes, nanosieves can be used for patterning the deposited metal, while short direct deposition yields insulated clusters with nanometer sizes on SAMs. The preparation of metal-SAM-metal junctions with different dimensions might be useful in the electronic analysis of SAMs and single molecules and in the fabrication of small electronic devices. Single molecules that can be assembled and disassembled on a surface shows a potential data storage system with nanometer size bits, that can be written, read and erased by reversible supramolecular processes.

Samenvatting

Het centrale onderwerp van dit proefschrift is de depositie van metalen op zelf-geassembleerde monolagen (SAMs) (één molecuul dikke, geordende, lagen op een oppervlak, die uit zichzelf gevormd worden). Metalen werden gedeponerd in de vorm van platte eilandjes met diameters kleiner dan een micrometer, clustertjes van enkele nanometers groot en supramoleculaire organometaal coördinatie-kooien. Verschillende SAMs op diverse substraten werden gemaakt and geanalyseerd om hun kwaliteit te bepalen en te zien of ze gebruikt konden worden als stabiele ondergrond voor metaaldepositie. Gepulste laser depositie (PLD) wordt gebruikt als metaal depositietechniek in combinatie met nanozeef schaduwmaskers voor patronering. Deze combinatie kan gebruikt worden om metaal op organische SAMs te deponeren in sub-micrometer patronen zonder de monolaag te beschadigen.. Kleine clustertjes konden ook worden gedeponerd met behulp van PLD. Met behulp van “scanning tunneling microscopy” (STM) (waarin een klein draadje vlak boven een oppervlak wordt bewogen om zo de elektronische eigenschappen te bepalen) en “conducting probe atomic force microscopy” (CP-AFM) (waarin een dun naaldje een oppervlak aftast en tegelijkertijd de stroom door het sample meet) werd bewezen dat deze clustertjes geïsoleerd van het substraat op de SAM lagen. Nanometer dunne patronen van platina, palladium en goud-clusters konden worden versterkt met behulp van electroless depositie (ELD) (een methode om uit een oplossing metaal te deponeren op oppervlakken) van koper. Grote cavitandmoleculen, met thioether functionaliteiten konden worden geassembleerd op goudoppervlakken en worden geanalyseerd als individuele moleculen. Door middel van organometaal coördinatie konden kooicomplexen worden opgebouwd en weer afgebroken, en dit kon op de schaal van één molecuul worden gevolgd met behulp van “*tapping mode*” AFM (waarin een dun vibrerend naaldje voorzichtig over een oppervlak wordt bewogen).

In Hoofdstuk 2 wordt een literatuuroverzicht van het gebied van de moleculaire elektronica gegeven. De nadruk ligt op het gebruik van monolagen in functionele elektronische structuren en de elektronisch eigenschappen meten van monolagen en op een oppervlak verankerde individuele moleculen. De belangrijkste elektronische structuren en meetopstellingen worden bediscussieerd. Moleculair-

elektronische structuren (kleine apparaatjes die moleculen gebruiken als stroomdraadjes en schakelaars) zoals SAM veld-effect transistoren (SAMFETs), diodes, schakelaars en capacitors worden beschreven. Op het moment ligt de focus op het correct en reproduceerbaar meten van elektronische eigenschappen van moleculen en monolagen om als het ware een meetstandaard te verkrijgen.

In hoofdstuk 3 wordt de bereiding en analyse van monolagen op goud gemaakt uit gedifunctionaliseerde moleculen beschreven. monolagen gemaakt van 1,9-nonaandithiol (NDT) lijken geschikt om in nanoschaal elektronische structuren te worden gebruikt. XPS, elektrochemie (cyclische voltametrie en elektrochemische impedantie spectroscopie) en contacthoek metingen geven aan dat de moleculen zich in een rechtopstaande positie op het goudoppervlak bevinden, terwijl een vrije thiolgroep uitsteekt. 1,16-Hexadecaandithiol vormde geen geordende monolagen. De meeste moleculen zijn met beide thiolgroepen aan het oppervlak gebonden. Bifenyldithiol en 1,4-di(fenylethynyl-4'-thioacetyl)benzeen vormden minder goed geordende SAMs hoewel de moleculen wel slechts met een S-groep aan het oppervlak gebonden zijn. De mogelijkheid om geconjugeerde moleculen te inserteren in decaanthiol(DT) monolagen werd onderzocht.

Hoofdstuk 4 beschrijft de bereiding van goud-monolaag-goud sandwiches door PLD van Au door siliciumnitride nanozeven. Patronen van goudeilanden met sub-micrometer diameters konden gemaakt worden over oppervlakken van enkele vierkante millimeters. Elektrochemische koperdepositie laat zien dat op octadecaanthiol (ODT) SAMs, 15 % van deze eilandjes gedeponerd bij een druk van 0.01 mbar elektronisch geïsoleerd van het goud oppervlak zijn. Wanneer lagere depositie drukken werden gebruikt konden er geen geïsoleerde eilanden verkregen worden. Op dunnere NDT monolagen konden geen geïsoleerde eilanden worden verkregen ongeacht de gebruikte druk

In Hoofdstuk 5 is de depositie met PLD van nm grote goud, palladium en platina clusters beschreven. Clusters met afmetingen afhankelijk van de depositie condities werden gemaakt op koolstofmembranen en geanalyseerd met transmissie elektronenmicroscopie (TEM). Deze clusters werden ook gedeponerd op monolagen. palladium clusters werden gedeponerd op DT monolagen en met STM werd aangetoond dat ze geïsoleerd van het goud substraat zijn. Een Coulomb blokkade werd geobserveerd voor dit systeem zelfs bij kamer temperatuur CP-AFM liet zien dat Au clusters gedeponerd op ODT en DT monolagen geïsoleerd van het goud substraat

waren door de monolaag. Het voltage dat nodig is om de clusters te visualiseren in het stroom (I) plaatje was zoals verwacht hoger voor de dikkere ODT SAMs dan voor de DT SAMs.

In Hoofdstuk 6 worden eilanden, gemaakt van diverse metalen gedeponerd op diverse monolagen op goud en siliciumdioxide, beschreven. De PLD techniek in combinatie met nanozeven en monolagen blijkt zeer veelzijdig en flexibel. Het gebruik van patronen van gedeponerde metaal clusters gemaakt met PLD door nanozeven en microzeven op monolagen voor de patroon versterking door ELD met koper is beschreven. Patronen, die gemaakt zijn door korte PLD, kunnen selectief verduidelijkt worden met koper. Deze methode minimaliseert de potentieel beschadigende gasfase depositie stap.

In Hoofdstuk 7 werden grote cavitanden en metaal (palladium) bevattende kooi complexen die gefunctionaliseerd zijn met thioetherketens geïnserteerd in mercaptoundecanol (MU) monolagen op goud. De geïnserteerde moleculen en complexen kunnen met AFM gedetecteerd worden omdat ze boven de monolaag uitsteken. Geïnserteerde kooicomplexen kunnen worden afgebroken met triethylamine als concurrerende ligande voor de palladiumcentrums. Kooien in oplossing kunnen uitwisselen met enkele oppervlakte gebonden cavitanden en zo nieuwe, gemengde kooien vormen.

De resultaten van het werk dat beschreven wordt in dit proefschrift laten zien dat PLD mogelijk bruikbaar is om metaal-molecuul contacten te maken op SAMs. Voor het maken van grotere elektrodes, kunnen nanozeven gebruikt worden, terwijl korte depositie kleine geïsoleerde clustertjes oplevert op monolagen. De bereiding van metaal-monolaag-metaal juncties met verschillende dimensies kan gebruikt worden voor elektronische analyse van monolagen of enkele moleculen, en voor de fabricage van kleine elektrische apparaatjes. Individuele moleculen die op oppervlakte kunnen worden geassembleerd en weer afgebroken vormen een potentieel dataopslag systeem met nanometerschaal bits, die kunnen worden beschreven, uitgelezen en gewist door middel van reversibele supramoleculaire processen.

Dankwoord

In de vier jaar die ik als AIO bij SMCT gewerkt zijn er veel mensen geweest die bedankt moeten worden voor samenwerking, supervisie, gezelligheid etc. Als eerste wil ik David Reinhoudt mijn promotor bedanken voor het mij de kans geven om een promotieonderzoek te doen bij SMCT. David, bedankt voor de vrijheid die ik had om dingen te gaan doen die misschien niet helemaal in onze groep pasten, en dat je toch altijd zorgde dat alles correct gebeurde en me liet focussen op de belangrijke dingen. De goede voorzieningen binnen MESA⁺ en de eenvoud om samen te werken met mensen uit allerlei disciplines zijn voor een belangrijk deel door jou geregeld, bedankt daarvoor.

Frank van Veggel, mijn dagelijks begeleider in de eerste anderhalf jaar, wil ik bedanken voor het mij bekend laten maken in een geheel nieuw gebied in de scheikunde. Om als “organisch” chemicus te beginnen op een zo fysisch gebied als het monolagen onderzoek vergt wel wat aanpassing maar met jou hulp ging dat eigenlijk gesmeerd.

Bart Jan Ravoo, die het van Frank overnam, wil ik bedanken voor het sturen van mijn onderzoek, het nakijken van hoofdstukken en artikelen etc., ondanks dat het voor jou ook nogal een switch in onderzoek was, was je een goed begeleider. Je kon me altijd motiveren en hebt me goed geholpen om in de laatste jaren veel resultaten te verkrijgen.

Jürgen Brugger, Nanolink director, heeft mij de eerste jaren inzicht gegeven wat er binnen MESA⁺ gebeurde, daarvoor bedankt. De Nanolink werk/ski-week in Zwitserland was onvergetelijk en heeft een goede basis gelegd voor de komende samenwerkingsverbanden met de verschillende MESA⁺ mensen. Al vrij snel zag ik dat organische chemie niet de enige weg naar succes was, maar dat er met lithografie, scanning probes, en nanozeven veel leuke dingen gedaan konden worden. I also worked together with Gyuman Kim at that time, thank you for the pleasant cooperation. Martin Bennink ook bedankt voor de Nanolink begeleiding in de laatste jaren en het maken van mooie plaatjes en posters.

From Parma came a few people with whom I cooperated on the work described in Chapter 7. First, Roberta Pinalli, then my first student Romina Ramingo and to finish it up Edoardo Menozzi, all from the group of prof. Enrico Dalcanale. It was a very pleasant cooperation and lead to a nice publication, thank you all. A special thanks for Prof. Dalcanale for his efforts to help arrange our workweek-meeting at the university of Parma.

Vlak daarna kwam Jeroen Bode afstuderen, eerst moest ik je nog delen met Monica maar later werkte je full-time voor mij. Ik heb uiteindelijk besloten om een andere weg op te gaan met mijn proefschrift, vandaar dat je resultaten hier niet vermeld zijn, evengoed bedankt natuurlijk.

Daniele Bonacchi thanks for showing me what single molecule magnets were. Our cooperation (as part of your thesis) showed me again some interesting different research.

Het grootste deel van mijn proefschrift heb ik met pulsed laser deposition gewerkt. Dave Blank en Guus Rijnders van harte bedankt om mij te laten werken in jullie labs, en vooral voor de discussies en het bedenken van nieuwe plannen. Frank Roesthuis, Jeroen Steen en Frank Vroegindeweij, wil ik bedanken voor de hulp met het PLDen.

Harold Zandvliet, Nuri Oncel en Ann-Sofie Hallbäck van vaste stof fysica bedankt voor de prettige samenwerking die op een goed moment kwam. Ik zocht een goede methode om kleine metaalclusterstjes op SAMs te analyseren, en wat beter dan dat op een state of the art STM te doen. Onze samenwerking heeft al tot een aantal publicaties geleid en hopelijk worden het er nog meer.

Barbara Dordi wil ik bedanken voor het met conducting probe AFM meten van mijn samples, ook dit was een belangrijk onderdeel van onze publicatie. Richard Egberink bedankt voor het synthetiseren en beschikbaar stellen van enkele geconjugeerde moleculen.

Marcel de Bruine, Ben Lammerink, Richard Egberink, Carla Weber, Izabel Katalanc bedankt voor de support op gebieden van computers, administratie, bestellingen, etc.

De mensen van de MTP groep wil ik bedanken voor het ons toelaten in het AFM-hok. En speciaal Holger Schönherr voor het altijd open staan voor al dan niet AFM gerelateerde vragen.

Bernard Boukamp van de AMK groep bedankt voor het beantwoorden van vragen aangaande elektrochemie.

De CMA-lab mensen Albert van den Berg, Mark Smithers en Enrico Keim bedankt voor het meten van TEM, SEM en XPS.

Dan het sociale aspect. Het gaat te ver om iedereen hier op te noemen maar een aantal mensen wil ik nog persoonlijk bedanken. De jongens van het SMCT voetbal team en speciaal, Alart, Wiljan, Steffen, Miguel en Paolo van het kampioenselftal. De vrijdag zaalvoetbal wedstrijden waren vaak hard, vaak liepen de emoties hoog op, soms raakte er eens iemand geblesseerd maar het was altijd plezier, en de nodige ontspanning naast het werken natuurlijk. Wiljan en Leon, en vrouwen bedankt voor de gezelligheid tijdens onze computer avondjes.

De donderdagavondgroep bij de Beiaard en dan vooral de hardcore van Barbara, Bas, Allesio, Olga, Fernando, Lourdes, Miguel, Mattijs, Marius, Bart Jan. En natuurlijk al die anderen van en buiten de universiteit die ik vergeten ben.

Dan Friso, Roel, Hugo, Jeroen, Niels, Nicky, Jorrit, en Roy, uit Zwolle; het is logisch dat die mooie stad onze verzamelpunt blijft. En als ik dan weer eens wat leuk voetbal wilde zien (dat mankeert er in Twente nog wel eens aan) dan waren de meeste van jullie daar, nooit te beroerd om eens goed uit te leggen wat er goed of fout ging.

Barbara en Bas bedankt voor de gezellige etentjes bij jullie en ons thuis. Ik denk dat we hard op weg zijn om food & wine “experts” te worden. Als we alle vier de chemie niet meer zien zitten kunnen we wel restaurant beginnen.

Jeroen van Ameijde, Dennis Lensveld, Guus Rijnders en Aldrik Velders bedankt voor het nalezen van mijn concept proefschrift, het wordt er toch altijd weer beter op na wat kritisch genakijk.

Dan wil ik Roel en Barbara, mijn paranimfen, bedanken. Roel ik hoop dat je je goed voorbereid hebt, en dat de internetinformatie over paranimfen correct was. Barbara, laten we hopen dat je er deze keer wel bij kunt zijn.

Mijn ouders bedankt voor jullie steun, niet alleen de laatste 4 jaar maar ook daarvoor. Ik ben blij dat jullie me scheikunde lieten studeren en altijd achter me stonden, Geesje ook bedankt.

Monica dankjewel dat je deze vier jaar met mij hebt gedeeld. Ondanks dat jij het ook druk had kon ik altijd op je steun rekenen, en motiveerde je me telkens weer. Nu we beiden deze 4 jaar al zijn doorgekomen zal de rest geen probleem meer zijn.

Curriculum Vitae

Emiel Speets werd geboren op 27 september 1976 te Midwoud. Na het behalen van zijn VWO-diploma aan de van der Capellen scholengemeenschap te Zwolle, begon hij in 1994 aan de studie scheikunde aan de Universiteit Utrecht, waar hij in 2000 afstudeerde bij de vakgroep metaalgestuurde organische synthese onder leiding van prof. Gerard van Koten. Zijn bijvak werd gedaan in de vakgroep anorganische chemie en katalyse van prof. Geus. Van oktober 2000 tot en met oktober 2004 voerde hij een promotieonderzoek uit, onder supervisie van prof. David Reinhoudt en dr. Bart Jan Ravoo, bij de vakgroep SMCT aan de Universiteit Twente. De resultaten van dit promotieonderzoek staan beschreven in dit proefschrift.